Engineered-Polysaccharide Reinforced Hybrid Composites for Automotive Applications

by

Dinesha Ganesarajan

A thesis
presented to the University of Waterloo
in fulfilment of the
thesis requirement for the degree of
Master of Applied Science
in
Chemical Engineering

Waterloo, Ontario, Canada, 2019

Author's Declaration

I hereby declare that I am the sole author of this thesis. This is a true copy of the thesis, including any required final revisions, as accepted by my examiners.

I understand that my thesis may be made electronically available to the public.

Abstract

In recent years, the automotive industry has undergone severe changes that challenges their conventional methods of mass vehicle production. This is due to many factors that include legislation that demand for increase in fuel economy and public sentiment for environmental sustainability. Therefore, one of the most prominent solutions to combat the factors mentioned above is to rethink material utilization in automobiles. The purpose of this thesis is to reduce the material weight and increase the environmental sustainability of polypropylene composites for body interior and under-the-hood applications, specifically replacing inorganic sources with naturally, biodegradable filler materials.

Two polysaccharide morphologies were explored in this study which includes DuPont's Nuvolve™ (micro-polysaccharide) and nanocellulose. The natural fillers were incorporated with glass fiber in a polypropylene matrix to yield hybrid composites. The polysaccharide & glass fiber loadings were varied with the total filler concentration not exceeding 30 wt.%. Subsequently mechanical, thermal, rheological and morphological properties were evaluated and compared to Ford Motor Company's material specification for body interior and under-the-hood applications. The composites were prepared through twin screw extrusion and injection molding where a universal testing machine was used to assess the mechanical properties. Thermal properties were analyzed using thermal gravimetric analysis (TGA) and differential scanning calorimetry (DSC). Melt rheology was evaluated using a parallel-plate controlled strained rheometer. Scanning electron microscope (SEM) was used to study the filler-matrix interface of the hybrid composites.

The results showed that for the micro-polysaccharide (Nuvolve™) hybrid composites a density reduction of up to 13% was achievable with improvements to tensile strength and impact strength

compared to Ford Motor Company's material specification. The addition of Nuvolve™ negatively affected the thermal stability of the composites due to the low thermal stability of the polysaccharide. Additionally, the analysis of the thermal transitions of the composites showed that the Nuvolve™ did not have a nucleating effect to enhance crystallization which in turn improves part-production. SEM images showed good filler distribution of Nuvolve™. Nuvolve™ revealed areas of poor dispersion seen as agglomeration up to 100μm; which can lead to poor transfer of stress between filler and the polymer matrix. Glass fibers were also well distributed in the polypropylene matrix with typical fracture mechanisms present such as fiber-pull out.

Nanocellulose reinforced hybrid composites showed a greater density reduction above 15% compared to Ford Motor Company's material specification. The optimal performing composite contained 2.5 wt.% of nanocellulose and 10 wt.% of glass fiber yielding a total filler content of only 12.5 wt.%. The mechanical properties of the optimal formulation agreed with most of the material specification outlined by Ford Motor Company for body interior and under-the-hood applications. Furthermore, the thermal stability was slightly enhanced with the inclusion of nanocellulose compared to neat polypropylene. Similarly, with Nuvolve™, nanocellulose did not show a nucleating effect on the crystallization temperature. SEM micrographs demonstrated agglomeration of cellulose nanofibrils (CNF) and cellulose nanocrystals (CNC) reinforced hybrid composites.

The hybridization of Nuvolve™ and nanocellulose combined with glass fiber in a polypropylene matrix yielded high performing composites that offer superior performance properties while permitting lightweighting that provides an intermediate but necessary step towards environmental sustainability within the automotive space.

Acknowledgements

I would like to extend my deepest appreciation and gratitude to my academic advisor Dr. Leonardo Simon for his constant support and guidance during this incredible journey. I would also like to express my appreciation to our research group that kept me sane throughout the process of pursuing my Master's study; in particular Charles Dal Castel, Ian Tivendale, Douglas Casseta, Andrew Finkle and Ryan Park. Thank you very much!

Furthermore, I would like to take the opportunity to thank Ford Motor Company for providing the facility to carry out the experimental work. Dr. Alper Kiziltas and Dr. Deborah Mielewski for their full support and guidance as well as training on the equipment used in this thesis. Without your continual support and loving nature; I would not be able to complete this very important milestone. I would also like to thank DuPont Industrial BioSciences for providing the opportunity to work with Nuvolve™ and with the help from Dr. Christian Lenges and Dr. Natnael Behabtu; I was given the tools to succeed in this research topic.

I owe a huge debt of gratitude to my family members: Geetha (mother), Jeny (sister) and Thanooshan (brother). This work would not be possible without the patience and everlasting support of my family whom I owe everything. I do not know how to thank my partner Shabeeka for her support; your love and encouragement transcended to the very fiber of my being. Thank you always! I want to dedicate this thesis work to my father Kanagaratnam. I hope this can solidify your legacy. Finally, I would like to thank my committee members Dr. Tizazu Mekonnen and Dr. Ting Tsui for generously giving their time to be part of my thesis reading committee.

Table of Contents

List of Figures

List of Tables

Chapter: 1 Introduction

1.1 Background & Motivation

Petroleum-based plastics have vastly contributed to quality of life in modern society such as the advent of Polyethylene (PE) which is widely used in consumer goods, wire & cable insulation, industrial piping, linings, coatings and it was historically deployed in World War II for electrical insulation of submarines and radarshields [1]. In particular, the usage of plastics in the automotive industry increased from 6% in 1970 to 16% in 2010 and it is due to reach 18% by 2020 [2]. The increased usage of plastics contributes to post-consumer waste where shortage of landfill space, ocean pollution and the depletion of petroleum resources invigorated engineers and scientists to shift their focus on to the development of biodegradable and renewable plastics. Next generation materials should exemplify principles of sustainability, industrial ecology and green chemistry.

Moreover, in the United States of America the corporate average fuel economy (CAFE) regulated by the national highway traffic safety administration (NHTSA) set the fuel economy standard for passenger vehicles and light-duty trucks to be 54.5 miles per gallon (MPG) by 2025 [3]. The projected added cost to a 2025 model vehicle is 1800 USD however, the improved fuel economy for those consumers who drive their vehicle for its entire lifetime would save on average 3400-5000 USD [3]. This standard further amplified the necessity for automakers to find innovative ways to improve fuel efficiency, where the concept of lightweighting sparked great interest within the automotive realm. Newton's Second Law states that acceleration of an object is dependent on the forces acting upon the object and the object's mass, therefore it takes less energy to accelerate a lighter object. Application of this fundamental law has shown that 10% reduction in vehicle weight can improve fuel economy by 6-8% [4].

Lightweighting primarily focuses on substituting heavier objects such as metal with lighter materials such as carbon fiber in high performance vehicles. This is extremely hard to achieve for large volume vehicles due to the cost and metal's structural importance in the construction of engine, chassis and body exterior parts. Metals used in non-structural parts of the vehicle can be replaced with reinforced thermoplastics without compromising performance while delivering reduction in weight. Composites are attractive, combining materials properties in ways not found in nature and in the automotive industry glass fibers and talc are common materials used for reinforcing plastics due to their low cost and good mechanical properties. Naturally sourced materials such as cellulose and poly-α-1,3-glucan have potential to provide good reinforcing properties at a lower density (~1.5 g/cm3). The advantages of bio-based filler materials are that they provide good mechanical properties, biodegradability, lower wear on processing equipment and lower density. The limitations of such materials are their restricted thermal stability, shrinkage in comparison to traditional inorganic fillers, hydrophilic nature of the filler and higher than usual cost per pound of material in comparison to inorganic fillers. Therefore, completely replacing inorganic filler material with naturally sourced material is not viable in today's economic environment, however combining inorganic and natural fillers could provide an intermediate and necessary solution to achieving performance properties, lightweighting and sustainability.

Improvements to fuel efficiency are initial steps to achieving a circular economy. However, there is also a need for a holistic approach to engineering design for next generation automotive parts that consider the source of materials, processing and disposal at end of usage which all contribute to the total carbon footprint [5].

1.1.1 Objectives

The purpose of this research was to develop hybrid composites combining various polysaccharides of unique morphologies with glass fiber in a polypropylene matrix to optimize overall composite properties. In particular, this study evaluates nanocellulose crystals, nanocellulose fibrils and DuPont's poly α -1,3 glucan (derived from sucrose feedstock) as viable options to reinforce polypropylene in combination with glass fiber for body interior and under-the-hood applications such as IP substrate, center console and battery cover in passenger vehicles & light-duty trucks. Composites were produced at various loadings of polysaccharide and glass fiber using melt blending (twin screw extruder) and injection molding. The effect of the combination of filler loading on the composite properties were investigated (mechanical, thermal & rheological) to gain insight of strategies to optimize performance properties of the composites. This research attempts to provide a comprehensive study on the development of hybrid composites containing naturally sourced materials to deliver optimum mechanical and thermal properties suited for body interior and under-the-hood applications for passenger vehicles and light-duty trucks while achieving significant lightweighting opportunities.

The major challenge of incorporating polysaccharides in polyolefins such as polypropylene is surface compatibility due to the hydrophilic nature of polysaccharides and hydrophobic nature of polypropylene. Filler-matrix adhesion is critical, as the role of the matrix in a fibre-reinforced plastic is to transfer the load to the stiff fibres through shear stresses at the interface; which requires good adhesion [5]. It is desired to have strong binding capabilities between the filler and the matrix and having weak binding sites promotes void structures and particle agglomeration. Therefore, it is essential to design and maximize the interfacial interaction of the filler and matrix to acquire improved material properties and functionality.

1.2 Structure of Thesis

A general overview of engineering thermoplastic composites reinforced with naturally sourced, biodegradable material and glass fiber are given in Chapter 2. Chapter 2 also discusses polypropylene being used as a commodity plastic in society as well as exploring the importance of filler-matrix interactions with respect to the overall composite properties. The thesis layout is displayed in Figure 1.2-1.

1.2.1 DuPont Nuvolve™ reinforced hybrid composites

Chapter 3 discusses the effect of incorporating DuPont Nuvolve™ (α -1,3 glucan) with glass fiber in a polypropylene matrix and evaluates the mechanical, thermal, morphological and rheological properties of the composites.

1.2.2 Nanocellulose reinforced hybrid composites

Nanotechnology in materials science has been a topic of discussion in recent years where technologies are created by manipulating chemistries at atomic and molecular levels to achieve superior material performance for a variety of applications. In Chapter 4, the deployment of nanocellulose as an effective reinforcing filler in combination with glass fiber in polypropylene is discussed; specifically evaluating the mechanical, thermal and morphological properties of various formulations.

Figure 1.2-1: Thesis Layout

Chapter: 2 Literature Review

2.1 Background on Polypropylene

The use of petroleum based-plastics erupted during the 20th century, with polyolefins being the top of the global production of synthetic polymers. Polyolefins are a class of polymers that are derived from olefins (alkenes) such as polyethylene produced by polymerizing the olefin ethylene and polypropylene being made from the olefin propylene. The global production of polyolefins exceeded 178 million tons in 2015, where isotactic polypropylene ranked as the least expensive polymer to produce [6]. Polyolefins can be processed by common techniques that include extrusion, injection molding, blow molding and thermoforming. Their ease of processing, low cost and good chemical & mechanical properties make it one of the most versatile and popular type of polymers being used in today's society.

Polypropylene (Figure 2.1-1) is a member of the polyolefin family which can be produced using a coordination catalytic-driven polymerization process. Prior to the discovery of polypropylene, in 1933 Eric Fawcett and Reginald Gibson accidently discovered polyethylene while running ethylene at high pressures. One of the autoclaves had leaked during the experiment and introduced oxygen in the system which decomposed and thereby provided free radicals for the formation of polyethylene [6]. This first discovery led to technological advances during the 1940s and several companies were motivated to find catalytic enabled polymerization methods at moderate process conditions (temperature and pressure) to lower costs such as the discovery of the Phillips catalyst for the production of high-density polyethylene (HDPE).

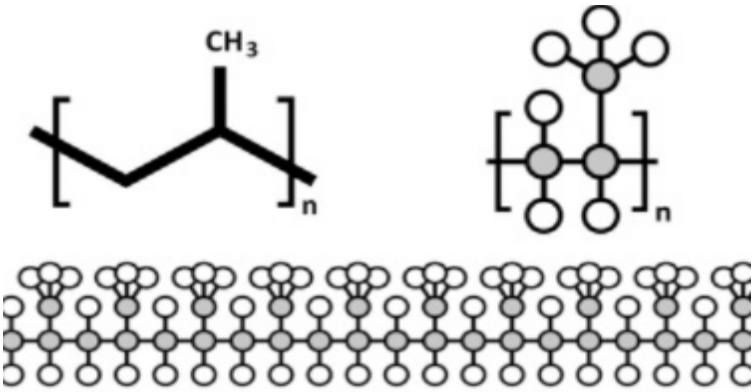

Figure 2.1-1: Structure of Polypropylene; top right image: i) hydrogen (white) ii) grey (carbon) [7]

In 1953, Karl Ziegler discovered that combining titanium tetrachloride and triethylaluminum yielded polyethylene at a lower temperature and pressure (<55bar) [6].This work led to Giulio Natta polymerizing isotactic polypropylene and introducing the concept of stereoregularity in the polyolefin industry; the catalyst is known as the Ziegler-Natta Catalyst. The co-catalyst (tridiethylaluminum) activates the catalyst by the reduction and alkylation of the transition metal.

Ziegler-Natta catalysts have developed over the last fifty years to maximize the activity and to improve stereoregularity such as catalysts being supported on $MgCl_2$ surface and therefore it is an ongoing area of interest [6]. In the 1970s continuous experimentation with the Ziegler-Natta catalyst led to the discovery of a new co-catalyst called methylaluminoaxane (MAO) with the general formula $(\text{-Al-O(-Me)-})_n$. The traditional Ziegler-Natta catalysts are heterogeneous systems with multiple active sites whereas, metal complexes in combination with MAO are categorized as homogenous catalysts with the simplicity of having a single active site. In respect to the production of polypropylene (isotactic), it is hard to distinguish the degree of influence that tacticity and molecular weight have on the structural performance since those two factors are strongly coupled when polymerized using the Ziegler-Natta catalyst. Metallocene polypropylenes are homogenous

in tacticity and molecular weight distributions, meaning that chains resemble one another much more than when using Ziegler-Natta catalysts due to the existence of only one active site in metallocene catalysts [8].

Polypropylene has three main configurations which are isotactic, syndiotactic and atactic. The following configurations depend on how the methyl groups are positioned along the polymer backbone. If the methyl groups are positioned along the same side of the macromolecule polymer then it is referred to as isotactic. Alternating positions along the backbone are referred to as syndiotactic and finally randomly positioned methyl groups are called atactic. Tacticity affects the physical properties of polymers as the regularity of the macromolecular structure influences the ability for polymer to crystallize. For example, isotactic polypropylene (iPP) readily crystallizes as opposed to atactic polypropylene (aPP), which is an amorphous polymer where limited crystallization occurs. Isotactic polypropylene that is commercially available contains around 2-5% of atactic polypropylene. The fraction of isotactic chains in polypropylene grades are quantified by the isotacticity index which is measured as the mass fraction of polypropylene insoluble in boiling heptane [9].

2.1.1 Polypropylene: North-American Market

Polypropylene (PP) is used in a wide range of applications that include consumer and industrial products. As discusses earlier there are three forms of PP, the main form being isotactic polypropylene (iPP) where the largest consumed PP are injection molded grades for packaging, electronic parts, electrical appliances, toys and other household goods [10]. The price of homopolymer injection grade polypropylene ranges between 0.60-0.80 USD/lb in the U.S [10]. Figure 2.1-2 show production capacity of PP in the US in 2018.

The US PP demand is expected to grow especially due to the newly announced Braskem facility to be built in La Porte, Texas with a capacity of 450,000 tonne/year [10]. Therefore, the US market shows growing number of production facilities to accommodate demand and most importantly the popularity of PP as a commodity globally.

US PP CAPACITY '000 TONNES/YEAR

Company	Location	Capacity
Total Petrochemicals	La Porte, Texas	1,200
Formosa Plastics USA	Point Comfort, Texas	740
Braskem	Marcus Hook, Pennsylvania	414
Pinnacle Polymers	Garyville, Louisiana	410
INEOS	Chocolate Bayou, Texas	400
ExxonMobil Chemical	Baytown, Texas	396
Phillips 66	Linden, New Jersey	352
ExxonMobil Chemical	Baton Rouge, Louisiana	335
Flint Hills Resources	Longview, Texas	330
Braskem	Seadrift, Texas	225

Figure 2.1-2: US PP Capacity (ktonne/year) in 2018 [10]

2.1.2 Polypropylene in the Automotive Industry

In the previous section, the importance of PP in daily life was discussed as well as the North American market for PP. It is clear that PP is one of the most utilized plastics and this can also be seen in the automotive industry [11]. PP accounts for more than half of all the plastic constituents used in automobiles due its low cost, outstanding mechanical properties and moldability. In 2007, 3.4 million tonnes of PP (8% of the world's total PP consumption of 41

million tonnes) were used in automotive applications [11]. Table 2.1-1 shows typical engineered plastics used in automotive parts.

Table 2.1-1: Engineered plastics used in a typical vehicle [12]

Component	Main types of plastics	Average Weight in car (kg)
Bumpers	PS, ABS, PC, PC/PBT	10
Seating	PUR, PP, PVC, ABS, PA	13
Dashboard	PP, ABS, SMA, PPE, PC	7
Fuel systems	HDPE, POM, PA, PP, PBT	6
Body (incl. panels)	PP, PPE, UP	6
Under-bonnet components	PA, PP, PBT	6
Interior trim	PP, ABS, PET, POM, PVC	20
Electrical components	PP, PE, PBT, PA, PVC	7
Exterior trim	ABS, PA, PBT, POM, ASA, PP	4
Lighting	PC	5
Upholstery	PVC, PUR, PP, PE	8

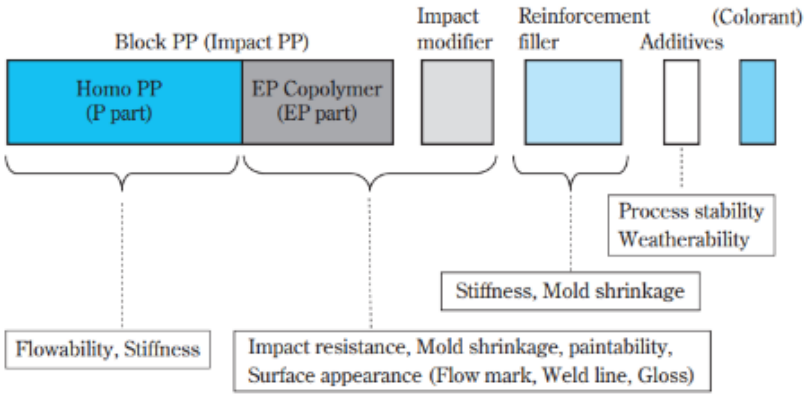

Figure 2.1-3: Component of PP compound for automotive application [11]

Figure 2.1-3 shows the general constitution of PP grades in automotive applications. Impact PP refers to a combination of homopolymer of PP and ethylene propylene copolymer (EP copolymer). PP compounds are used in a variety of parts, including bumper fascia, instrumental panels (IP), center console and door trims. Traditionally, in the automotive industry uses inorganic fillers to improve performance of PP, such as glass fiber, talcum, silica and mica.

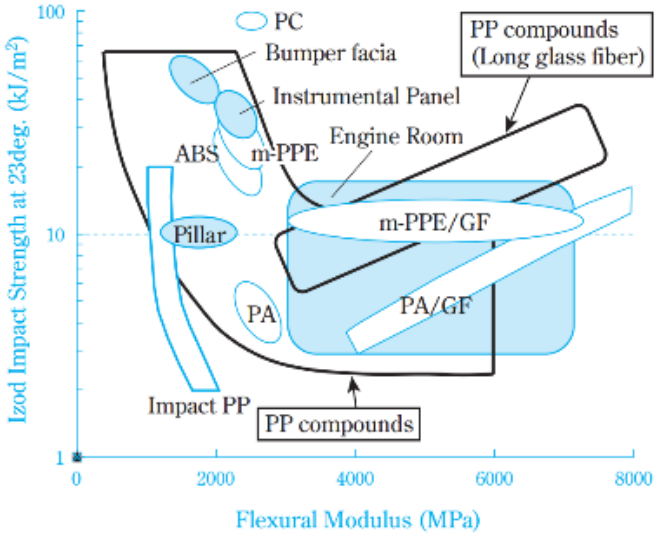

Figure 2.1-4: Impact & Flexural Modulus of PP compounds and usage in vehicles: PC=Polycarbonate, ABS=Acrylonitrile Butadiene Styrene, PA=Polyamide and m-PPE=Modified Polyphenylene Ether [11]

Figure 2.1-4 shows the mechanical properties of various PP grades and their application) [11]. The automotive industry requires lower weight, improved moldability and enhanced mechanical properties and the various grades of PP compounds can fill the void and replace conventionally used engineered plastics (ABS, PA and PC).

2.2 Crystallization of Polymers

2.2.1 Nucleation and Growth

The attractiveness of using thermoplastics specifically in the automotive industry is due to the mechanical properties, ease of manufacturing and cost as seen in the previous section. Thermoplastics can be used in load-bearing and non-load bearing applications, therefore the robust choice of application makes thermoplastics extremely useful in the automotive industry. Furthermore, the increasing use of thermoplastics and thermoplastic composites requires further knowledge about the microstructures and their effect on the overall end-user properties. Thermoplastics can be divided into two distinct groups among polymer families i) semi-crystalline ii) amorphous. Semi-crystalline polymers have both crystalline and amorphous domains co-existing. Crystalline domains are ordered polymer chains and these domains are understood to positively impact strength and stiffness properties of the polymer. Whereas amorphous domains represent disordered, tangled polymer chains and this is understood to give flexibility and energy absorption (impact) properties [13]. For engineering thermoplastics, it is important to maximize the crystallinity of a given polymer due to its impact on the strength and stiffness of the polymer (high strength-to -failure and stiffness-to-failure).

The crystallization mechanism is divided into two processes:

1. Nucleation
2. Growth

Nucleation is the start of crystal growth, as temperature decreases molecular vibrations decrease and intermolecular interactions (e.g. Van Der Waals) between the molecules start to occur. These intermolecular interactions of molecules allow for close packing of molecules

resulting in an embryonic crystal. Growth mechanism occurs when the critical nuclei size is formed, this can be depicted in Figure 2.2-1. This is thermodynamically modelled by the Gibbs free energy (Figure 2.2-1), where the energy peak has to be overcome for spontaneous crystal growth. This is understood to happen at the crystallization temperature where sufficient thermal energy overcomes such a barrier [14].

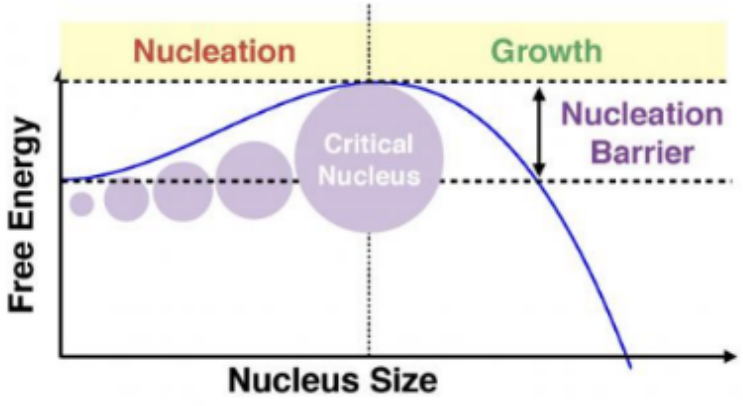

Figure 2.2-1: Gibbs free energy as a function of crystal nucleus size [15]

The crystal growth further aggregates to form lamellae structures that represent folded polymer chains in an ordered manner. On the surface of lamellae structures, there are regions of the polymer chains that are not ordered intending to re-order into the lamellae structures; this is especially true for long-chained polymers such as polyethylene. There are generally two acceptable models of this re-entry process known as i) adjacent re-entry-model and ii) switchboard -model Figure 2.2-2. The arrangement in the lamellae is a dynamic process where chains are assumed to come back and forth into the lamellae structure to forms loops with identical lengths resulting in a clear defined cuboid shape, which was used to explain the spherulite structure. However, Flory demonstrated that the first model cannot precisely describe the crystal formation of long chain molecules [14].

Long chain polymers cannot always re-enter the lamellae at an adjacent site, it most likely a random re-entry process which is described by the second model (switchboard-model).

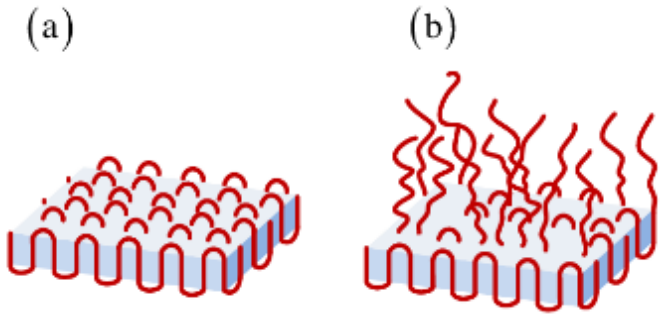

Figure 2.2-2: A schematically view of (a) adjacent-entry model (b) switchboard-model [14]

Figure 2.2-3 shows the hierarchical structure of crystallization starting in the atomic scale to micro dimensions. The lamellae structures further aggregate to form spherulites that grow radially from the crystal nucleus and the lamellae structures are sandwiched with amorphous regions as seen in Figure 2.2-4.

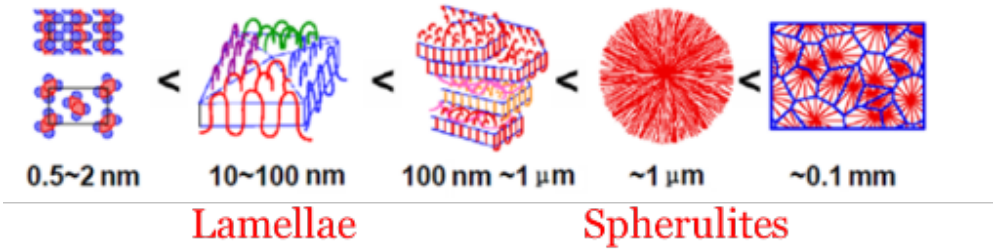

Figure 2.2-3: Hierarchical representation of crystallization, taken from Prof. A Toda (University of Hiroshima)

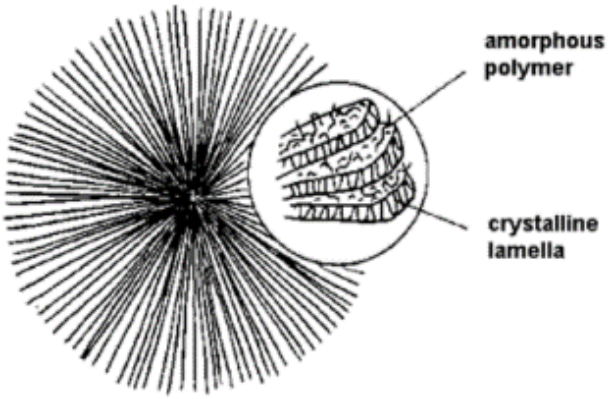

Figure 2.2-4: Spherulite structure [16]

2.2.2 Transcrystallinity

In the previous section, homogenous nucleation was described where crystallization occurs from the polymer melt. Heterogeneous nucleation can also occur, and this is more apparent in composites that incorporate several materials. Fibers may act as heterogeneous nucleating agents and nucleate crystallization along the interface forming transcrystalline layers (TC), provided that there is a high density of nuclei present at the fiber surface. The nuclei will grow perpendicular to the fiber surface and will eventually impede the spherulite growth from the melt. Figure 2.2-5 shows that the energy barrier is lowered with heterogeneous nucleation resulting in faster crystallization process, which is beneficial in automotive part production (lowering cycle times).. Some authors have shown that the mechanical properties improved due to the formation of TC layers and some have reported negligible contribution to the composite properties [17]. The formation of TC layer depends on the fiber topography, surface coating of the fiber, processing conditions (cooling rate) and roughness of the fiber [17].

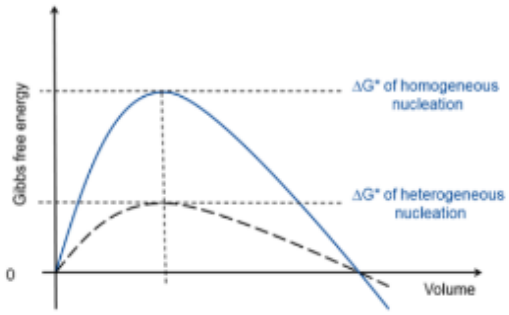

Figure 2.2-5: Schematic showing the energy barrier reduction with heterogeneous nucleation [18]

Transcrystallinity in polypropylene reinforced by glass fiber is largely dependent on the sizing used during the glass fiber manufacturing. Sizing is referred to the protective layer which is a mixture of lubricants (abrasion), antistatic agents (reduce static friction between filaments) and coupling agents that promotes adhesion [19]. It was reported that glass fibers sized with aminosilanes induced TC layers in polypropylene [17]. This statement was further supported by Q.Li *et al* [20] showing that acid treatment of glass fibers induced TC layers and the glass fibers that had no treatment did not induce TC layers as seen in Figure 2.2-6.

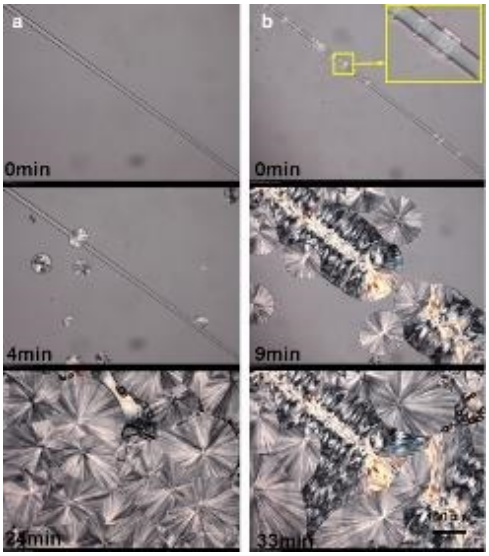

Figure 2.2-6:left) untreated GF-PP right) acid-treated GF-PP at 130ºC using a polarized optical microscope [20]

The images on the right show nucleation sites forming on the glass fiber surface at zero minutes during isothermal crystallization and this could be due to the rough surface topography of the fibers after acid treatment (Figure 2.2-6). Therefore, the surface treatment used in fibers/fillers is an important factor to induce TC layers.

2.3 Inorganic Fillers Used in the Automotive Industry

As mentioned in the previous section, PP has limitations to its performance and to improve mechanical properties inorganic fillers are added for example PP has low ductility at low temperatures [21]. Table 2.3-1 shows typical properties of polypropylene homopolymer compared to other polymer matrices. The addition of inorganic fillers like glass fiber can raise the tensile strength, young's modulus and flexural properties of PP and contribute to the stiffening effect. Table 2.3-2 shows the different type of inorganic fillers used for PP compounds in automotive applications.

Table 2.3-1: Typical Properties of Polymer Matrices [22]

Property	PP	LDPE	HDPE	Nylon 6	Nylon 6,6
Density (g/cm^3)	0.899-0.920	0.910-0.925	0.94-0.96	1.12-1.14	1.13-1.15
Glass Transition (T_g)	-10 to -23	-125	-133 to -100	48	80
Melting Temperature (T_m)	160-176	105-116	120-140	215	250-269
Heat Deflection Temperature (ºC)	50-63	32-50	43-60	56-80	75-90
Coefficient of Thermal Expansion (mm/mm/ºC $x10^5$)	6.8-13.5	10	12-13	8-8.6	7.2-9
Tensile Strength (MPa)	26-41.4	40-78	14.5-38	43-79	12.4-94
Elastic Modulus (GPa)	0.95-1.77	0.055-0.38	0.4-1.5	2.9	2.5-3.9
Elongation (%)	15-700	90-800	2.0-130	20-150	35-100
Izod Impact Strength (J/m)	21.4-267	>854	26.7-1,068	42.7-160	16-654

Table 2.3-2: Typical inorganic fillers for PP compounds [11]

Inorganic Filler Type	Examples
Oxide	Silica, Titanium Oxide, Magnesium oxide, Antimony oxide
Hydroxide	Aluminium hydroxide, Magnesium hydroxide, Calcium hydroxide
Carbonate	Calcium Carbonate, Dolomite
Silicate	Talcum, Mica, Glass fiber. Glass beads, Calcium Silicate, Montmorilonite
Carbon	Carbone black, Graphite, Carbon fiber

Figure 2.3-1 shows the stiffening effect of glass fiber, talcum and calcium carbonate as a function of filler content (wt. %). Glass fiber shows the greatest stiffening effect and given the consideration of cost (0.60-0.90 cents/lb [23]), performance and process ability; glass fiber is the most utilized filler for PP in automotive applications.

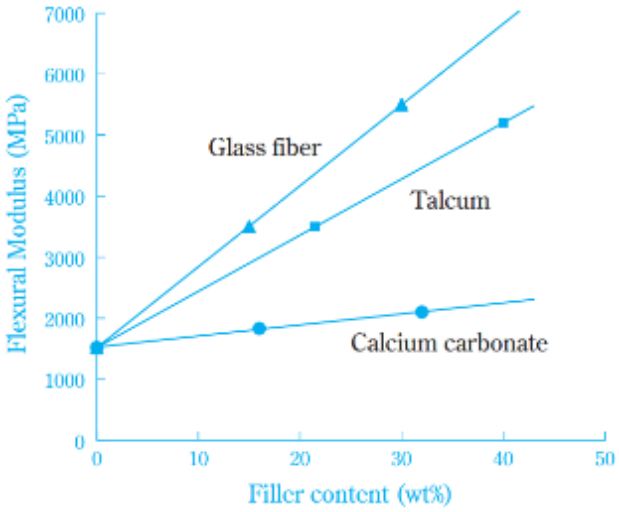

Figure 2.3-1: Stiffening Effect of Glass Fiber, Talcum & Calcium Carbonate in injection molding PP grade [11]

2.3.1 Glass Fiber & Glass Fiber Reinforced Plastic (GFRP)

Glass fibers exhibit useful properties such as hardness, transparency, chemical resistivity, thermal stability and inertness as well as desirable fiber properties including strength, flexibility, and stiffness. There are various grades of glass fibers and the general-purpose grades can be broken down into two categories: 1) Boron-containing E-glass and 2) Boron-free E-glass. Typically, E-glass contains 5-6 wt. % boron oxide and about 60% Silica [24]. The boron oxide is added for ease of processing as it reduces the melting temperature and increases thermal resistance and mechanical strength. However, due to environmental concerns, boron-free E-glass was developed to prevent boron leaking to the environment during processing.Table 2.3-3 shows the letter designations of fiber glass used in industry. The automotive industry uses E-glass for glass reinforced plastics (GFRP). Table 2.3-4 shows typical properties of fiber glass types.

Table 2.3-3: Letter designations for different types of fiber glass [24]

Letter Designation	Property
E	Low electrical conductivity
S	High Strength
C	High chemical durability
M	High Stiffness
A	High alkali/soda lime glass
D	Low dielectric constant

Table 2.3-4: Typical properties of fiber glass [24]

Fiber glass type	Bulk density (g/cm^3)	Dielectric Strength (kV/cm)	Tensile Strength (MPa)	Young's Modulus (GPa)
E-glass	2.54-2.55	103	3100-3800	76-78
Boron-free-E-glass	2.62	102	3100-3800	80-81
D-Glass	2.16	------	2410	888-91
S-Glass	2.48-2.49	130	4380-4590	69

With respect to glass fiber reinforced plastic (GFRP), adhesion at the fiber-matrix interface is crucial to attain improved mechanical properties. Glass fiber is inorganic whereas plastics such as polypropylene are organic; raising incompatibility issues. To increase interfacial compatibility between fiber and polymer matrix, fiber treatments and chemical modification to the polymer can be done. This includes silanization of glass fiber and grafting maleic anhydride on PP. The combination of both techniques achieves optimal interfacial bonding as mentioned by P.F Chu [25]. Figure 2.3-2 shows the fiber treatment using alkoxysilanes on glass fiber. The mechanism of maleic anhydride grafted on polypropylene will be discussed in Section 2.4.1.

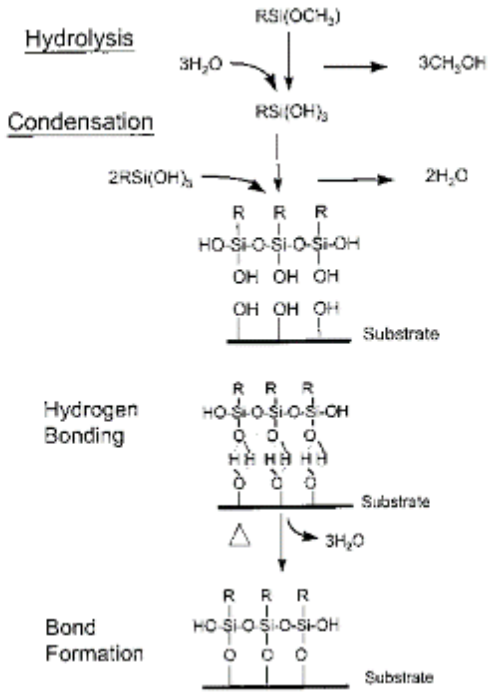

Figure 2.3-2: Reaction process of alkoxysilanes [25] [26]

As defined previously sizing is referred to the protective layer which is a mixture of lubricants, antistatic agents and coupling agents that promotes adhesion between fiber and matrix [19]. The effect of type of sizing used in glass fiber on GFRP was evaluated by P.F Chu [25]. Table 2.3-5 shows the mechanical properties when different sizing systems were used.

Table 2.3-5: Influence of glass fiber sizing on the mechanical properties of GFRP [25]

Properties	A-Silane +PP	B-PP dispersion	C-Silane	D-Unsized
Glass loading (% wt.%)	22.9	22.2	23.7	26.7
Tensile Strength (MPa)	67.8	58.2	35.9	32.9
Modulus (GPa)	3.87	3.58	2.70	3.40

Elongation (%)	2.5	2.4	3.6	4.4
Flexural Modulus (GPa)	103	95	61	60
Notched Izod Impact (kJ/m^2)	12.3	9.82	7.87	4.11

Sample A uses commercially available PP and silane treatment (968 PP glass) on homopolymer PP (Profax 6523) and sample B uses polypropylene dispersion whereas sample C and D use silane and no treatment respectively. The results demonstrate that there is a clear improvement in mechanical properties albeit elongation (%) for sized fibers as opposed to use of no sizing system. Figure 2.3-3 shows SEM micrographs of sample A, C and D at fracture surface. It is evident that sample A has PP engulfed for improved adhesion whereas sample C and D show no bonding to PP matrix (clean fiber surface). Sample A shows an optimized system with tensile strength and impact strength improvements of 106% and 199% compared to sample D.

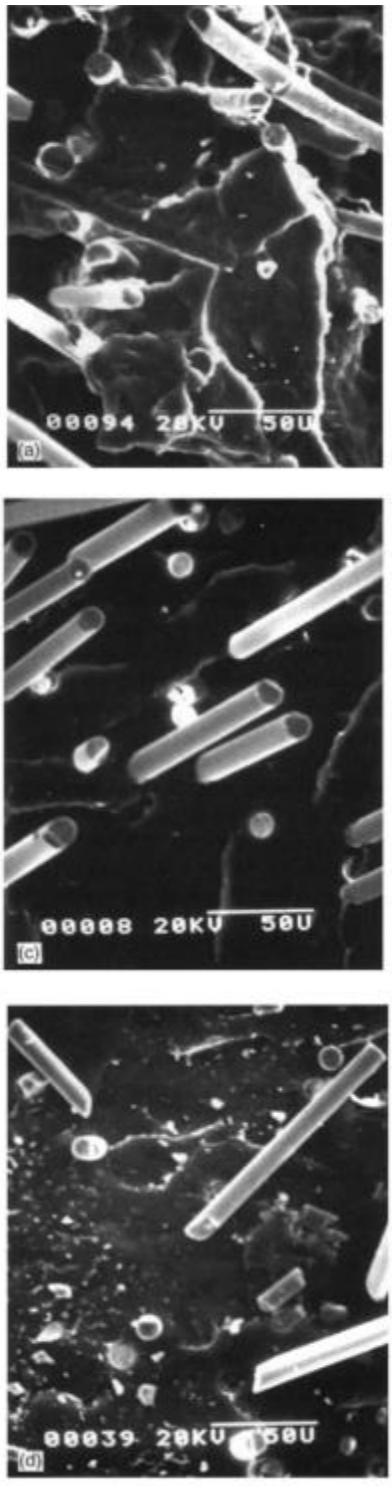

Figure 2.3-3: SEM micrographs of sample A (top), C (middle) and D (bottom) [25]

The influence of sizing system employed in glass fiber manufacturing has a significant effect on the mechanical properties of the GFRP. Another factor that can affect the performance of GFRP is the fiber diameter. The general understating in the glass fiber industry is that smaller glass fiber diameters lead to improved composite strength. Research presented by P.F Chu [25] examines mechanical properties (tensile strength, notched impact strength) of GFRP using glass fibers treated with silane and PP (969 PP glass) and homopolymer PP at varying fiber diameters and glass fiber loading (% wt.). The results showed that the tensile and impact strength decrease with increasing fiber diameter at 30% wt. glass fiber loading and for 10 & 20% wt. glass fiber loading the fiber diameter has negligible effects on the mechanical properties. Although with smaller fiber diameters incremental changes in composite properties can be achieved, it would be a trade-off with the increased cost of production to attain finer fiber diameters. Furthermore, the increase in melt viscosity as a result of smaller fiber diameters can be problematic for injection molders. F.Ramsteiner [27] examined the Young's modulus of short fiber glass reinforced polyamide composites at various fiber diameters. The results showed that fiber diameter does not influence modulus and that aspect ratio controls such property. This is supported by various micromechanical models such Halpin Tsai, where only the aspect ratio not fiber diameter controls the geometric factor [27].

The major setback from utilizing glass fiber in composite technology is the environmental footprint, Table 2.3-6 shows the environmental impact from glass fiber and china reed fiber, production. It can be seen that glass fiber emits about 4 times more of carbon dioxide (kg/kg) compared to china reed fiber (naturally sourced filler) and the total energy to produce glass fiber is 16 times more than china reed fiber. Therefore, glass fibers offer impressive reinforcing

capabilities at a low cost but, the environmental impact constitutes necessity to innovate in filler technology.

Table 2.3-6: Environmental impact from glass fiber and china reed fiber production [23]

Environmental Impact	Glass Fiber	China Reed Fiber	Polypropylene
Energy use (MJ/kg)	48.33	3.64	77.19
CO_2 emissions (kg/kg)	2.04	0.66	1.85
CO emissions (g/kg)	0.80	0.44	0.72
SO_x emission (g/kg)	8.79	1.23	12.94
NO_x emissions (g/kg)	2.93	1.07	9.57

2.3.2 Talc

Another inorganic filler type to consider is talc which has been used to reinforce polypropylene since the 1960s for under-the-hood automotive parts. In the 1970s, ultrafine talc in thermoplastic olefins (TPO) replaced polyurethane and acroylonitrile-butadiene-polystyrene (ABS) blends in fascia and kick plates because of the lower cost and meeting the 5 mile/hr automotive crash test [28]. Talc is a mineral that is found in deposits around the world, known as a hydrous magnesium silicate. The typical concentration of talc consists of 31.7% MgO, 63.5% SiO2 and 4.8% H2O; this can change depending on the ore. Talc is a layered structure as seen in Figure 2.3-4.

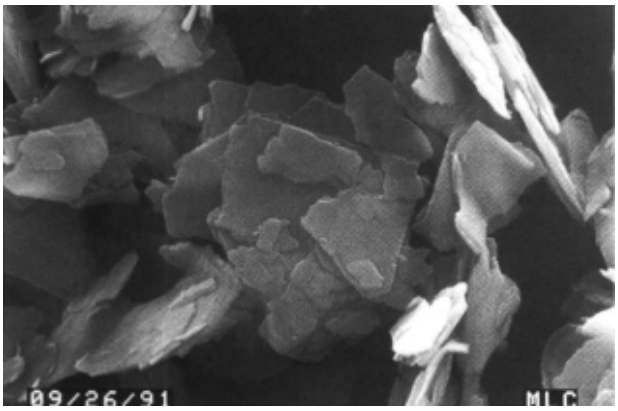

Figure 2.3-4: SEM Micrograph showing layered structure of talc [28]

The plate like morphology of talc self-orients with the flow of the molding process which allows for good reinforcement in stiffness and heat deflection temperature. The stiffness of the composite is influenced by the aspect ratio of the filler and talc can be found in macrocrystalline and microcrystalline forms. Macrocrystalline talc has a higher aspect ratio and therefore contributes more significantly to the stiffness effect of talc. Particle size has a huge influence on impact properties (Figure 2.3-5), the increasing particle size decreases the impact properties of the final composite. Figure 2.3-6 shows SEM micrographs of talc with varying particle size reinforcing an impact copolymer and producing two different failures: brittle and ductile. Therefore, to achieve a stiffness-impact balance the particle size and aspect ratio need to be considered. In the automotive industry, talc is usually combined with other minerals along with glass fiber to reinforce polypropylene for body interior and under-the-hood applications [29].

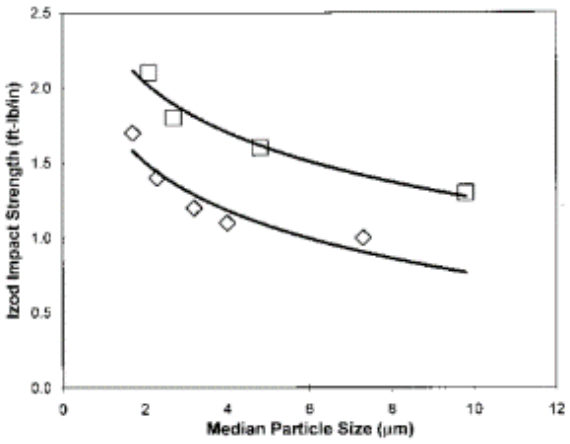

Figure 2.3-5: Particle size effect on Izod impact strength. Diamond represents commercial grade Jetfil® and square represents commercial grade Cimpact®

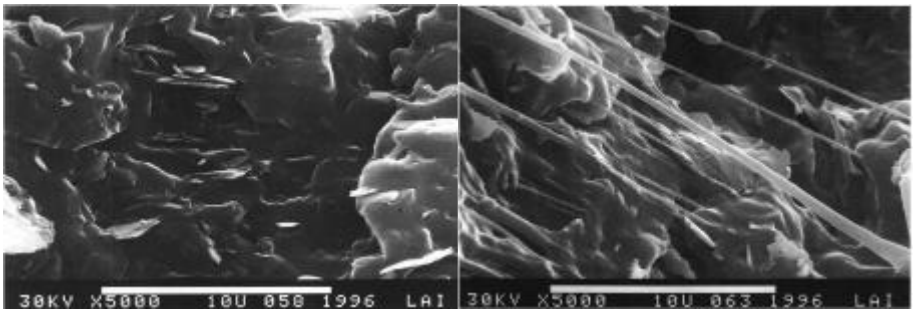

Figure 2.3-6:Left) Brittle failure due to large particles Right) Ductile Failure due to small talc particles

2.3.3 Carbon Fiber

The automotive industry has shifted its focus on technological advancement in composites to meet stringent fuel economy and emissions standards. Lightweighting through carbon fiber reinforced plastic (CFRP) composites is possible due to the high specific strength and stiffness (1.8 GPa and 517 GPa [30]) and thermal stability of carbon fiber. Carbon fiber's chemical structure consists of sheets of carbons atoms arranged in a hexagonal pattern and the precursor material for making carbon fiber is polyacrylonitrile (PAN) [30] [31]. The chemical processes involved in carbon fiber production are shown in Figure 2.3-7.

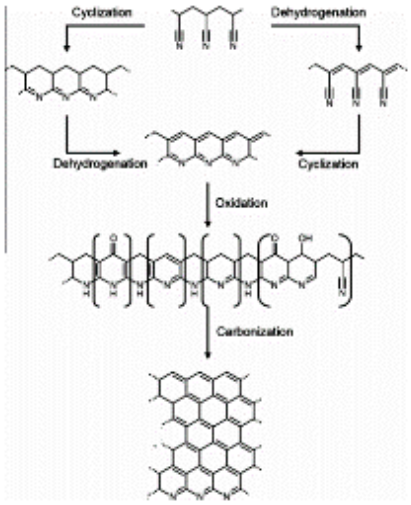

Figure 2.3-7: Chemical reactions during the stabilization and carbonization of PAN based carbon fibers [31]

A study conducted by F. Rezaei [32], evaluated the mechanical and thermal properties of short carbon fiber reinforced polypropylene (PP) composites for the application of a car bonnet (comparing to conventional carbon steel bonnet). The results showed that strength, stiffness and impact increased with carbon fiber content (% wt.) and thermal degradation was also improved. When compared to commercially available steel bonnet, the short carbon fiber reinforced PP composites exhibited superior specific strength and modulus thus providing the opportunity for weight savings for the application of the car bonnet. However, implementation of carbon fiber in the automotive industry is difficult due to poor economies of scale, which keeps this technology only available in premium markets. Furthermore, a study conducted by J.R Duflou [33] evaluated the life cycle assessment of structural car components by a CFRP composite alternative. The results showed that significant fuel economy savings were achievable with the implementation of CFRP composites, however the study noted that the improvements in fuel economy were offset by the energy intensive nature of carbon fiber production.

2.4 Naturally Sourced-Fillers

The popularity of engineered plastics during the 20th century grew immensely, as global plastic production reached 292 million tonnes in 2015 (Figure 2.4-1). Polyolefins are one of the most dominant plastics due the relatively inexpensive cost of production via natural gas and being one of the lightest synthetic polymer families. This enormous increase in global plastic production sparked concerns over recyclability and biodegradability. Petroleum-based polymers do not readily degrade and persist in the environment; therefore, concerns over emissions from incineration and entrapment from plastics spurred governmental bodies to adopt efforts to develop solutions [23]. For the automotive industry, the driving factors for innovative solutions are i) to increase fuel economy (lightweighting) in response to governmental regulations and ii) decrease carbon dioxide emissions due to public unrest on climate change. Composites offer a unique solution to this problem where glass fiber or traditionally inorganically sourced filler material can be replaced by natural fillers to produce lighter and better performing composites. There is a premium for incorporating natural fiber and hybridization with glass fiber in thermoplastics offers an economically feasible and necessary step for advanced composites in the automotive industry.

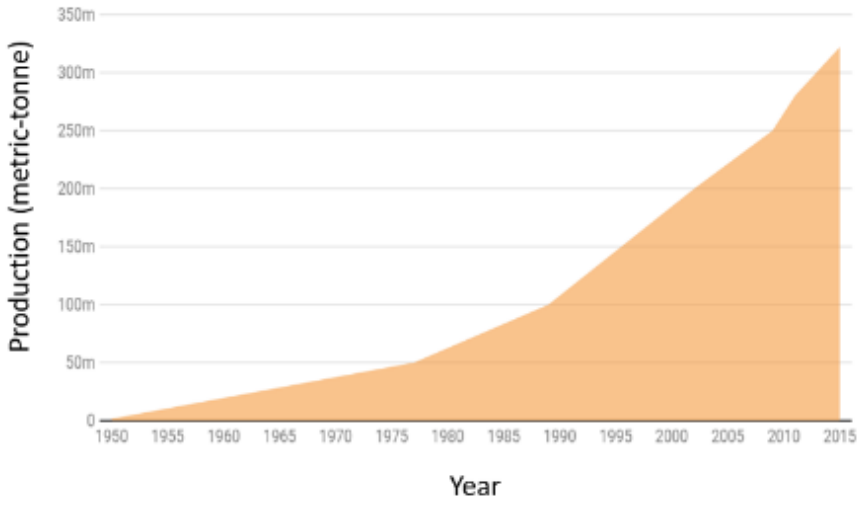

Figure 2.4-1: World production of plastics [34]

2.4.1 Natural Fibers

The most common natural fibers are hemp, jute, ramie, coir, sisal, flax and cotton. The emergence of bio-composites represent a value-added source of income for the agriculture industry. For example, India accounts for 20% of the total world production of jute and coir and sisal is harvested in tropical areas such as Africa, West Indies and the Far East [23].

Natural fibers major constituents are cellulose, lignin, hemicellulose, pectin and wax. Cellulose is composed of repeating β- 1,4 -glucose molecules linked in a long chain. The multiple hydroxyl groups on the glucose from one chain form hydrogen bonds with oxygen atoms on the same (intramolecular) or neighbouring (intermolecular) chain, holding the chains firmly together side by side as seen in Figure 2.4-2 [35] [36]. Therefore, cellulose is hydrophilic in nature. Hydrogen bonds give cellulose unique properties of mechanical strength and chemical stability. Although various types of natural fibers consist of cellulose, the mechanical properties are dependent on molecular weight and degree of polymerization (DP) of cellulose.

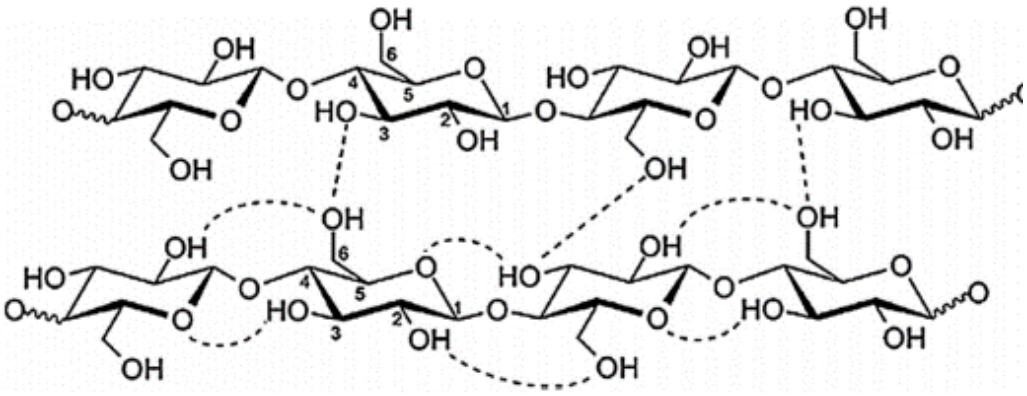

Figure 2.4-2: Cellulose Structure with Hydrogen Bonding (dashed lines) [35]

Hemicellulose belongs to a group of heterogeneous polysaccharides and is found in the cell wall of plants. In comparison to cellulose, hemicellulose is short-chained (DP of 50-200) and has a random amorphous structure with little strength; it can also be hydrolyzed by acid or base [37] [38].

Lignin acts as an adhesive and cements the cellulose and hemicellulose together. Lignin is a high molecular weight phenolic compound with the exact chemical structure relatively unknown. The main functional groups have been identified as hydroxyl and methoxy groups where high carbon and low hydrogen content suggest that lignin is highly unsaturated, aromatic and hydrophobic [23]. Figure 2.4-3 shows a proposed structure of lignin [39]. Lignin and cellulose work together to provide structural function in plants analogous to that of epoxy resin and glass fibres in a fiberglass boat. Essentially lignin acts as an adhesive in the fibre network. Similarly, pectin acts as an adhesive to the fibre network, holding the fibre together. Therefore, natural fibers provide good mechanical strength, stiffness and chemical compatibility that can be applied in the automotive industry [5].

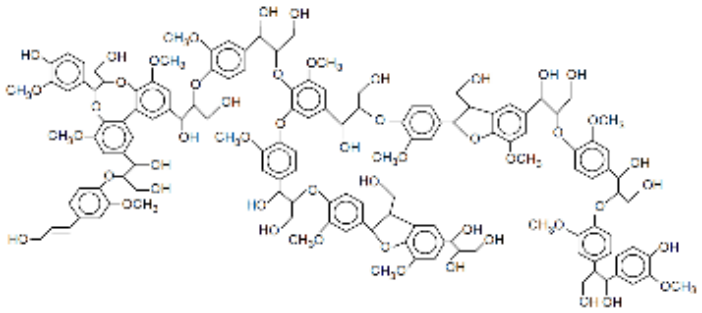

Figure 2.4-3: Lignin Structure [39]

Table 2.4-1 shows the physical properties of natural fibers in comparison to manmade fibers.

Table 2.4-1: Physical properties of natural fiber and manmade fibers [40] [41]

Fiber	Cellulose (%)	Density ($g/cm^{3)}$	Diameter (µm)	Tensile Strength (MPa)	Young's Modulus (GPa)	Elongation (%)
Jute	61-71	1.3-1.45	25-200	393-773	13-26.5	1.16-2
Flax	71	1.5	10-25	345-1100	27.6	2.7-3.2
Hemp	68	1.5	25-35	690	15-23	1.6
Ramie	68.6-76.2	1.5	10-25	400-938	61.4-128	1.2-3.8
Sisal	65	1.45	50-200	350-640	9.4-22	3-7
Coir	32-43	1.15	100-450	131-175	4-6	15-40
E-glass	---	2.5	8-15	2000-35000	70	2.5
Carbon	---	1.7	5-100	2400-4000	230-400	1.4-1.8

Natural fibers are generally incorporated in short fiber reinforced composites because the fiber can be processed in conjunction with the polymer matrix such as injection molding or extrusion for thermoplastics. A.C Karmaker [42] investigated the mechanical properties of injection molded short jute fibers (with and without compatibilizer) in polypropylene. The research showed high fiber attrition due to injection molding process and the mechanical properties were not optimal without the use of coupling agents for improving adhesion between filler and matrix. It is commonly understood that in order to introduce the full reinforcing effect of fibers in the matrix; it is important that the fiber lengths exceed the critical fiber length described by Equation 1. The critical fiber length is denoted as L_c, fiber tensile strength as σ_F, shear stress at the interface as τ_I and fiber diameter as d_F.

$$L_c = \frac{\sigma_F d_F}{2\tau_I} \tag{1}$$

The critical fiber length significantly reduced when adhesion between the fiber and matrix is optimal. In injection molding of composites, the fibers are subjected to extensive stresses that inevitably cause fiber breakage and nonuniform fiber distribution (fiber attrition) which can affect the reinforcing capabilities of the fiber itself. The critical length of jute fiber without compatibilizer was found to be 530 μm, while the median fiber length without coupling agent was found to be 350 μm [42]. This result further explained that the poor mechanical results of short jute fiber reinforced polypropylene composites without the addition of compatibilizer is due to fiber attrition and weak interfacial adhesion between the fiber and matrix.

2.4.2 Nanocellulose (Cellulose Nanocrystals & Cellulose Nanofibrils)

Cellulose is a member of a class of polymers known as polysaccharides which are sugar molecules linked via glyosidic linkages This group of natural polymers exhibit great performance properties for reinforcing commercial polymers such as PP and PE, while having a degree of biodegradability and lightweighting capabilities

Cellulose can be further broken down into a subcategory known as nanocellulose where at least one dimension is in the nanoscale. This new material has been regarded as the next generation renewable reinforcement for the production of high-performance bio-composites [43]. Nanocellulose can be obtained via two methods 1) top-down by mechanical methods/disintegration of plant materials 2) bottom up by fermentation of low molecular weight sugars using bacteria from *Acetobacter* genus. Therefore, cellulose can be extracted from wood, plants, bacteria and algae. Figure 2.4-4 shows the hierarchical structure of cellulose starting from the cell wall in plant biology.

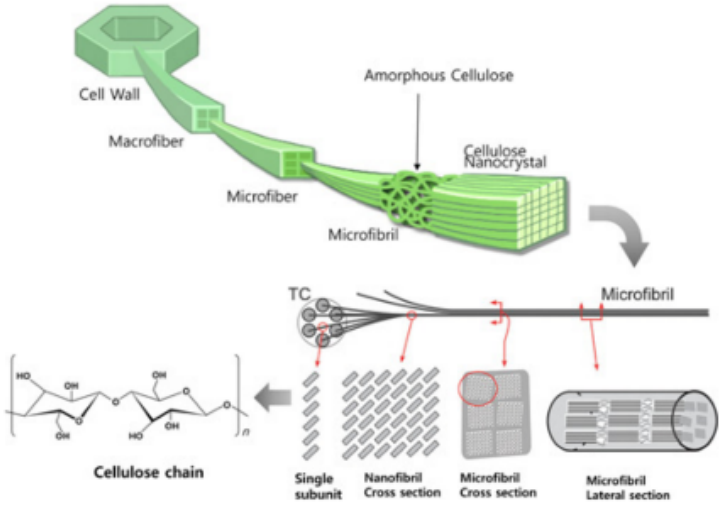

Figure 2.4-4: Hierarchical structure of cellulose [44]

Cellulose is a semi-crystalline polymer meaning that cellulose has amorphous (disordered) and crystalline (ordered) regions. It can be seen (Figure 2.4-4) that the cell wall can be broken down into microfibers where, the crystalline regions are hard to break because of strong hydrogen bonding between hydroxyl groups in cellulose. There are several polymorphs of crystalline cellulose (I, II, III, IV). Cellulose I is naturally produced by a variety of organisms (trees, plants, tunicates, algae, and bacteria), it is sometimes referred to as ‘‘natural’’ cellulose. The structure is thermodynamically metastable and therefore can be converted to either cellulose II or III. Native cellulose has two different crystal structures known as I_β and I_α. Cellulose I_β is composed of a monoclinic unit cell containing two parallel chains and cellulose I_α composed of a triclinic unit cell [45]. The portions of I_β and I_α vary in cellulose of different origins, for example bacteria cellulose is rich in I_α whereas plant-based cellulose is rich I_β. The unique properties of cellulose are linked to the hydrogen bonding formed within and with other chain. Figure 2.4-5 shows the proposed hydrogen bonding network that is widely accepted; the intrachain hydrogen bonding specifically at oxygen close to the carbon 5 atom and the hydrogen attached to the oxygen at the carbon 3 atom contributes to the high axial chain stiffness of cellulose [45].

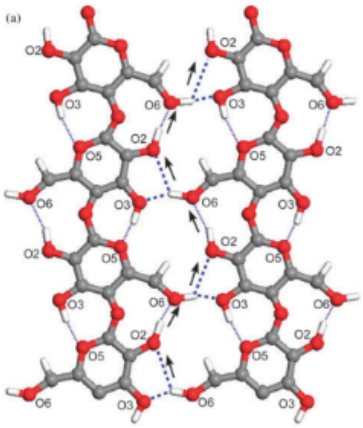

Figure 2.4-5: Schematic of hydrogen bonding network. Thin dotted lines represent intrachain bonding and thick dotted lines represent the interchain bonding. Arrows represent the donor-acceptor-donor direction [45]

It was reported by K.Y Lee [46] that bacterial cellulose reinforced epoxy nanocomposites with lower nanocellulose loading had resulting higher tensile strength values compared to nanofibrilated cellulose (NFC) reinforced expoxy composites. This was attributed to the higher critical surface energy of BC (57 mN m^{-1}) compared to NFC (42 mN m^{-1}) , where higher surface energy provides for improved adhesion to the polymer matrix according to Young's Equation (Equation 2). Solid-vapor surface energy is defined as γ_{SV}, solid-liquid surface energy as γ_{SL}, liquid-vapor surface tension as γ_{LV} and contact angle with respect to the liquid θ [47].

$$\gamma_{SV} = \gamma_{SL} + \gamma_{LV} Cos\theta \quad (2)$$

The hierarchical structure of cellulose breaks down cellulose from the cell wall which is made from macrofibers of cellulose, hemicellulose and lignin (Figure 2.4-4). The macrofibers can be broken down into microfibrils which can be further broken down by chemical and mechanical treatments into nanocellulose known as cellulose nanocrystals (CNC) and cellulose nanofibrils (CNF). Nanocellulose offers high modulus, strength, dimensional stability, low thermal expansion coefficient and biodegradability. Figure 2.4-6 shows the specific modulus and strength of nanocellulose and various materials. It is clear that the inherent properties of cellulose show high specific strength and modulus that is comparable to ceramics and metals and therefore showcase potential to be employed as reinforcement in thermoplastic composites.

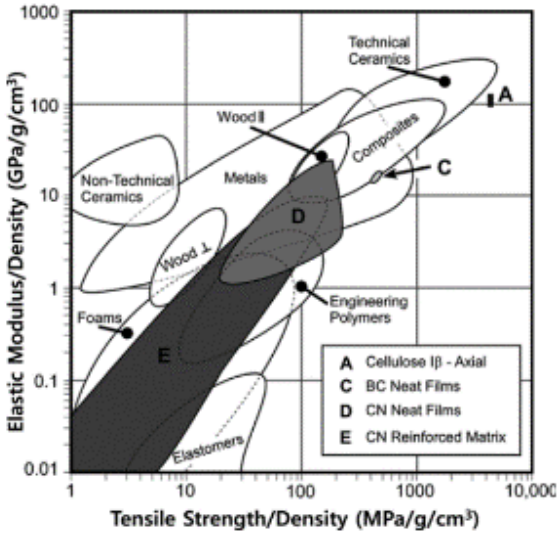

Figure 2.4-6: Specific strength and modulus of various materials including cellulose [44]

Cellulose nanocrystals (CNC) are needle-like cellulose crystals of 10-20 nm in width and several hundred nanometers in length. CNC is produced by strong acid hydrolysis where; the acid treatment removes the amorphous regions and leaves behind crystals and thus CNC is known to have high crystallinity. Cellulose nanofibrils (CNF) are long flexible fiber network that exhibits a complex, highly entangled structure with diameters ranging from 6 to 100nm in diameter. CNF is predominately produced by chemically treating the cellulose microfibrils by TEMPO-mediated oxidation (2,2,6,6-tetramethylpiperidine-1-oxyl radical) followed by mechanical disintegration of individual fibrils using a blender in water. Cellulose is not soluble in water, but TEMPO-mediated oxidation of cellulose allows for regioselective conversion of the hydroxyl groups to carboxylate groups yielding water-soluble cellulose. It was reported by T. Saito [48] that TEMPO-mediated oxidized cellulose had carboxylate groups on the cellulose fibril surfaces and no oxidation occurred in the cellulose crystallites maintaining inherent cellulose crystallite structures [48]. Figure 2.4-7 shows TEM images of CNC and CNFs, where the structural differences are highlighted and furthermore the complex structure (web-like) of CNF increases the resistance of

flow and results in gel-like behaviour of the material in comparison to CNC which has a lower aspect ratio and lacks entanglements [49].

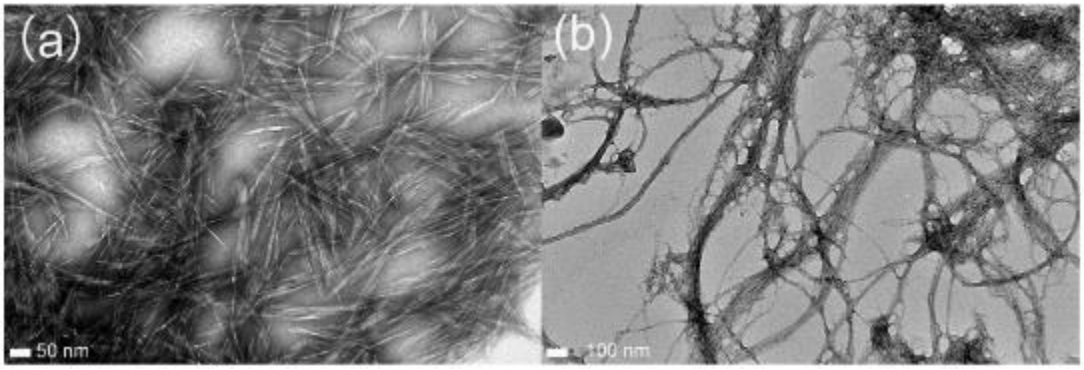

Figure 2.4-7: TEM images of a) CNC and b) CNF [49]

Table 2.4-2 explores the mechanical properties of common fibers used to reinforce composites and it can be observed that cellulose nanocrystals (CNC) is comparable and at times exceeds performance of commonly utilized fibers such as glass fiber. Therefore, it is evidential that nanocellulose has the potential to deliver enhanced mechanical properties, process-friendliness, biodegradability and reduction in carbon footprint when utilized in engineering composites needed for commercial industries [44]. There are limitations of cellulose due to the high moisture absorption rate, incompatibility with hydrophobic polymer matrices and lower thermal stability compared to inorganic fillers (e.g. glass fibers), but these problems can be addressed by surface modifications of the fiber surfaces.

Table 2.4-2: Mechanical properties of CNC compared to inorganic fillers [44]

Material	Tensile Strength (GPa)	Modulus (GPa)	Density (g/cm^3)	Specific Tensile Strength ($GPa.cm^3/ g$)	Specific Modulus ($GPa.cm^3/ g$)
CNC	7.5	145	1.6	4.7	90.6
Glass Fiber	4.8	86	2.5	1.9	34.4
Steel Wire	4.1	207	7.8	0.5	26.5
Kevlar	3.8	130	1.4	2.7	92.9
Graphite	21	410	2.2	9.5	186

2.4.3 Poly-α-1,3-Glucan

Poly-α-1,3-glucan is a water insoluble polysaccharide produced by microorganisms such as *Penicillium* spp., *Eupenicillium* spp., and *Aspergillus* spp. In addition, this polysaccharide is synthesized extracellularly by *Streptococcus* spp and *Leuconostoc* spp. present in the oral cavity, enhancing the formation of dental plaque [50].

The enzymatic polymerization mechanism of poly α-1,3-glucan is shown in Figure 2.4-8. Enzymatic polymerization allows for a novel, controlled path towards the engineering of nano to micron-scale structures within aggregated polysaccharide materials.

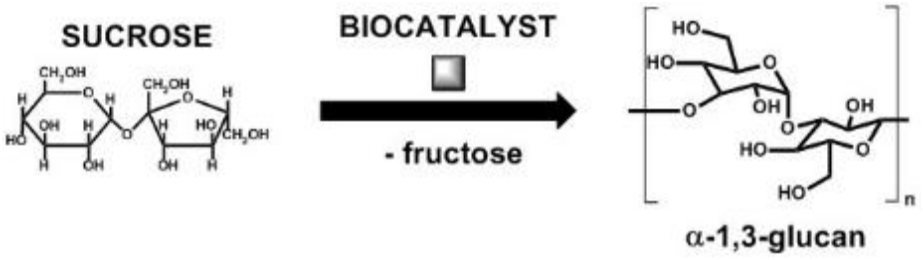

Figure 2.4-8Enzymatic polymerization of poly α-1,3-glucan [50]

S. Puanglek *et al* [50] synthesized this polymer in a one-pot *in vitro* process from a sucrose feedstock using the enzyme glucosyltransferase J (GtfJ) from *Streptococcus salivarius*. Figure 2.4-9 , shows the synthesis process for this polymer; at first GtfJ enzyme was produced by culturing E.coli expressing GtfJ cloned from *Streptococcus salivarius* ATCC 25975. The enzyme selectively breaks down sucrose which is composed of fructose and glucose and subsequently transfers glucosyl residues to a growing glucan chain. The turbidity is measured (qualitative) suggesting formation of the poly α-1,3-glucan.

Furthermore, the research suggested that the optimum pH of enzyme activity of GtfJ is between 5.3-5.8 with a reaction temperature of 30 °C, where the enzyme activity of GtfJ is defined as the amount of released fructose per minute (μ mole/min, U) per one mL of GtfJ at the initial state of reaction. Furthermore, a study of temperature effects on molecular weight was conducted which showed that at higher temperatures the molecular weight decreases while the polydispersity index (PDI [50]) increases during an experiment conducted with 2 weeks of reaction time. It is well known that temperature positively influences kinetics of a reaction and the governing mechanisms for polymerization are rate of propagation and rate of termination. It can be hypothesized that the rate of termination is increased at higher temperatures which will negatively affect the average molecular weight and thereby change the poly-dispersity index (PDI).

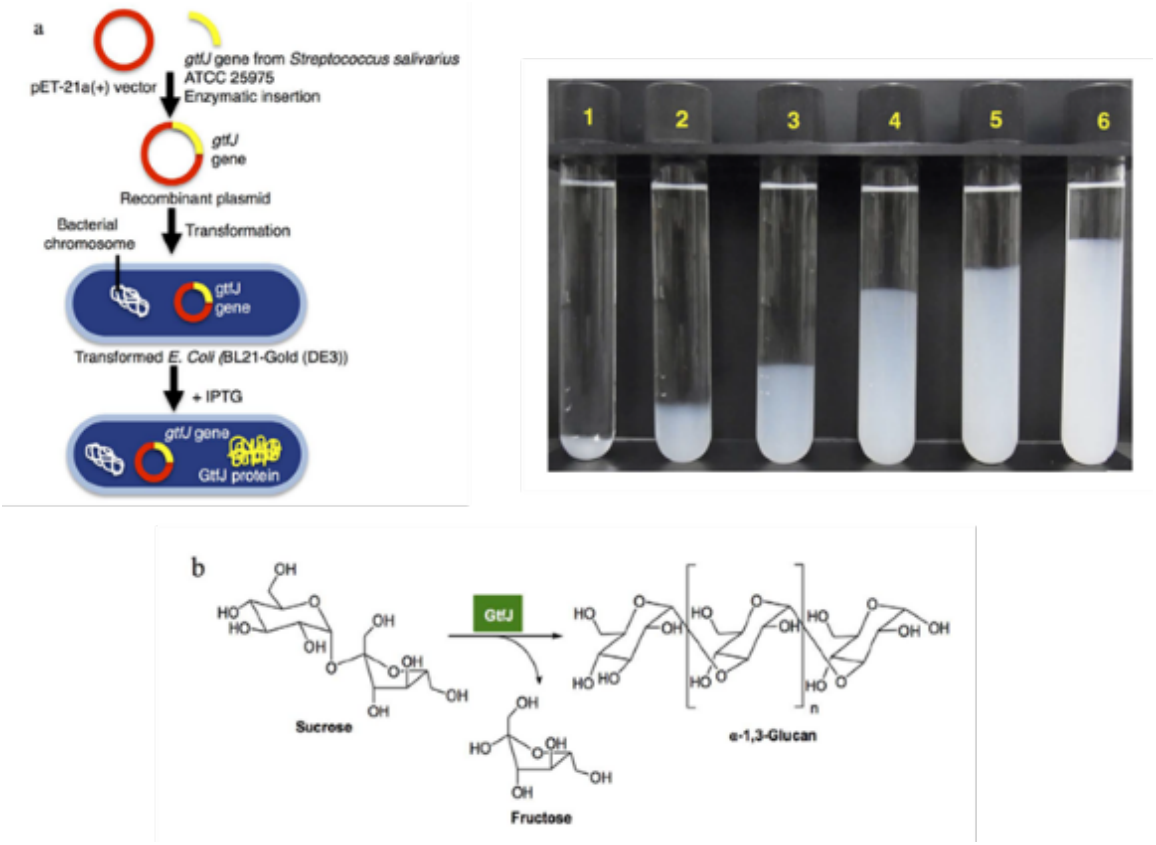

Figure 2.4-9: Synthesis of poly α-1,3-glucan [50]

Crystallinity of linear poly-α-1,3-glucan was studied by K. Kobayashi *et al* [51]. It was reported that the synthetic poly-α-1,3-glucan forms a fibril-like crystal structure and small lamellae structures (Figure 2.4-10). It was noted that for the fibril-like crystal structure the glucan chains folded perpendicular to the fibril axis. This was an interesting observation as folding is not typically seen in common polysaccharides e.g. cellulose where glucan chain form parallel to the fibril axis. The significance of such crystalline structures is still under investigation.

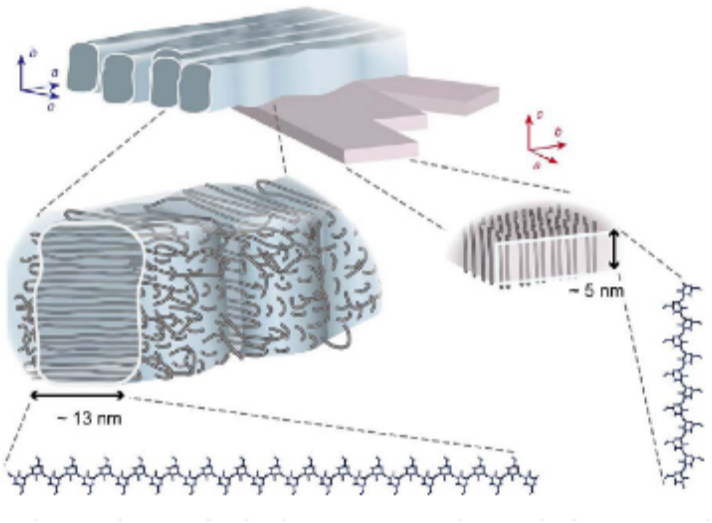

Figure 2.4-10: Schematic drawing of molecular orientations in the crystals of poly α-1,3-glucan [51]

DuPont Industrial Biosciences is developing a new product called Nuvolve™ which is a poly-α-1,3-glucan. The specific family of biocatalysts is selected from the general class of glucosyltransferase (GTF) enzymes and the polymer can be produced by reacting an aqueous solution of sucrose with this GTF enzyme. Poly-alpha-1,3-glucan has a typical degree of polymerization of 800 glucose repeat units with a polydispersity index (PDI) in the range of 1.7-2.0, as controlled by the polymerization process conditions. The polymer has a degree bulk density of 1.5 g/cm^3 and crystallinity index of 50%. The process is described in Figure 2.4-11. This product can be applied in paper coatings, composites and packaging [52].

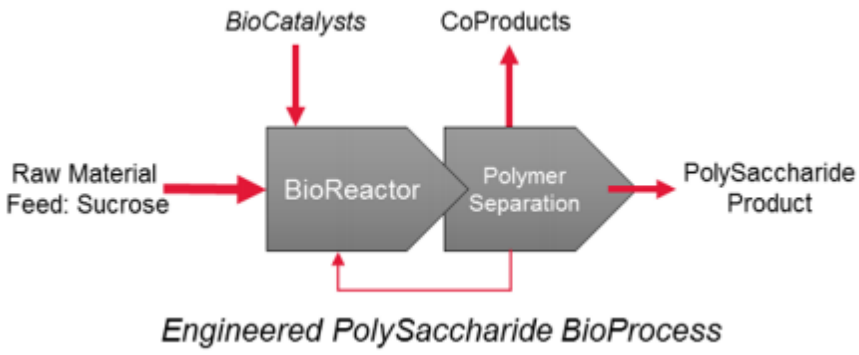

Figure 2.4-11: Process diagram of DuPont's Nuvolve™ Production [52]

Therefore, natural sourced filler materials provide a low-cost, abundant solution to reinforcing thermoplastic composites where good mechanical properties, renewability, recyclability, low energy consumption, low abrasion to processing equipment and biodegradability can be achieved. The clear limitations are that naturally sourced materials have a high moisture absorption rate, compatibility issues with hydrophobic polymer matrices and lower thermal stability compared to inorganic filler materials. Surface modifications on fiber surfaces and the incorporation of compatibilizers when compounding can fix the issues mentioned previously when incorporating naturally sourced fillers in hydrophobic polymer matrices.

2.5 Natural Filler Reinforced Thermoplastic Composites

The advantages of using naturally sourced filler material as opposed to inorganic fibers, are biodegradability, higher specific mechanical properties (low density), ease of processability and compatibility in various types of thermoplastic matrices with or without the use of coupling agents. Thermoplastics are popular due to their user-friendly processing as they can be melted, shaped and cooled into a variety of complex shapes/parts in a matter of seconds. For load-bearing applications, thermoplastics are not sufficient because of the lack of strength, stiffness and dimensional stability. Fillers/fibers on their own possess high strength and modulus values (Figure 2.4-6) and thus can be incorporated in a thermoplastic matrix to effectively transfer load between the continuous polymer and fiber/filler interface via shear stresses. Naturally reinforced thermoplastic composites fall under the broad term of "biocomposites" [5]. Many researchers have formulated and investigated performance properties of biocomposites that could be potentially used in consumer electronics, automotive, industrial & consumer packaging applications.

N.M. Robertson [53] formulated composites that incorporated hemp, flax, wood pulp, wood chips, wheat straw and triticale into low density polyethylene (LDPE). LDPE is hydrophobic and maleic anhydride (MA) was added to increase the interfacial adhesion between the matrix and natural fiber (hydrophilic). This study showed that for all fiber types the tensile strength and modulus increased while elongation at failure decreased with increasing fiber loading (wt. %). Tensile modulus increased by a factor of eight with the addition of 40% natural fiber compared to the modulus of pure LDPE. Furthermore, the addition of MA showed improvement in tensile strength and elongation over composites without the addition of MA.

M.D.R Batista [54] studied hybrid composites that comprised of cellulose fibers and long glass fibers in a PP matrix. Their findings showed the increasing contents cellulose decreased tensile strength and modulus of the hybrid composites while glass fiber had a more prominent role in the stiffening effect. However, composites that contained 30 wt.% of cellulose without long glass fiber showed an increase of 18% and 129% in tensile strength and modulus compared to neat PP. Moreover, their work showed that cellulose has a nucleating effect on the composites resulting in higher crystallization temperatures in comparison to neat PP. The higher crystallization temperatures enable part production to be faster and therefore adds a cost-down in the process flow. Overall, the authors of this paper conveyed the idea of putting in place a hybrid system that adds the benefit of the stiffening effect of the glass fibers in combination with the specific mechanical properties of the cellulose fibers to produce an optimal composite that addresses partial biodegradability (end of life) and performance. Much like the emergence of hybrid vehicles that combines a typical internal combustion engine system with an electric propulsion system; the hybrid composites offer an intermediate process step before natural fibers can be produced at a cost-effective or cost-neutral manner for 100% deployment in thermoplastic composites thereby replacing the need for inorganic fillers.

Polyamide-6 (PA-6) was reinforced with cellulose fibers (bleached and semi-bleached) in the research presented by F.C Fernandes [55]. Bleached cellulose fibers were extracted via the Kraft process to remove lignin and other impurities. Lignin has phenolic groups that contribute to the stabilization of polymers via deactivation of free radicals; when cellulose degrades via thermo-oxidative or photo-oxidative pathways free radicals are generated and hence destabilizing composites. Therefore, bleached cellulose contains less lignin than semi-bleached cellulose yielding less stable composites. According to this study, 30 wt. % loading of bleached cellulose

led to the best mechanical properties with good fiber-matrix interaction. Bleached cellulose at 40 wt.% loading showed decreased mechanical properties due to the poor transfer of mechanical stress in the presence of an excess amount of fibers. Furthermore, the specific tensile modulus of 30 wt. % of cellulose reinforced PA6 composite was greater than the 20 wt. % glass reinforced PA6 composite indicating the clear advantage of using natural fibers. Overall, this study showed that 30 wt. % bleached/semi-bleached cellulose yields enhanced mechanical properties compared to unreinforced PA-6. The semi-bleached cellulose showed slightly improved mechanical properties which can be attributed to the higher content of lignin.

M. Idicula [56] studied mechanical performance of short banana/sisal hybrid reinforced polyester composites. The study concluded that banana/PET, sisal/PET and banana/sisal/PET composites showed improved tensile strength and modulus with the increase n fiber content. However, impact performance worsened with the hybridization of banana/sisal reinforced PET composites. The study also showed that at higher fiber loadings, fiber agglomeration hinders effective stress transfer between fiber and the matrix. In this particular study, the cut-off fiber loading was 40 vol. % for maximum stress transfer. Therefore, natural fibers have the potential to be great reinforcing fillers for thermoplastic composites. There are few factors that affect the performance of fiber reinforced composites which are: fiber-matrix interaction (dispersion), aspect ratio and orientation of the fibers. To truly appreciate the reinforcing capabilities of fibers/fillers the factors mentioned above have to be optimized in a continuous polymer matrix.

2.5.1 Fiber/Filler-Matrix Interactions & Surface Treatments

Optimizing the fiber/filler-matrix interface is crucial to achieve optimal performance properties of composites. Composites combine properties of individual materials that are not found readily available in nature and hence performance properties depend on the individual components and their interfacial compatibility. The majority of naturally sourced fillers are inherently hydrophilic which is problematic when combined with hydrophobic matrices such as polypropylene and polyethylene. This heterogeneous system with a hydrophilic filler and hydrophobic matrix leads to inferior properties due to the lack of adhesion between both materials that impairs stress transfer. To aid the compatibility between incompatible materials, surface treatments on the fibers can be employed such as bleaching, grafting of monomers and acetylation. For example, maleic anhydride (MA) grafted on the polymer matrix (e.g. PP) can form covalent bonds with the hydroxyl groups of natural fibers/fillers as seen in Figure 2.5-1.

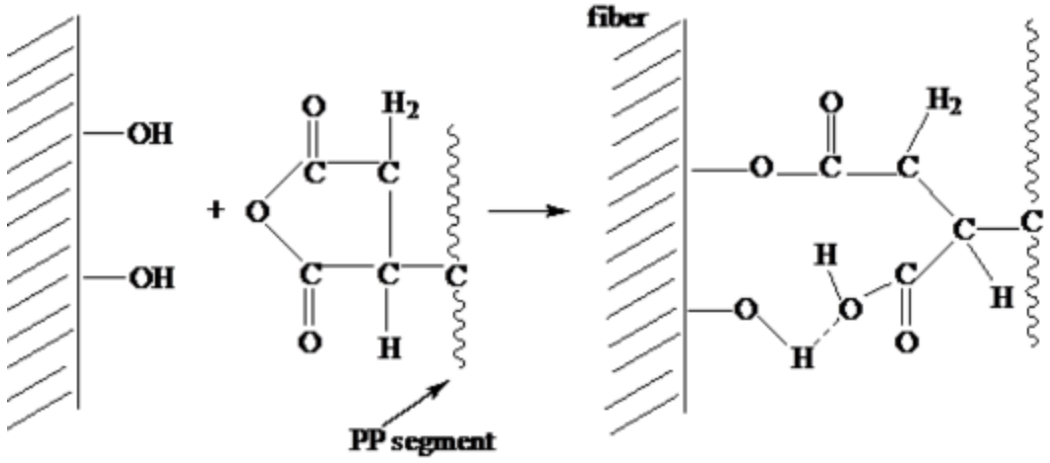

Figure 2.5-1: Covalent bond formation of Maleic Anhydride (MA) grafter PP and Natural Fiber Surface [57]

R. Gauthier [58] proposed a mechanism of maleic anhydride grafted PP synthesis which can be subdivided by preparation temperature. At low temperatures the MA can be grafted without modifying the length of the initial PP chains (PPgMA a). Whereas at higher temperatures, scission occurs and MA prepolymer is added at the scission end (PPgMA b) which leads to lower molecular weight PPgMA. Maleic anhydride is grafted in the presence of peroxide where free radicals are present (Figure 2.5-2).

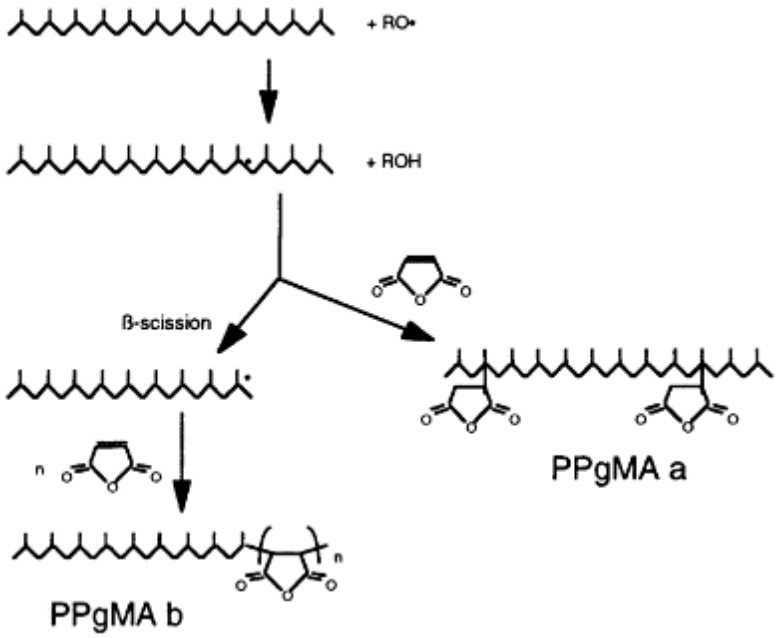

Figure 2.5-2: Mechanism of PPgMA synthesis [58]

A.V Gonzalez [59] studied the influence of surface treatments on henequen (agave fourcroydes) fibers adhesion in HDPE. In particular alkaline, silane treatment as well as surface impregnation of PE dilute solution. The composites were then characterized by the fiber pull-out test and single-fiber fragmentation test (SFFT). The alkaline treatment removes hemicellulose, waxes and lignin present on the surface of the fibers, leading to imperfections on the surface and increasing the roughness and thereby the opportunity for mechanical interlocking is increased

promoting improved fiber-matrix adhesion. Silanization enables the alkoxy groups to interact with the hydroxyl groups on the fiber surface whilst the vinyl group interact with the hydrophobic polymer matrix and improving interfacial load transfer efficiency. The fiber pre-impregnation of PE allows for better wetting, where normally this would not be achievable due to the high polymer viscosity. The single fiber fragmentation test showed that the silanization of the fibers yielded high interfacial shear strength indicating enhanced fiber-matrix interaction. Figures Figure 2.5-3 and Figure 2.5-4 show the different surface treatments employed in the study as well as the interfacial shear strength data measured using the single fiber fragmentation test. In conclusion, fiber surface treatments and the introduction of coupling agents can improve interfacial adhesion between hydrophilic fibers and hydrophobic polymer matrices which is crucial for optimal load transfer resulting in peak mechanical properties.

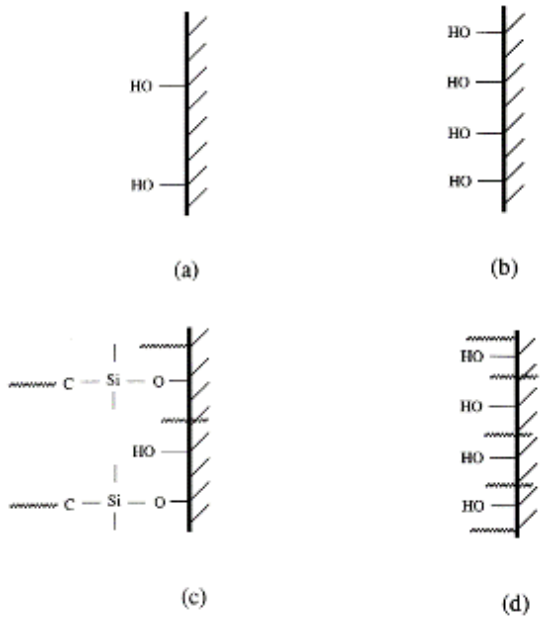

Figure 2.5-3: Schematic representation of the interphases formed on the henequen fibers for: (a) no surface treatment (FIB: control); (b) Alkaline Treatment (FIBNA); (c) Silane Treatment (FIBNASIL) and (d) Preimpregnation Treatment (FIBNAPRE) [59]

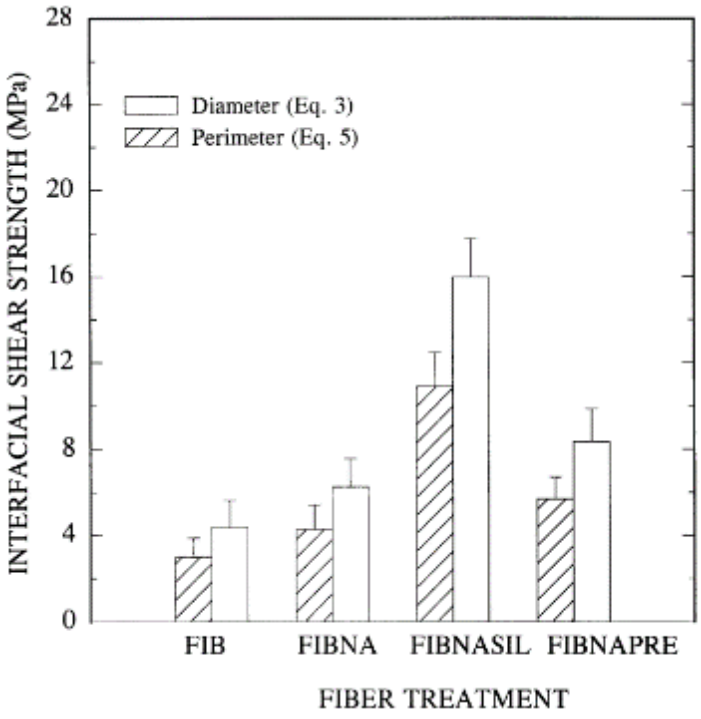

Figure 2.5-4: Effect of the surface treatment on the interfacial shear strength using the single fiber fragmentation test: native (FIB), alkali treated (FIBNA), silane treated (FIBNASIL) and preimpregnated henequen (FIBNAPRE) fibers [59]

2.5.2 Natural Fiber/Filler Reinforced Composites in the Automotive Industry

As mentioned in the previous section, the automotive industry traditionally uses glass fiber and inorganic minerals to reinforce plastics such as polypropylene. Glass fibers are inexpensive and have a great influence in the stiffening effect to achieve superior mechanical properties. However, the environmental impact of producing glass fibers are reminiscent of the CO_2 emissions released through the production of petroleum- based plastics (Table 2.3-6) [23]. Glass fibers density is also twice as much as naturally sourced filler materials based on polysaccharide chemistry e.g. cellulose and poly-α-1,3-glucan. With the growing pressures from society; industrial and governmental leaders have opted to implement renewable materials in the foreseeable future to combat increasing post-consumer waste products occupying landfills and limiting ocean plastic pollution [60].

In recent years the automotive industry has been focusing on global sustainability efforts, where the automaker's definition of sustainability is corporate responsibility that extends to its workers, customers and beyond [5]. In the early 1940s, Henry Ford a pioneer in the automotive industry used soybean oil to make a boot lid and claimed that the material had 10 times the shock resistance of steel; which he demonstrated by applying an exe to the lid. However, during World War II the development of natural-fiber reinforced composites were put on hold as other areas were addressed. Daimler-Benz explored the idea of replacing glass fibers in 1991, where jute fibers were used on door panels in the E-Class in 1996 [5]. Therefore, many attempts have been made by automakers to commercialize green materials and sustainable technology, but with the economic environment as well as the ease of processing glass fibers, these technologies never took off. In today's environment, incorporating renewable, biodegradable material in commodity plastics is not a choice but a necessity to achieve a circular economy.

Table 2.5-1 shows the different applications where natural fibers are utilized differentiated by automotive manufacturer [5]. Table 2.5-2 shows the typical applications of natural-fiber reinforced PP composites in the North American market [5]. These Tables show that there is real potential of cost savings via weight reduction, process-friendly material adaptation and end of life disposal pathways for natural fiber/filler reinforced thermoplastic composites. There are few issues to address with natural fibers/fillers being used as reinforcement for thermoplastic matrices such as incompatibility with hydrophobic matrices, water absorption, requirement for the fibers to be treated or addition of coupling agents (increasing production cost) and lack of sufficient adhesion (which is related to incompatibility issues with hydrophobic matrices) at the fiber-matrix interface [5].

The issues described above can be solved with time and progression in technology to produce natural fibers/fillers at lower costs. The fluctuating oil price and major governmental bodies pledge to pursue renewable materials (even at higher prices) makes the future look bright for this particular technology.

Table 2.5-1: Natural fiber reinforced composites in automotive application sorted by automaker [5]

Automotive Manufacturer	Application
Audi	Seat backs, side and back door panel, boot lining, spare tire lining
BMW	Door panels, headliner panel, boot lining, seat backs
Daimler	Door panels, windshield/dashboard
Ford	Door panels, boot liner
Rover	Rear storage shelf/panel, door panels
Volkswagen	Door panels, seat back, boot lid finish panel, boot liner

Table 2.5-2: Natural fiber reinforced composites in the North American automotive market (interiors) [5]

Application	Fiber Type
Door panel	Kenaf/hemp
Inserts	Wood fiber
Rear parcel shelves	Kenaf, flax, wood
Seat backs	Flax
Spare tyre covers	Flax, wood
Other interior trim	Kenaf, flax

Chapter: 3 Determining Mechanical, Thermal, Rheological and Morphological Properties of DuPont Nuvolve™ Reinforced Hybrid Composites

3.1 Introduction

In Chapter 2, the potential of naturally sourced filler materials replacing inorganic filler materials were discussed specifically in the automotive industry. In today's automotive industry automakers have pledged ongoing efforts to improve mechanical properties, enable lightweighting opportunities and incorporate biodegradable components in their composite technologies. In this Chapter, DuPont's Nuvolve™ (poly-α-1, 3-glucan) an engineered polysaccharide was combined with glass fiber in a polypropylene matrix to produce hybridized composites at various polysaccharide and glass fiber loadings for body interior and under-the-hood automotive applications. The samples were prepared via twin-screw extrusion followed by injection molding into ASTM test specimens. Mechanical, thermal and morphological analyses were conducted in accordance to ASTM standards to asses overall mechanical properties, individual filler contribution to reinforcing PP, thermal stability, filler-matrix compatibility and melting & crystallization characterization for process development of the composites for large scale operations.

Nuvolve™ is a synthetic polysaccharide produced via bio-catalytic reaction from a sucrose feedstock. The enzymes used to selectively isolate glucose from fructose and subsequently polymerize glucose monomers at the 1,3 carbon forming glyosidic linkages are derived *Streptococcus, Leuconostoc* and *Lactobacillus* species. The polymer has a degree of

polymerization of about 800, PDI of 2, bulk density of 1.5g/cm^3 and crystallinity index of 50% [52]. Nuvolve™ is a spherical particle as opposed to the rod-like shape of glass fiber.

3.2 Experimental

Polypropylene (PP) injection mold grade homopolymer pellets (MFI 12.1 dg./min) and chopped glass fiber filled PP pellets were provided by local suppliers and poly α-1,3-glucan of two particles sizes (5 and 20 microns) were supplied by DuPont Industrial BioSciences under the tradename Nuvolve™. Polypropylene grafted maleic anhydride (PP-g-MA: locally sourced) was used as a coupling agent to help with the compatibility of hydrophobic PP and hydrophilic polysaccharide.

The composites were prepared using a two-step process extrusion followed by injection molding. Nuvolve™ masterbatch (30 wt.%) with PP was compounded using twin-screw extruder: ThermoHaake Rheomex Model PTW25 (Figure 3.2-1) Table 3.2-1 shows the extrusion temperature profiles used. Prior to extrusion all materials were dried to reduce moisture content (60°C for 12 h). The dry PP, PP-g-MA and Nuvolve™ were separately starve-fed into the twin-screw extruder via K-Tron gravimetric feeders and the screw speed was set at 120 RPM. After extrusion, the materials were immediately quenched in a water bath and kept at room temperature. The compounded materials from the twin-screw extruder were granulated using a lab-scale grinder/chopper and dried (60°C 12 h) before the injection molding step.

Table 3.2-1: Extrusion Profile

Zone	1	2	3	4	5	6	7	8	Die
Temperature (ºC)	175	175	177	180	180	185	185	190	190

Nuvolve™ masterbatch (30 wt.%) (now grounded pellets) was then combined with glass fiber filled PP pellets and neat PP using the injection molder (Boy Machines Model 80M) to achieve the desired formulations presented in Table 3.2-3. ASTM test specimens were molded for tensile (ASTM-D638), flexural (ASTM D790) and impact (ASTM D256) testing respectively (Figure 3.2-2). Table 3.2-2 shows the injection molding temperature profiles used, the mold temperature was set at 40ºC with an injection pressure of 1300 psi.Table 3.2-3 shows the formulations studied.

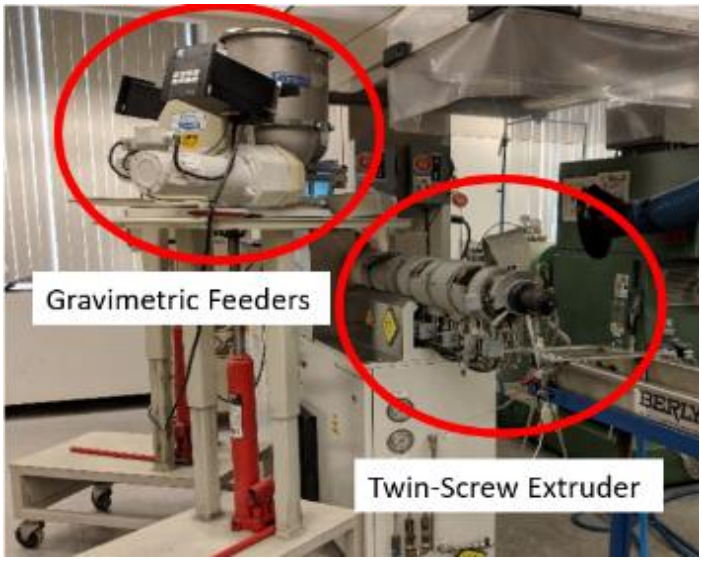

Figure 3.2-1: Equipment and experiment set-up

Table 3.2-2: Injection Molding Profile

Zone	1	2	3	4	Nozzle
Temperature (ºC)	174	179	190	185	188

Table 3.2-3: Composition of the composites i) A = Nuv-A ii) B = Nuv-B

Formulation	Nuvolve™ (wt.%)	Glass Fiber (wt.%)	Total Fiber (wt.%)
Neat PP	---	---	---
0/5	---	5	5
0/10	---	10	10
30A/0	30	---	30
10A/10	10	10	20
10A/15	10	15	25
10A/20	10	20	30
15A/15	15	15	30
20A/10	20	10	30
30B/0	30	---	30
10B/10	10	10	20
10B/15	10	15	25
10B/20	10	20	30
15B/15	15	15	30
20B/10	20	10	30

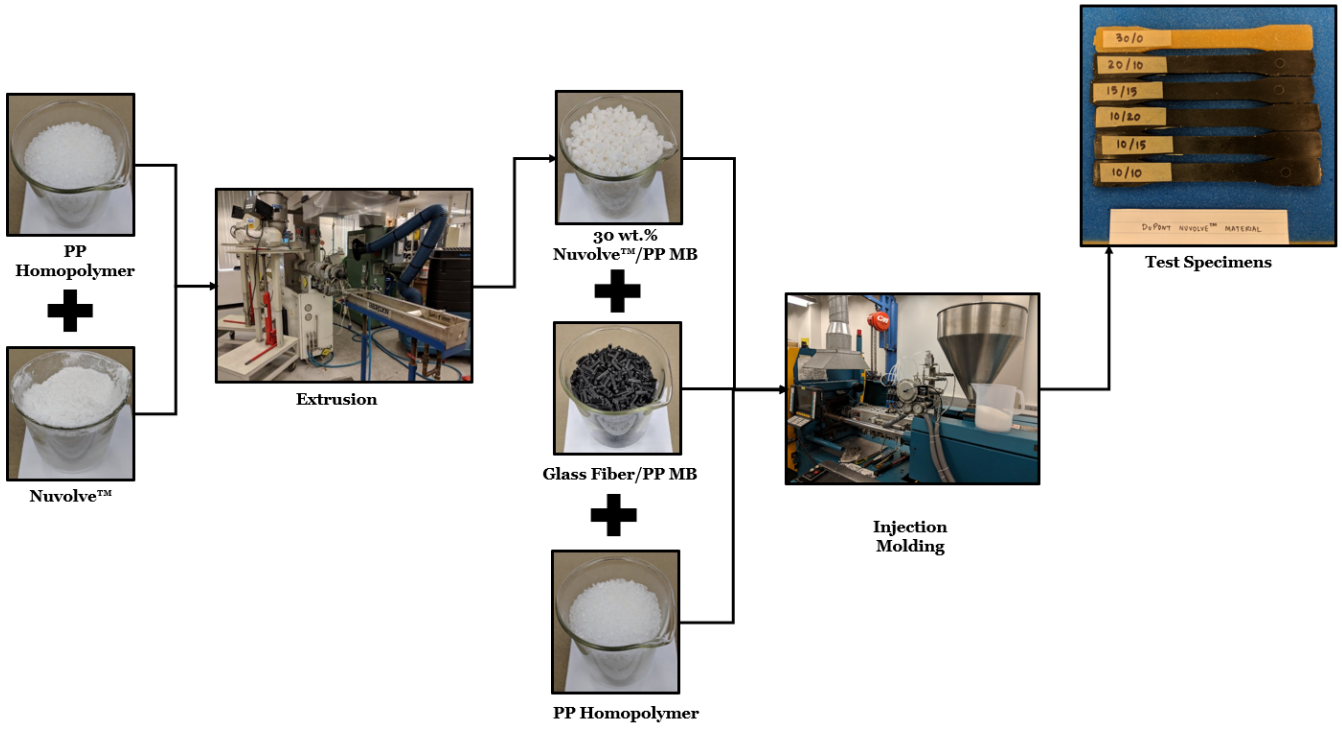

Figure 3.2-2:Fabrication process of the hybrid composites

Two particle sizes of DuPont's Nuvolve™ (Nuv A=5 µm, Nuv B=20 µm) were supplied and the control samples were 5 , 10 wt.% glass fiber reinforced PP and neat PP. Furthermore, the hybrid composites were compared to Ford Motor Company's material specification for body interior and under-the-hood applications. It is also important to emphasize the exclusion of a second extrusion step to incorporate the glass fiber in the Nuvolve™ masterbatch (30 wt.%) with PP. The elimination of a second extrusion process can speed up part production, lower manufacturing costs and reduce thermal degradation and fiber attrition.

3.2.1 Mechanical Test & Density Measurement

Tensile, flexural and Izod notched impact tests were conducted using a universal testing machine (Instron 3366) and a pendulum tester (Testing Machines Inc. 43-02-03 model) in compliance with ASTM D638, ASTM D790 and ASTM D256 respectively (Figure 3.2-2). The properties of interest were: tensile strength, tensile strain at break, tensile modulus, flexural modulus, flexural strength and impact strength. All mechanical tests were run in an environmentally conditioned room at 23 °C ± 2 °C and 50 ± 5 % relative humidity, the samples were also conditioned prior to testing. Density was measured using an analytical balance (readability down to 0.1 mg) and density kit ME-DNY-43 from Mettler Toledo (ASTM D792).

3.2.2 Thermal Characterization

Thermal transitions of the composites and the virgin polymer matrix were analyzed using a differential scanning calorimetry instrument (DSC: TA Instruments Q2000). The samples were prepared by cutting the injection molded ASTM test specimens into small chips (6-10mg) obtained from multiple locations of multiple test specimens to minimize possible effects of poor material distribution within the composites. At first the samples were heated from room temperature to 190°C at a rate of 50°C/min and held isothermally for 5 min to remove any thermal history incurred from the fabrication of the composites. Thereafter, the samples were cooled to 70°C at 10°C/min and isothermally held for 5 min before reheating to 190°C at 10°C/min. The melting and crystallization transitions were collected from the heat flow versus temperature curves where, melting temperature (T_m) is an endothermic transition and the crystallization temperature (T_c) is an exothermic transition denoted by the peak minimum and maximum respectively. Crystallinity, heat of fusion (ΔH_f) and heat of crystallization (ΔH_c) were also calculated.

Thermal gravimetric analysis (TGA: TA Instruments Q500) was used to study thermal stability of neat PP and the hybrid composites. For the thermal stability analysis of the hybrid composites, the samples were heated at 20°C/min and subjected to nitrogen from 35°C to 800°C at a flowrate of 40mL/min. For the activation energy determination of Nuvolve™, the TGA experiments were carried out at 5, 7.5, 10, 15 and 20 ºC/min in air and nitrogen. Samples were prepared similarly to the DSC sample preparation.

3.2.3 Melt Rheology

The linear viscoelastic properties were measured in accordance with ASTM D 4440 using a TA Instruments ARES-G2 controlled-strain rheometer equipped with a parallel plate geometry inside a forced convection oven. The geometry consists of two stainless steel 25 mm plates with smooth surfaces. Discs with a diameter of 25 mm and a thickness of 1.2 mm were prepared from coarsely chopped pieces of the dog bones by compression molding in a 25 mm diameter mold under vacuum at a temperature of 180 °C using a heated lab press.

After confirmation of the melt stability (time sweep) and determining the linear viscoelastic region (strain sweep), the linear viscoelastic properties were measured at 190 °C. A frequency sweep was performed between 100 and 0.015 rad/s using a strain that was within the LVR (varied with each sample). The test atmosphere was 25 L/min of heated nitrogen.

3.2.4 Morphology (SEM)

Zeiss 1550 (LEO) scanning electron microscope with accelerating voltage of 5 keV was used to observe the morphology of the composites and the neat PP as well as distribution of fillers within

the polymer matrix. The samples were obtained from post notched Izod impact testing, exposing the fracture surface and the samples were sputter-coated with gold to avoid surface charging

3.3 Results & Discussion

3.3.1 Mechanical Properties: Tensile and Flexural Properties

The effects of different fiber combinations on the tensile, flexural and impact properties of the hybrid composites are explored in this section. The hybrid composites are compared to control samples (neat PP, 5 and 10 wt.%. glass fiber in PP) and Ford Motor Company's material specification for body interior and under-the-hood applications.

The addition of glass fiber led to a considerable increase in tensile and flexural modulus attributed to the high modulus and aspect ratio of glass fiber [25] as seen in Figure 3.3-1 and Figure 3.3-2. The incorporation of Nuvolve™ (30/0) led to a lesser improvement in modulus compared to the addition of glass fibers which is due to the lower aspect ratio of Nuvolve™. The diameter of the glass fiber is approximately 12μm with lengths up to several hundred microns (Figure 3.3-3) thereby showing a higher aspect ratio than Nuvolve™ (Figure 3.3-4 and Figure 3.3-5). Riley et al [61] reported that the flexural modulus of four types of filers such as carbonate, clay, talc and mica increased with increasing aspect ratio of the filler particles in PP. Therefore, the addition of glass fiber has a greater effect on the modulus of the overall composite compared to Nuvolve™. The combination of Nuvolve™ and glass fiber yielded composites such as 10/20 that showed a 190 % increase in tensile and flexural modulus compared to neat PP.

Furthermore, the tensile strength increased with the addition of glass fiber as seen in Figure 3.3-6. This is expected as the tensile strength of glass fiber is about 84 times higher than that of PP

[62]. For the Nuvolve™ containing composite (30/0) a decrease in tensile strength (16 %) is observed compared to neat PP. This can be attributed to dispersion and agglomeration of the Nuvolve™ particles due to strong intermolecular forces keeping the molecules intact such as hydrogen bonding and van der Waals forces. This observation is supported by the work of M.A Khan and *et al* on hybrid composites containing jute and cellulose fibers in polypropylene/ethylene co-polymer matrix; where it was observed that an increasing amount of natural fiber above 20 wt.% had an adverse effect on the tensile strength of the composite [53]. The addition of glass fiber showed a greater improvement in strength and modulus compared to Nuvolve™. This was further supported by M.D.R Batista *et al* work reporting that the addition of glass fiber had a greater effect on the strength and stiffness of the cellulose/glass fiber reinforced PP composites [54]. The strongest performer of the hybrid composites was formulation 10/20 followed by 10/15 and 10/10 which utilizes 20-25 % of total filler content in comparison to Ford's incumbent material specification (35 % total filler content).

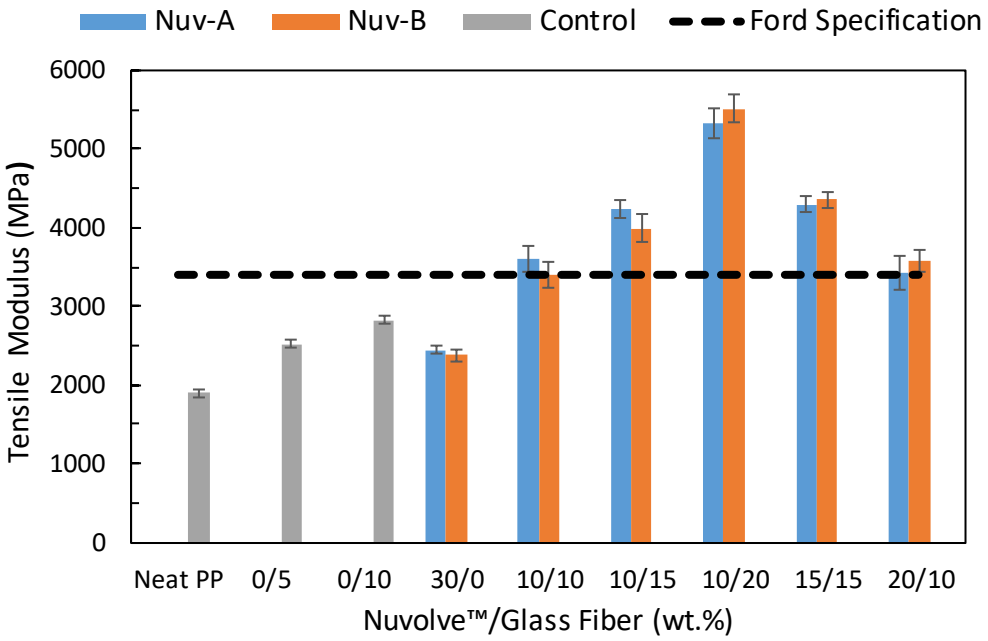

Figure 3.3-1: Tensile Modulus (MPa) of all composites and neat PP

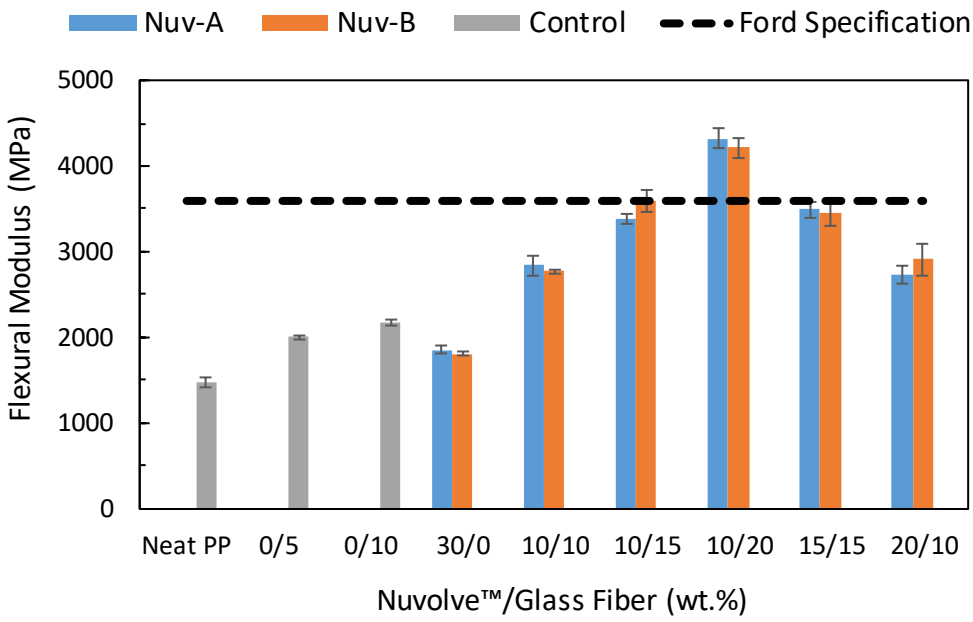

Figure 3.3-2: Flexural Modulus (MPa) of all composites and neat PP

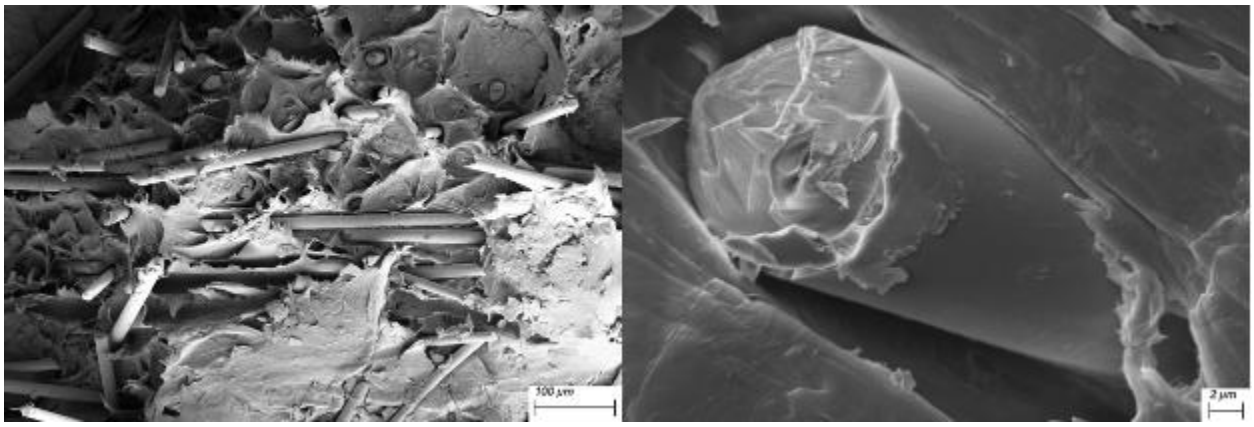

Figure 3.3-3: SEM micrograph of glass fibers embedded in the hybrid composites at 500x (left) and 2000x (right) magnification

Figure 3.3-4: SEM micrograph of Nuv-A (5 µm) at 500x magnification

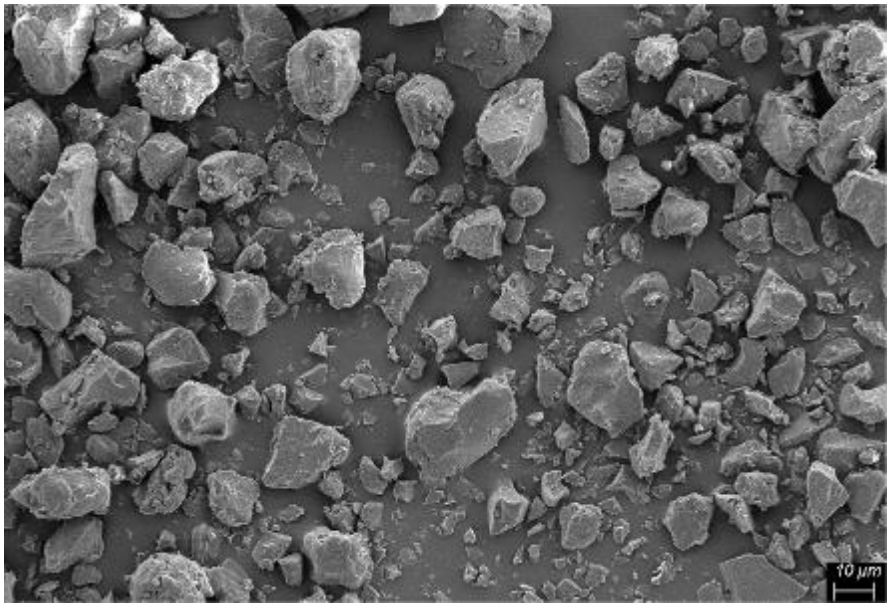

Figure 3.3-5: SEM micrograph of Nuv-B (20 µm) at 500x magnification

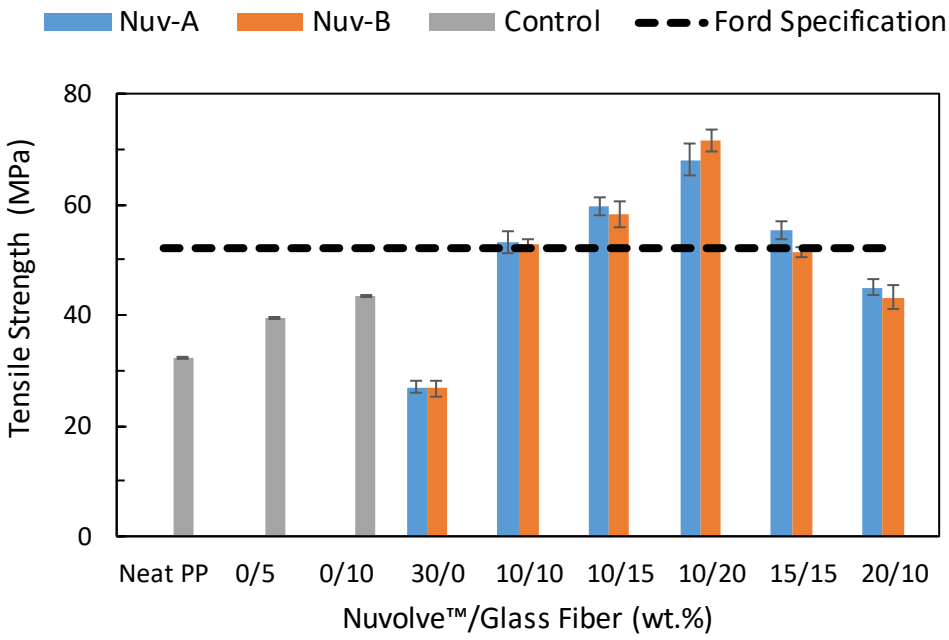

Figure 3.3-6: Tensile Strength (MPa) of all composites and neat PP

Tensile strain at break of the composites were lower than neat PP (Figure 3.3-7). Figure 3.3-8 shows the density reduction (%) compared to Ford Motor Company's material specification for body interior and under-the-hood applications; where formulations 10/15 and 10/20 show a density reduction of 13 and 10 % respectively.

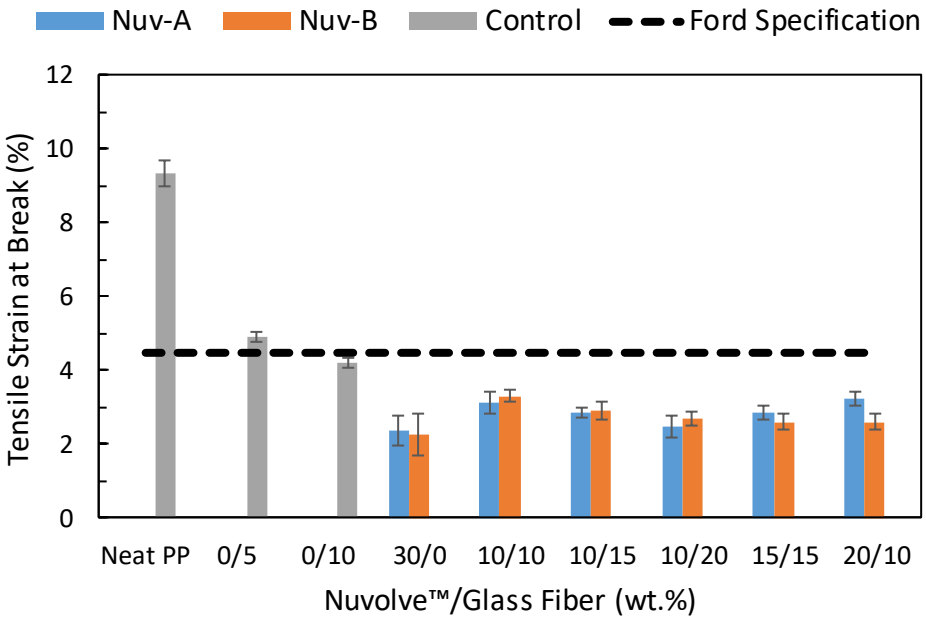

Figure 3.3-7: Tensile Strain at Break (%) of composites and neat PP

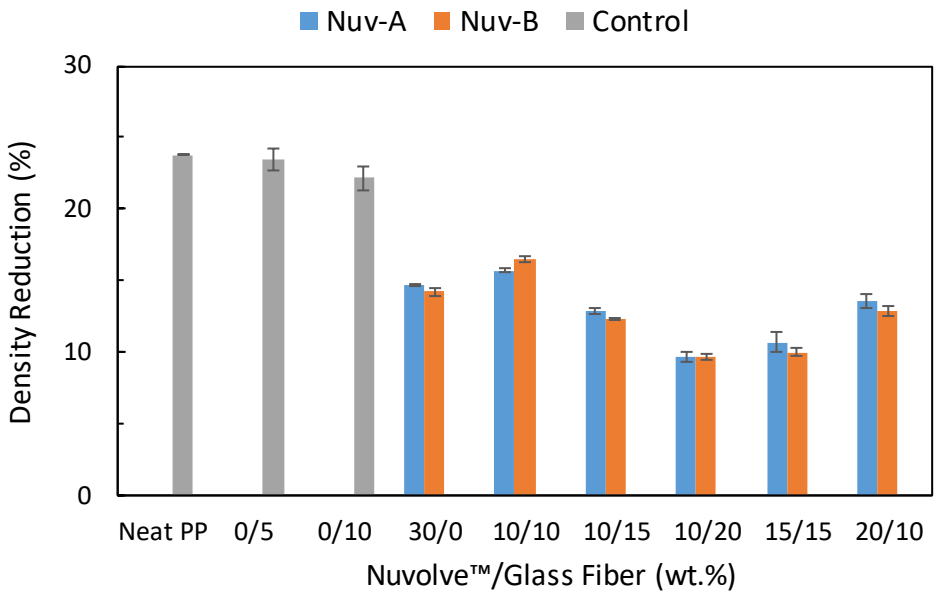

Figure 3.3-8: Density Reduction (%) of all composites and neat PP in reference to Ford's incumbent material specification

3.3.2 Mechanical Properties: Impact Properties

Impact strength or resistance of a material is the capacity to absorb and dissipate energies under impact loading. This impact strength of filler/fiber reinforced composites depend on filler geometry and filler-matrix interface as the filler's role is to interact with the crack formation in the matrix and act as stress transferring medium [63].

Figure 3.3-9 shows that impact strength decreased by 54 % for formulation 30/0 and this can be attributed to filler agglomeration promoting stress concentrations requiring less energy for crack propagation to occur [64] [65]. The glass fiber reinforced composites (0/5 and 0/10) showed an increase in impact strength and this is likely due to the extra energy dissipation mechanisms available with the addition of glass fiber such as fiber-pull out [66]. In a composite, the load is transferred through shear; and when the shear force exceeds the fiber matrix interaction force, the fiber matrix debonding takes place e.g. fiber pull-out [63].The hybrid composites showed a synergistic effect of Nuvolve™ and glass fiber yielding an increase in impact strength up to 123% (10/20) compared to neat PP and this is largely attributed to glass fiber content. This is also consistent with Panthapulakkal and Sain's [67] findings, where it was reported that hemp/glass fiber hybrid PP composites had enhanced impact strength with an increase of glass fiber content.

Generally, the addition of DuPont's Nuvolve™ and glass fiber in a PP matrix enhanced mechanical performance. The greatest contributing factor is the concentration of glass fiber in the composite, however the addition of Nuvolve™ also positively impacts the mechanical properties (to a lesser degree) while offering superior weight savings per material part. Formulation 10/15 was the optimal solution as it was able to meet Ford Motor Company's materials specification

except for tensile strain at break and achieving a density reduction of 13 % enabling lightweighting opportunities in non-structural components of an automobile.

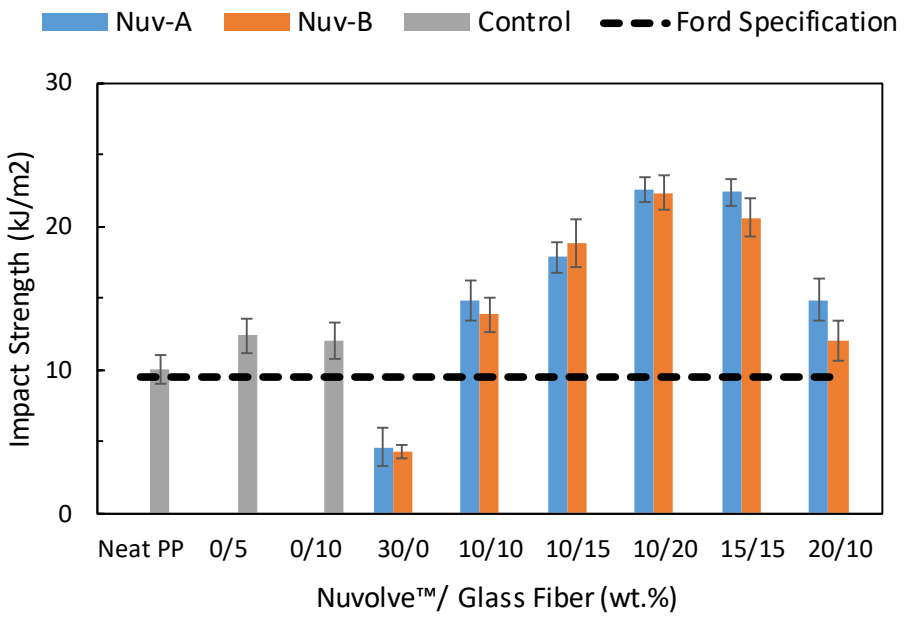

Figure 3.3-9: Impact strength (kJ/m2) of all composites and neat PP

3.3.3 Morphological Properties

The effect of Nuvolve™ and glass fiber on the overall composite morphology was studied using scanning electron microscope (SEM). The purpose of this morphological study is to understand the interfacial interaction between the fillers and the polymer matrix. Figure 3.3-10 shows an SEM image of neat PP, where a continuous phase is apparent. Figure 3.3-11 and Figure 3.3-12 show SEM images of 30A/0 and 30B/0 formulation only containing Nuvolve™. It can be seen that the texture of the composite changed in comparison to the neat PP; exhibiting a coarser morphology. Furthermore, agglomeration of Nuvolve™ is observed with an approximate size of 100 µm (Figure 3.3-11) Agglomeration of particles lead to localized stress concentrations resulting

in weaker mechanical performance properties as seen in Section 3.3.2; where formulation 30/0 exhibited poor impact strength compared to the other composites.

Furthermore, to understand the particle distribution of Nuvolve™ in PP; formulation 30B/0 was treated with concentrated sulfuric acid (99.9 %). The sample was taken from an ASTM test specimen where it was cooled using liquid nitrogen and immediately broken via manual force. The broken piece of the sample was submerged in sulfuric acid for two hours and left to dry overnight. SEM images were taken of the treated and untreated 30B/0 composite. It can be seen (as voids) that the particle size distribution of Nuvolve™ varies between 10-100 µm (Figure 3.3-13) with signs of agglomeration (~100 µm) present in the sample indicating lack of dispersion. However, the distribution of Nuvolve™ within the polymer matrix is good.

Figure 3.3-10: SEM micrograph of neat PP at 100x magnification

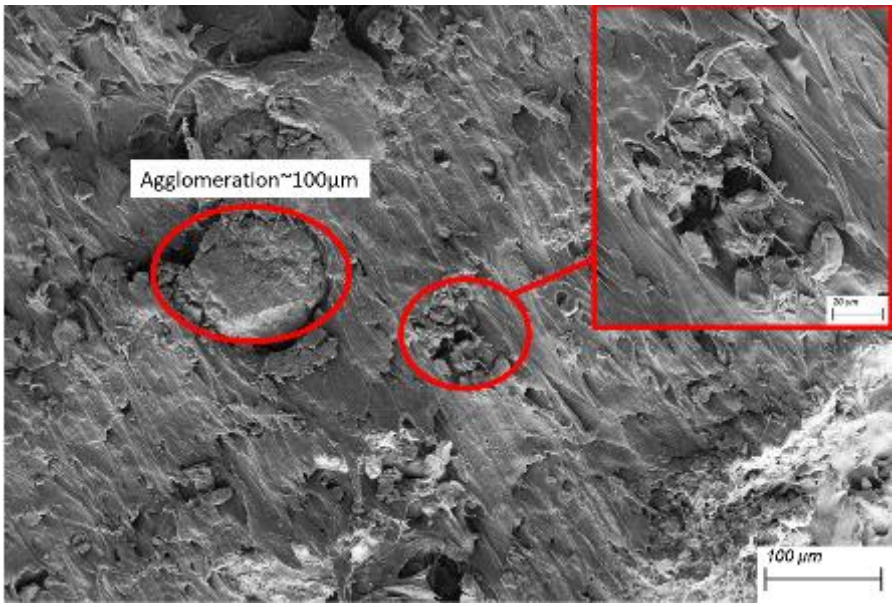

Figure 3.3-11: SEM micrograph of 30A/0 at 500x magnification

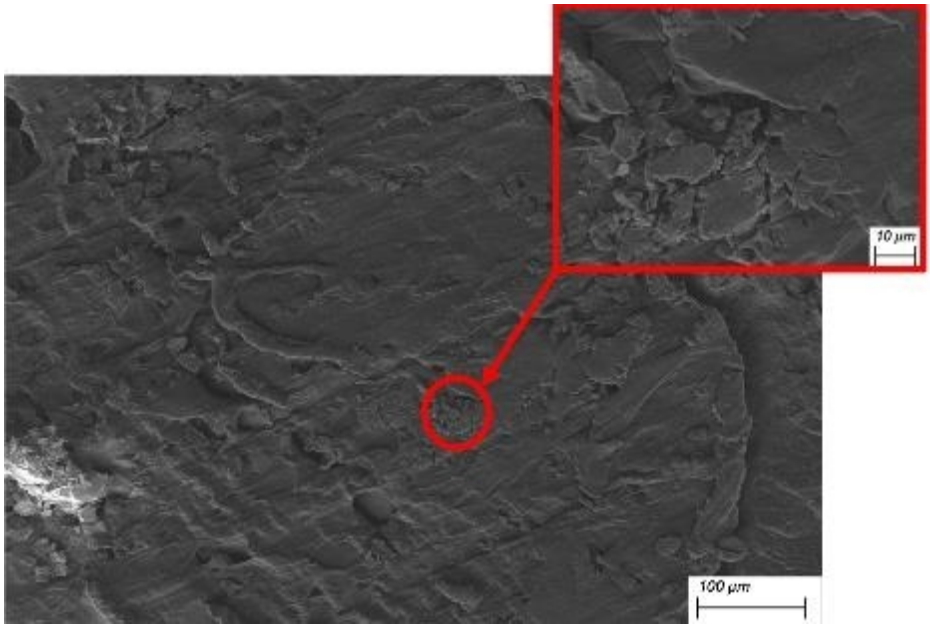

Figure 3.3-12: SEM micrograph of 30B/0 at 500x magnification

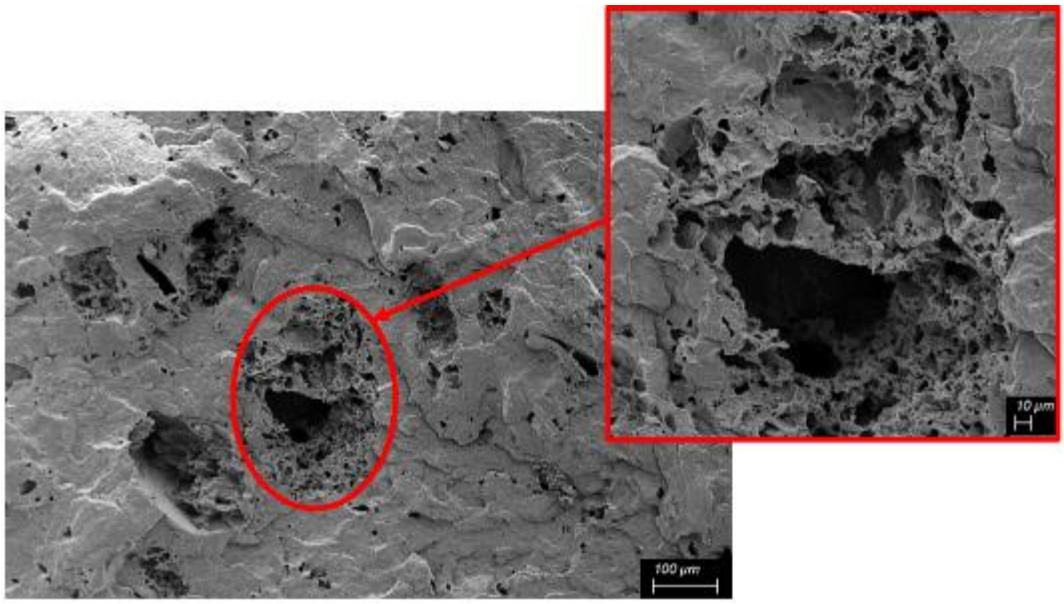

Figure 3.3-13: SEM micrograph of 30B/0 (treated with sulfuric acid) at 250x magnification

Figure 3.3-14: SEM micrograph of 30B/0 (untreated) at 250x magnification

Figure 3.3-15 and Figure 3.3-16 showed areas with good wetting of PP on glass fiber (designated in red) for formulation 10A/15 and 15B/15.This maximizes the stress transfer between filler and matrix for optimum reinforcing capabilities. Figure 3.3-16 shows an agglomerated Nuvolve™ particle lacking adhesion with the polymer matrix indicated by the absence of total surface coverage from PP as seen with glass fiber (in the same figure). Nuvolve™ and PP are hydrophilic and hydrophobic by nature and it is difficult to attain good adhesion at the interface between the filler and matrix (Figure 3.3-16). Optimizing the interfacial interaction between filler and matrix is directly related to the composite's mechanical performance as the filler's sole duty is to effectively transfer load from the polymer matrix through shear stresses [54] [5]. The addition of maleic anhydride grafted on PP (PP-*g*-MA) has shown to increase compatibility between hydrophilic natural fibers and hydrophobic PP and thereby improve mechanical properties of the composites [68] [69]. This could be improved in the case of Nuvolve™ and PP by further addition of PP-*g*-MA to enhance the compatibility between the two entities.

Figure 3.3-17 shows a SEM micrograph of formulation 10A/15 where good adhesion of glass fiber and PP is present (red box) . The PP homopolymer covers the surface of glass fiber signifying good wetting of the fiber. Additionally, fiber-pull out can be observed denoted by the green circles (Figure 3.3-17). The effect of this is shown in the impact strength of the hybrid composites in Section 3.3.2. The relatively long glass fibers exhibit additional energy dissipation mechanisms through enabling improvement in impact strength of the composites [66] [70]. This is further amplified by the good adhesion between glass fiber and PP. Moreover, the glass fiber shows good distribution within the polymer matrix.

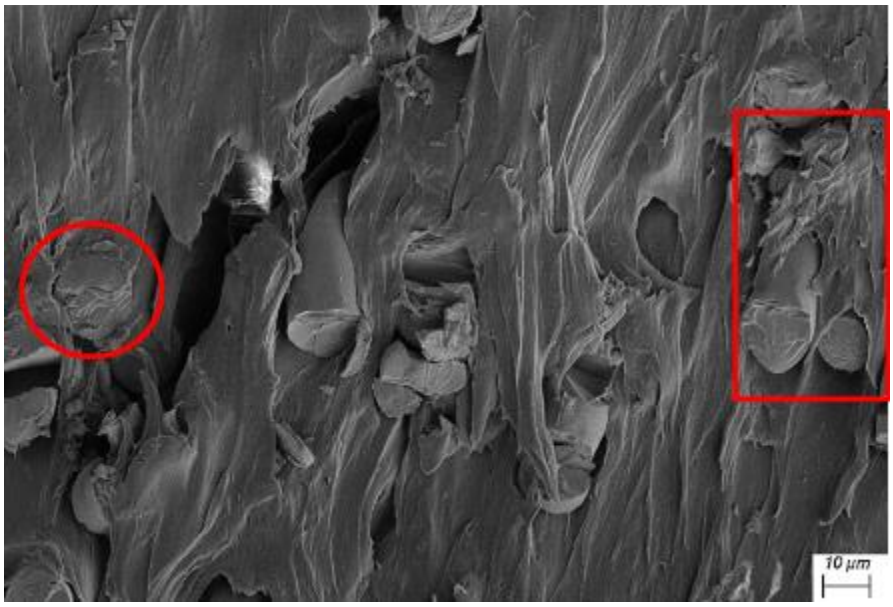

Figure 3.3-15: SEM micrograph of 10A/15 at 2000x magnification

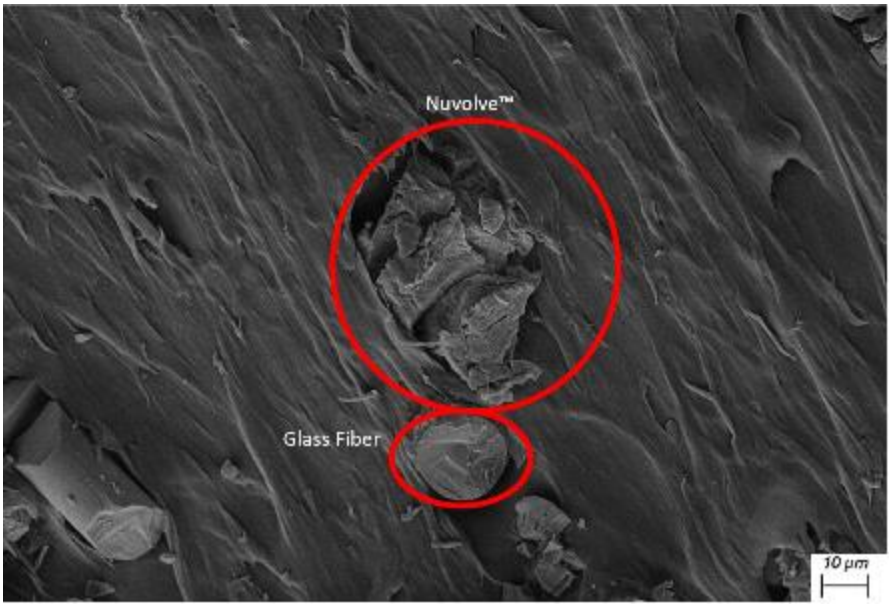

Figure 3.3-16: SEM micrograph of 15B/15 at 2000x magnification

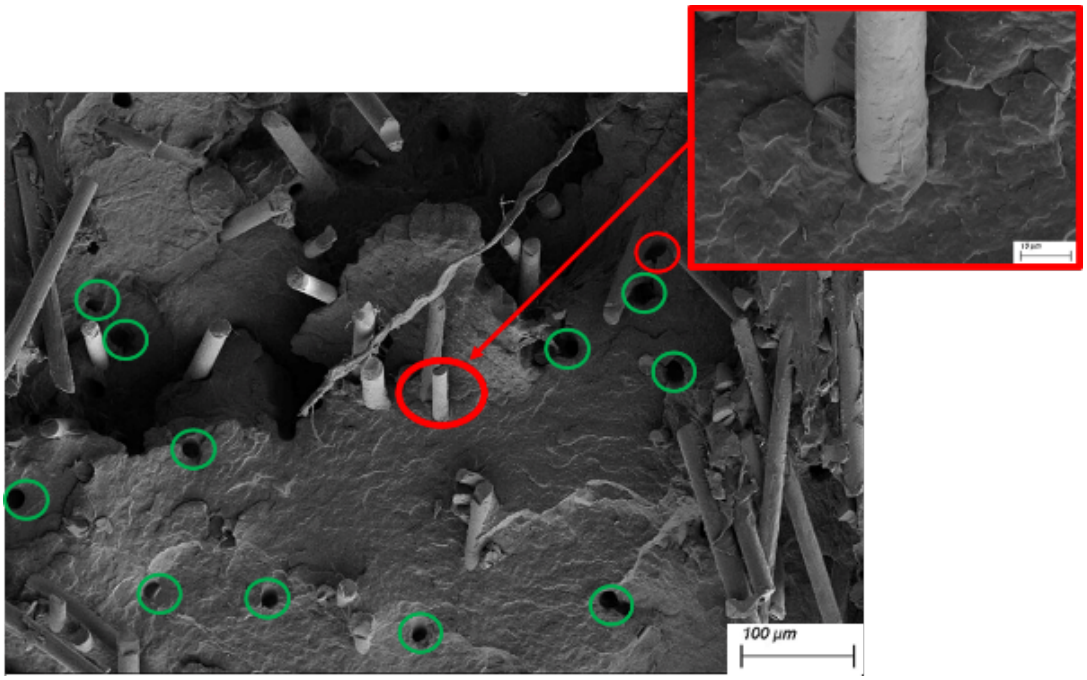

Figure 3.3-17: SEM micrograph of 10A/15 at 500x magnification, fiber pull-out (green circles)

3.3.4 Performance and Cost Analysis of the Hybrid Composites

In the automotive industry, one of the most useful and cited metrics for material selection is the flexural modulus which is a measure of stiffness. Figure 3.3-18 shows significant improvements in density by the hybridization of glass fiber and Nuvolve™ in PP compared to Ford Motor Company's material specification for body interior and under-the-hood applications. Figure 3.3-19 shows the specific flexural modulus of the hybrid composites as a function of total filler loading (wt.%). The incorporation of Nuvolve™ at 10, 15 and 20 wt.% showed that the following composite systems met the material specification from Ford Motor Company while offering lightweighting opportunity and reduction in total filler loading (wt.%).

Cost analysis is critical to determine the commercial viability of the materials used to formulate the hybrid composite systems. Figure 3.3-20 shows the cost of the hybrid composites ($/L).

Assumptions on the cost of the filler materials are presented in Appendix 7.6. The data presented in Figure 3.3-20 shows that the hybrid composites cost more than control samples and the Ford Motor Company's material specification; this is attributed to the higher cost of Nuvolve™ compared to glass fiber. There is 0.12 $/L difference between the best performing composite (10/20) and the material specification from Ford Motor Company; showing a slight premium cost of utilizing the hybrid composites for body interior and under-the-hood applications.

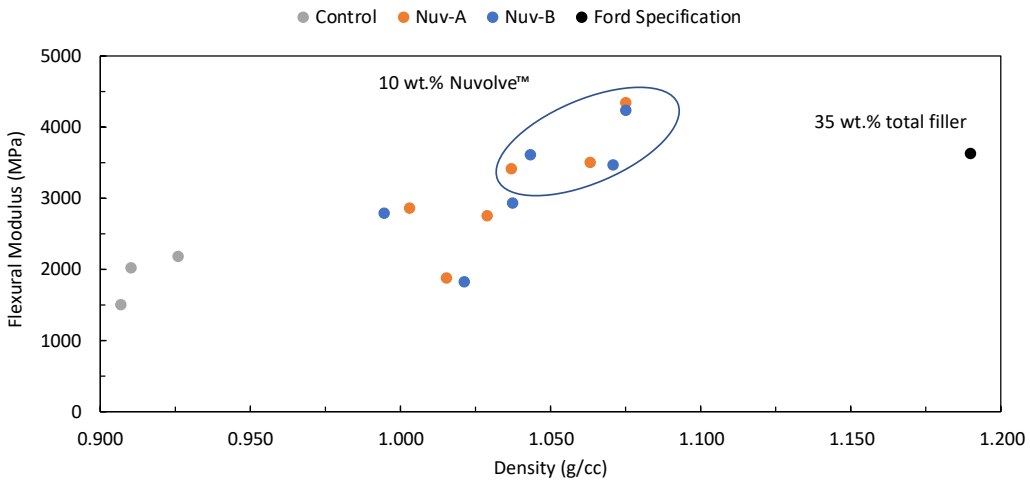

Figure 3.3-18: Flexural Modulus (MPa) vs. Density (g/cc)

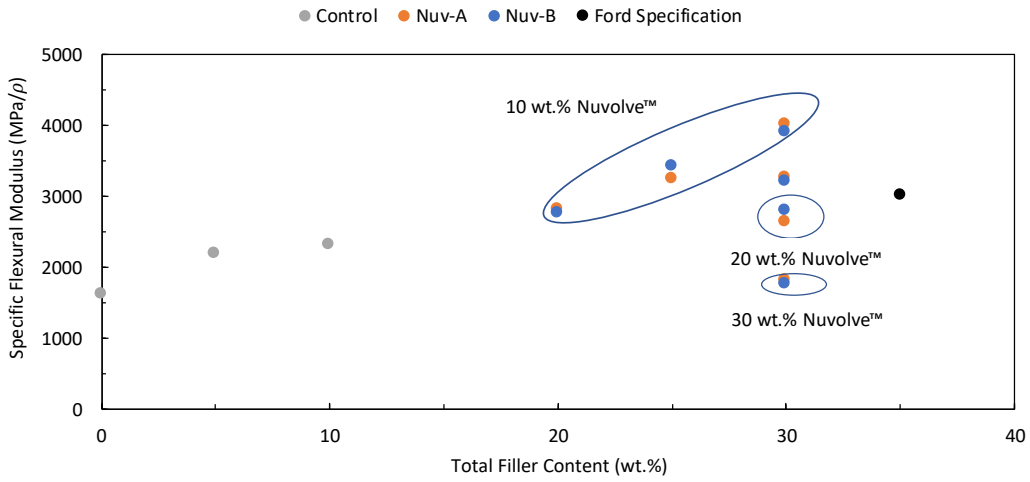

Figure 3.3-19: Specific Flexural Modulus (MPa/ρ) vs. Total Filler Concentration (wt.%)

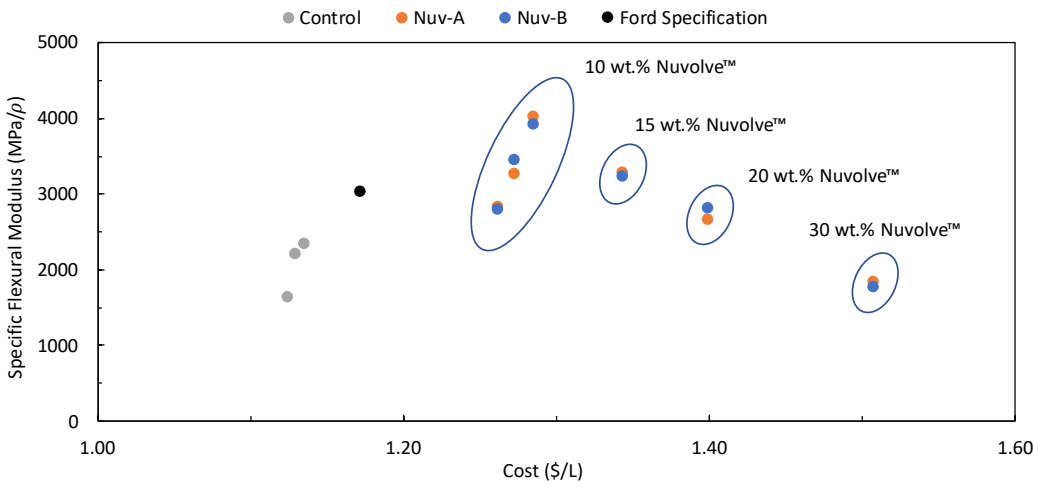

Figure 3.3-20: Specific Flexural Modulus (MPa/ρ) vs. Cost ($/L)

3.3.5 Thermal Characterization

Thermal characterization of all composites was carried out to determine the thermal stability of Nuvolve™ reinforced hybrid composites; specifically analyzing the onset decomposition temperature of polypropylene and the temperatures exhibiting 10 and 15 % weight loss for all composites. The thermal stability was investigated using thermal gravimetric analysis (TGA) at a heating rate of 20 ºC per minute in nitrogen. Furthermore, the crystallization and melting transitions were evaluated using differential scanning calorimetry (DSC) to determine crystallinity and melting behaviour of the composites.

Figure 3.3-21 and Figure 3.3-22 show the thermal gravimetric analysis curves for Nuv-A and Nuv-B reinforced hybrid composites. It can be seen that the hybrid composites have two transitions as opposed to the control samples (neat PP, 5 wt.% GF-PP and 10 wt.% GF-PP.). The transition that occurs before the major weight loss change (>400 ºC) is the degradation of Nuvolve™ with

the major transition being attributed to the degradation of polypropylene. The onset of degradation of Nuvolve™ occurs at around 315 ºC.

The hybrid composites exhibit lower thermal stability than neat PP, which is due to the low thermal stability of Nuvolve™ (~315 ºC) and this is represented by the temperatures at 10 and 15 % weight loss (Table 3.3-1). Formulation 30/0 (only containing Nuvolve™) shows a decrease by 105 ºC in temperatures at 10 and 15 % weight loss compared to neat PP. At this point, greater than 20 % of the weight is lost during the degradation of Nuvolve™. This observation is supported by A. Kiziltas *et al* [71] work on microcrystalline cellulose (MCC) reinforced PET-PTT composites; where it was reported that temperature at 10 % weight loss decreased with the increasing addition of MCC. This is due to the lower thermal stability of MCC (~340 ºC). The control samples (0/5 and 0/10) showed an increase up to 8 ºC in temperatures at 10 and 15 % weight loss attributed to the high thermal stability of glass fiber. The hybrid composites showed a harmonious effect exhibiting slightly greater values in temperatures at 10 and 15 % weight loss compared to formulation 30/0 but yet still showing lower values in contrast to neat PP.

Although, the hybrid composites showed a decrease in thermal stability compared to neat PP; the onset degradation temperature of PP was retarded by the addition of filler material as seen in Table 3.3-1 presenting the onset degradation temperatures of the PP in all composites quantified by 1% conversion of the material. The formulation that contained only Nuvolve™ (30/0) showed a 12% increase of degradation temperature of the PP compared to neat PP. All of the hybrid composites utilizing Nuv-A and Nuv-B showed an increase in degradation temperature compared to neat PP. Similar findings were shown by M.D.R Batista *et al* [54] with respect to micro-cellulose reinforced PP composites.

With respect to processing, Nuvolve™ showed that it will be thermally stable when melt blended with neat PP in a twin-screw extrusion process with typical melt temperature ranges of 190-210 ºC [72]. For the application of under-the-hood components; operating temperatures are within 120 ºC [73]. Therefore, the hybrid composites showed good thermal stability that can be employed in under-the-hood components (e.g. battery cover) while also incorporating renewable content in the composite and ultimately enabling lightweighting.

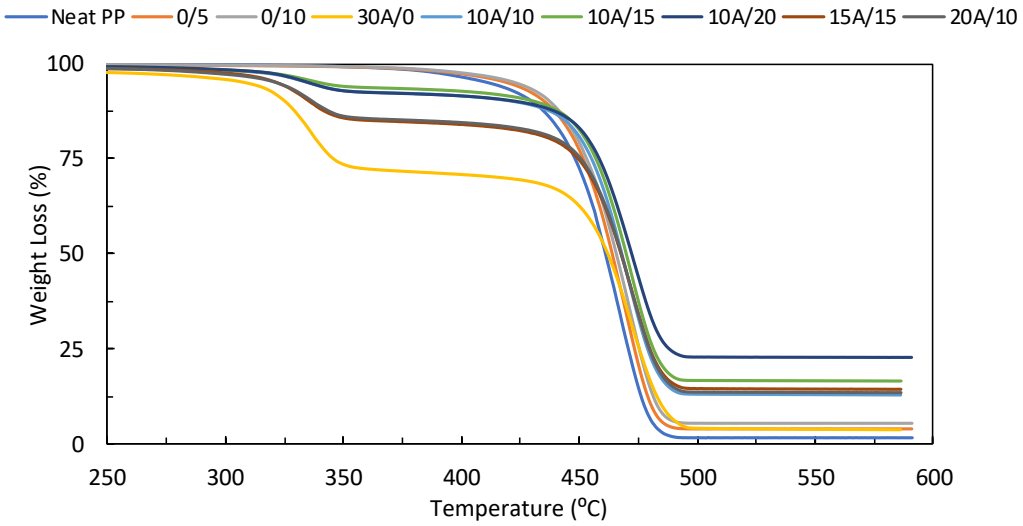

Figure 3.3-21: TGA curves of Nuv-A containing hybrid composites

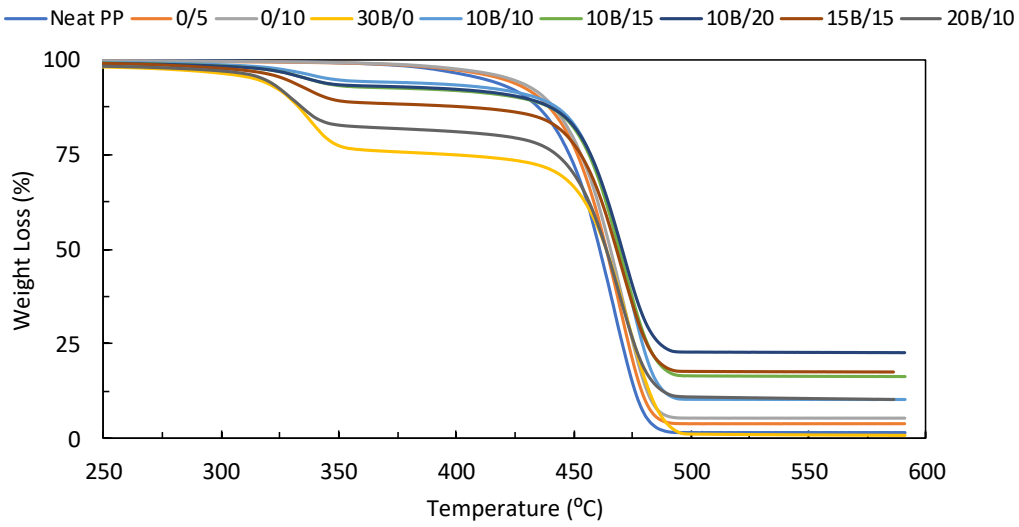

Figure 3.3-22: TGA curves of Nuv-B containing hybrid composites

Table 3.3-1: Thermogravimetric data for hybrid composites reinforced by Nuv-A and Nuv-B

Formulation	Onset Degradation Temperature of PP (°C)	Temperature at 10% Weight Loss (°C)	Temperature at 15% Weight Loss (°C)
Neat PP	368	430	439
0/5	371	435	443
0/10	371	438	445
30A/0	406	326	333
10A/10	408	423	444
10A/15	405	432	447
10A/20	408	424	447
15A/15	409	336	364
20A/10	406	337	386
30B/0	411	329	336
10B/10	406	434	448
10B/15	409	427	446
10B/20	406	429	446
15B/15	409	345	434
20B/10	407	329	339

Figure 3.3-23 and Figure 3.3-24 show the DSC cooling curves for Nuv-A and Nuv-B reinforced hybrid composites. The data on Table 3.3-2 suggests that the onset and peak crystallization temperature of the hybrid composites decreased up to 6 ºC compared to neat PP. The onset crystallization temperatures were estimated at a defined temperature range of 105-160 ºC for consistency. Literature suggests that the addition of filler material is expected to act as a nucleating agent and thus increase the crystallization temperature. Y.Feng *at el* [74] reported the addition of sorbitol in polypropylene contributed to an increase in crystallization temperature. This was further supported by the work of Y. Amintowlieh *et al*, [75] where wheat straw reinforced polyamide 6 composites showed an increase in crystallization temperature with the addition of wheat-straw compared to virgin polyamide 6. The heterogeneous nucleation induced by filler content can lead to faster part production and lower cycle times during processing e.g. injection molding. Table 3.3-2 indicates that this is not the case with Nuvolve™ reinforced hybrid composites. Therefore, the addition of glass fiber/ Nuvolve™ did not result in a nucleating effect on the crystallization of PP. The typical onset and peak crystallization temperatures of PP homopolymer are 127 and 113 ºC respectively [76]. This suggests that the commercial-injection molding grade PP used in this study likely has an additive package that promotes crystallization to occur at a higher temperature.

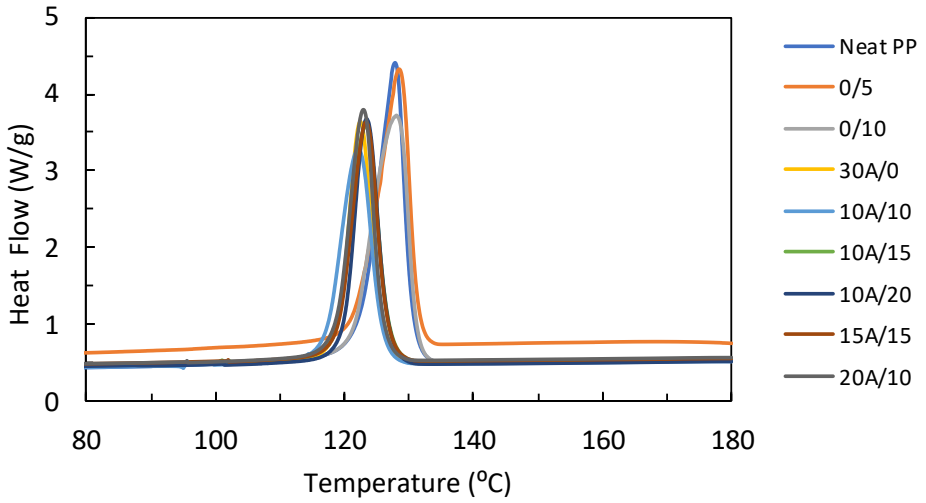

Figure 3.3-23:DSC cooling curves for Nuv-A reinforced hybrid composites

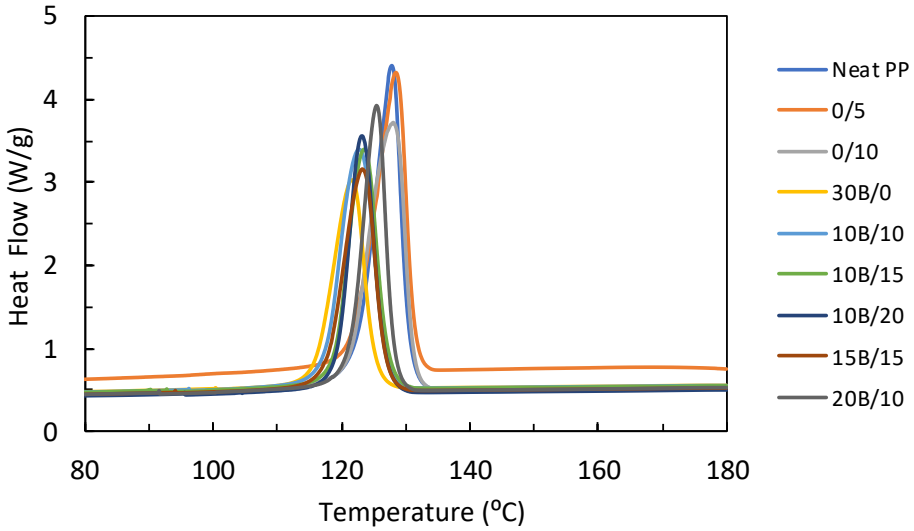

Figure 3.3-24: DSC cooling curves for Nuv-B reinforced hybrid composites

Furthermore, crystallinity of the composites was calculated using Equation 3, where the heat of fusion ($\Delta H_{f,pp}$) is determined from the DSC curves (Figure 3.3-20 and Figure 3.3-24). The standard heat of fusion of polypropylene at 100% crystallinity ($\widehat{\Delta H}_{f,pp}$) is taken from TA

instruments data bank of polymers [77]. The equation is corrected by the mass fraction of polypropylene (m_{pp}). Similar to the onset crystallization temperature, the heat of fusion was estimated at the predefined temperature range (105-160 ºC) for consistency. Table 3.3-2 shows the resulting crystallinity of the composites where the neat PP homopolymer (injection molding grade) has a crystallinity of 64 %. This value is slightly higher than the reported value of 55-60 % in literature for general use PP [78]. Similarly, this is likely due to the additive package used in this commercial-injection molding grade PP. It is expected that the addition of filler material would hinder the movement of polypropylene chains with viscosity increasing as seen in Section 3.2.3 where complex viscosity increased with the addition of filler material. This mechanism would reduce the ability of the chains to fold into crystalline structures and interfere with the growth of crystallites. The results shown in Table 3.3-2 indicate an inconclusive trend. The addition of 5 wt.% glass fiber in PP increased the crystallinity compared to neat PP by 6 %. When a further amount of glass fiber is added (10% wt.) the increase in crystallinity compared to neat PP is only 2 %. Formulation 30/0 showed at decrease in crystallinity by 1 % compared to neat PP utilizing 30 wt.% of Nuvolve™ and this agrees with the hypothesis made earlier. However, the hybrid formulations with a total filler content of 30 wt.% show an increase in crystallinity up to 4% compared to neat PP contrary to what is expected to happen. It should also be noted that the crystallinity values range from 63 to 70 % with a median value of 66 % and standard deviation of 2 %. Therefore, the differences in crystallinity among the composites is insignificant and no trend can be observed.

$$X_c = \frac{\Delta H_{f,pp}}{\widehat{\Delta H}_{f,pp} * m_{pp}} * 100 \tag{3}$$

In contrast, the peak and onset melting temperatures stayed constant for all composites in comparison to neat PP, suggesting that the effect of Nuvolve™ is minimal on the melting temperature (Figure 3.3-25 and Figure 3.3-26). A. Kiziltas *et al* [71] reported similar findings with micro-crystalline cellulose reinforced PET-PTT composites, where there was no significant influence of the MCC addition on the melting temperature of the composites.

Overall, the DSC results showed that the fillers did not act as nucleating agents to aid with accelerated crystallization which translates to a potential increase in part production and reduction in cycle times. The melting temperatures stayed consistent in all composites compared to neat PP Moreover, the two variants of Nuvolve™ differentiated by particle size performed equally well and showed little to no significant differences resulting in commercial potential for Nuv-B due to the lower cost of production. The hybridization of Nuvolve™ and glass fiber in PP showed good thermal stability that can be utilized in challenging conditions for application in body interior and under-the hood with the added benefit of lightweighting and incorporation of sustainable material within the composite technology.

Table 3.3-2: Differential scanning calorimetry (DSC) data

Formulation	Peak Crystallization Temperature (ºC)	Onset Crystallization Temperature (ºC)	Crystallinity (%)
Neat PP	128	131	64
0/5	128	131	70
0/10	128	131	66
30A/0	122	126	63
10A/10	122	126	67
10A/15	123	127	65
10A/20	123	127	67
15A/15	123	127	68

20A/10	123	126	65
30B/0	122	125	63
10B/10	123	127	69
10B/15	123	127	65
10B/20	123	127	65
15B/15	123	127	68
20B/10	125	128	68

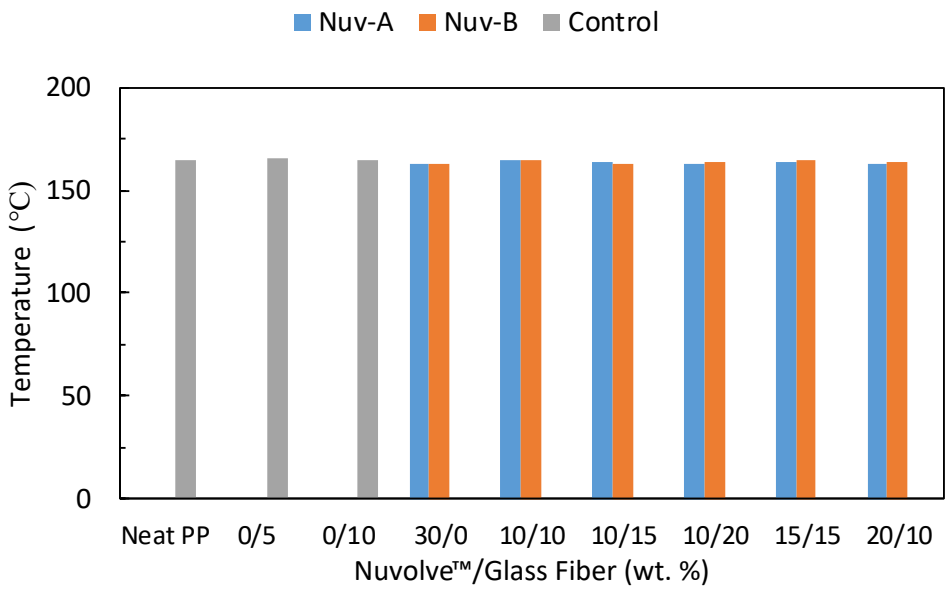

Figure 3.3-25: Peak melting temperature of all composites

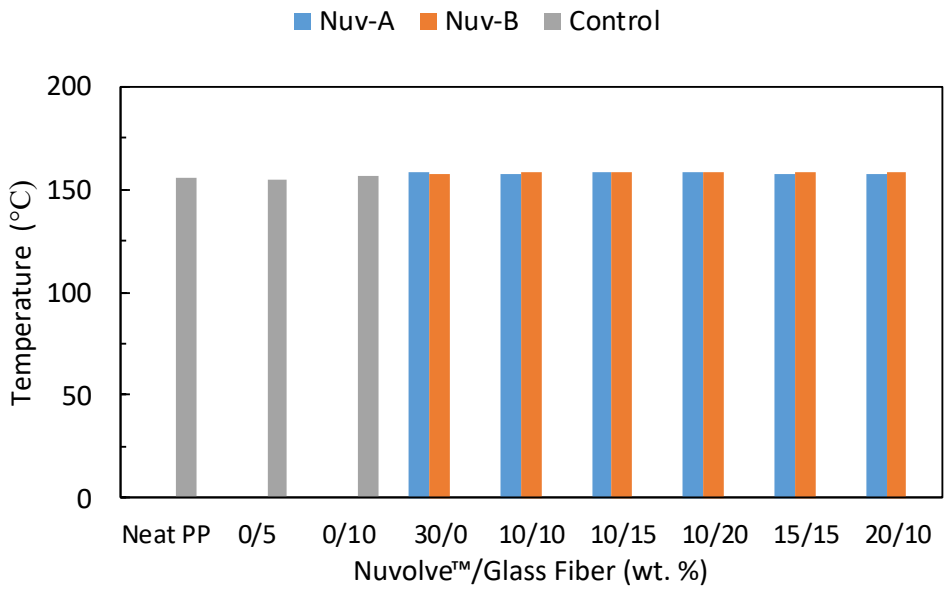

Figure 3.3-26: Onset melting temperature of composite

3.3.6 Kinetics of Thermal Degradation

The degradation mechanism of Nuvolve™ was studied using Friedman's iso-conversional differential method. The method outlines steps to determine the activation energy of the degradation process of Nuvolve™. The measurements were carried out at 5, 7.5, 10, 15 and 20 ºC/min using the thermal gravimetric analysis (TGA): TA Instruments Q500) at predefined heating rates (ºC/min) and conversion levels (%) as well as exposure in different chemical environments (nitrogen and air). The objective of this study is to calculate the activation energy at each conversion level and specific chemical environment.

The fundamental governing rate equation is described in Equation 4, where the rate of thermal degradation $\frac{d\alpha}{dt}$ is a function of temperature T and conversion α. Conversion can be defined by

Equation 5; where $w_{initial}$ is the initial weight of the sample (mg) and w_{final} is the final weight of the sample (mg).

$$\frac{d\alpha}{dt} = k(T)f(\alpha) \tag{4}$$

$$\alpha = \frac{w_{initial} - w}{w_{initial} - w_{final}} \tag{5}$$

The initial and final weight of the samples were carefully selected for each TGA curve. This was done by computing the derivative of the weight loss (%) signal (DTG) from the individual TGA curves, and the range was selected where the DTG curved had a defined baseline. Figure 3.3-27, Figure 3.3-28, Figure 3.3-29 and Figure 3.3-30shows the TGA curves for Nuvolve™-B and Nuvolve™-A at various heating rates and in a nitrogen environment.

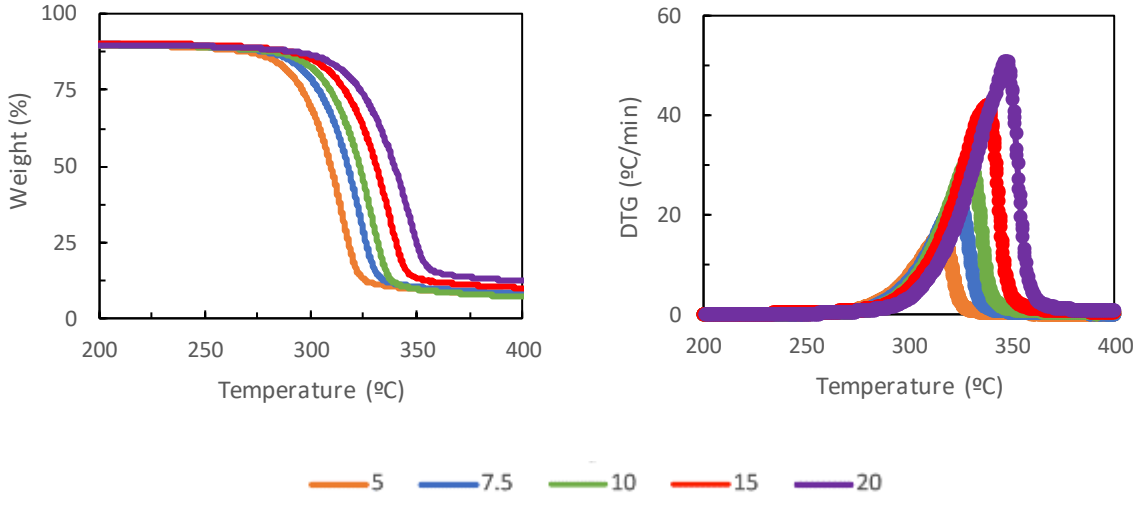

Figure 3.3-27: TGA and DTG curve for Nuvolve™ B in nitrogen at different heating rates (5, 7.5, 10, 15 and 20 °C/min

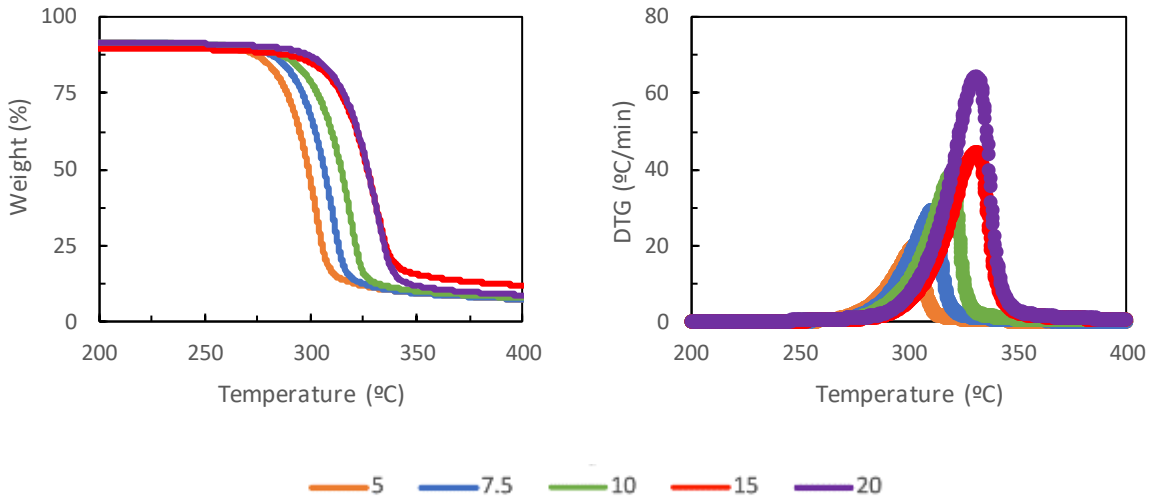

Figure 3.3-28: TGA and DTG curve for Nuvolve™ B in air at different heating rates (5, 7.5, 10, 15 and 20 °C/min)

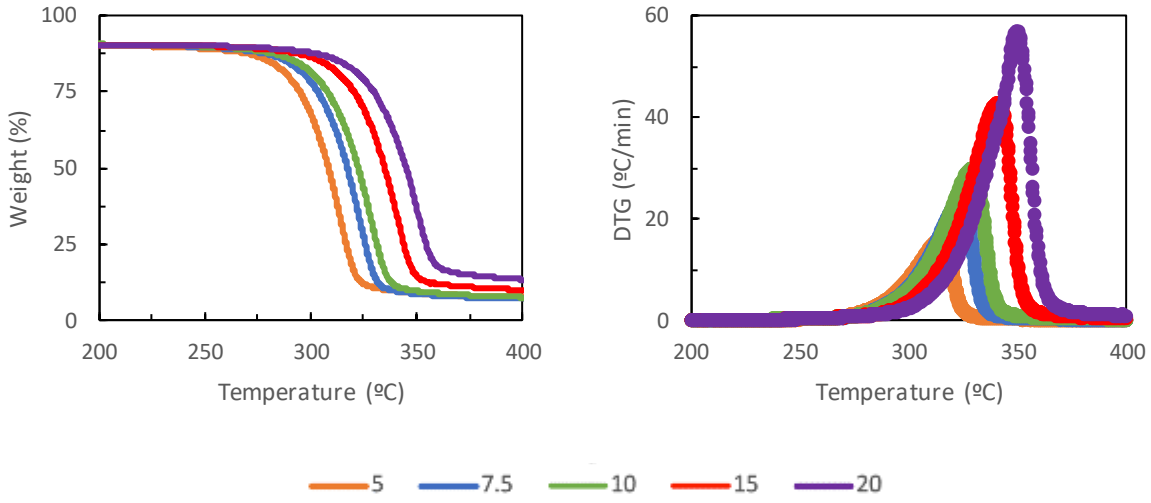

Figure 3.3-29: TGA and DTG curve for Nuvolve™ A in nitrogen at different heating rates (5, 7.5, 10, 15 and 20 °C/min)

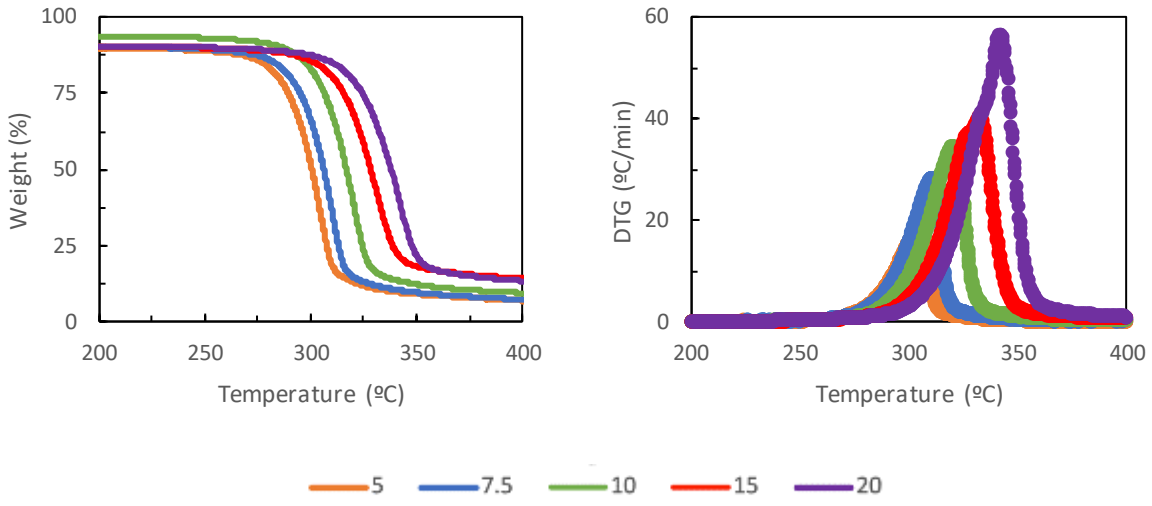

Figure 3.3-30: TGA and DTG curve for Nuvolve™ A in air at different heating rates (5, 7.5, 10, 15 and 20 °C/min)

Equation 4 can be further simplified using the Arrhenius equation to model the rate constant $k(T)$ in Equation 5; where A is the pre-exponential factor, E_a is the activation energy and R is the gas constant.

After mathematical manipulation, the final form of the rate equation is shown in Equation 7.

$$k(T) = A * \exp\left(-\frac{E_a}{RT}\right) \tag{6}$$

$$\frac{d\alpha}{dt} = Aexp\left(-\frac{E_a}{RT}\right)f(\alpha) \tag{7}$$

$$\ln\left(\frac{d\alpha}{dt}\right) = ln\big(Af(\alpha)\big) - \frac{E_a}{RT} \tag{8}$$

The logarithm is taken to linearize the equation in the form of $y = mx + b$, where y corresponds to $\ln\left(\frac{d\alpha}{dt}\right)$ and x corresponds to $1/T$. Equation 8 yields a linear line where the slope is used to approximate the activation energy as seen in Equation 9.

$$E_a = -\frac{R}{b} * slope \tag{9}$$

Figure 3.3-31 and Figure 3.3-32 show the resulting activation energies of Nuvolve™ A and B at the defined conversion levels (5,10 and 15 %) and chemical environment (air & nitrogen). The results show that in a nitrogen environment the activation energy is higher than in air which is supported by A. Buchenauer [79] work on wood-fiber reinforced polyamide composites. It should also be noted that Nuvolve™-B attained higher activation energy values in air and nitrogen compared to Nuvolve™-A and the result of this would suggest that Nuvolve™-B is slightly more stable since it has a higher energy barrier for thermal degradation to occur. The activation energies of common polysaccharides such as cellulose and starch are 135 and 180 kJ/mol which is comparable to the results attained in this study for Nuvolve™ [80] [81].

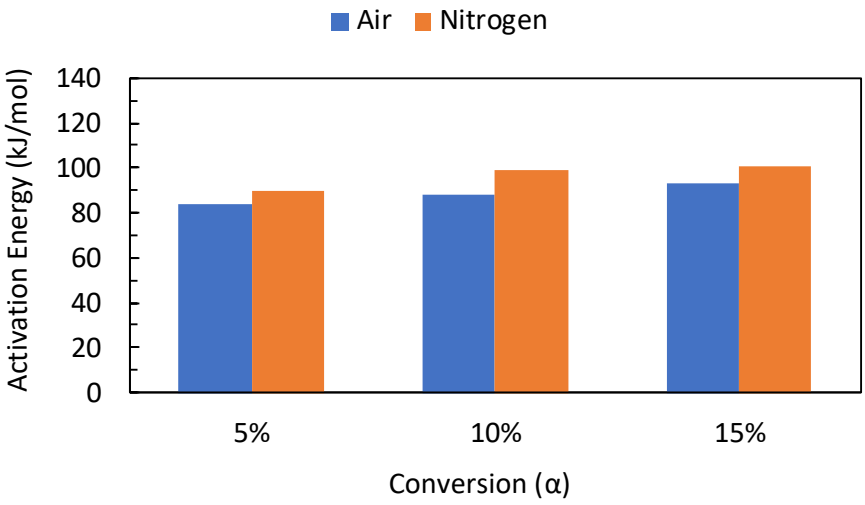

Figure 3.3-31: Activation energy values for Nuvolve™-A in air and nitrogen

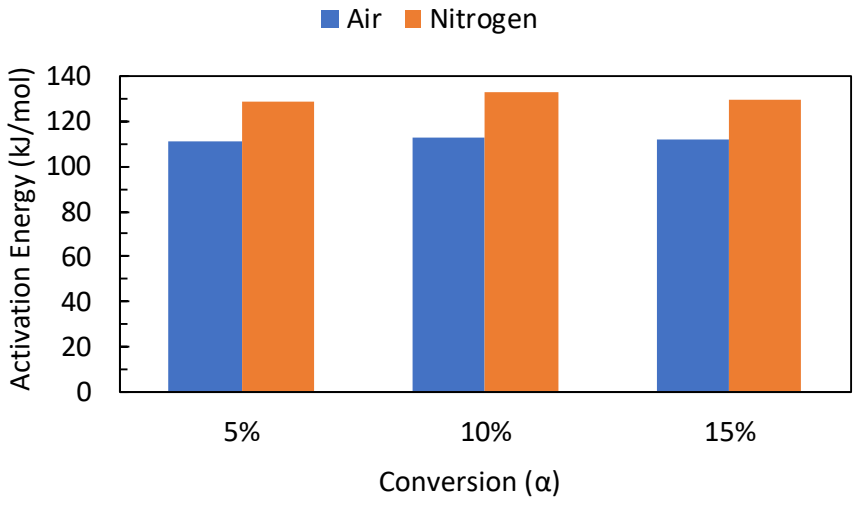

Figure 3.3-32: Activation energy values for Nuvolve™-B in air and nitrogen

The reaction model can be determined from the master plots with the introduction of the generalized time (θ) which is defined as [82]:

$$\theta = \int_0^t e^{\frac{-E_a}{RT}}\, dt \tag{10}$$

$$\frac{d\theta}{dt} = e^{\frac{-E_a}{RT}} \tag{11}$$

Equation 10 can then be substituted into Equation 7 to yield:

$$\frac{d\alpha}{d\theta} = \frac{d\alpha}{dt} e^{\frac{E_a}{RT}} \tag{12}$$

Plotting $\frac{d\alpha}{d\theta}$ as a function of conversion can produce the reaction model for the degradation mechanism of Nuvolve™; where the curve is compared to established reaction models presented by A.Khawam *et al* [83]. Figure 3.3-33 shows the plot of $\frac{d\alpha}{d\theta}$ as a function of conversion at heating rates of 5, 7.5, 10, 15 and 20 ºC/min. From this data, it is evidential that the degradation mechanism of Nuvolve™ follows a power-law model; specifically model P4 up until 50% conversion as shown in Table 3.3-3.

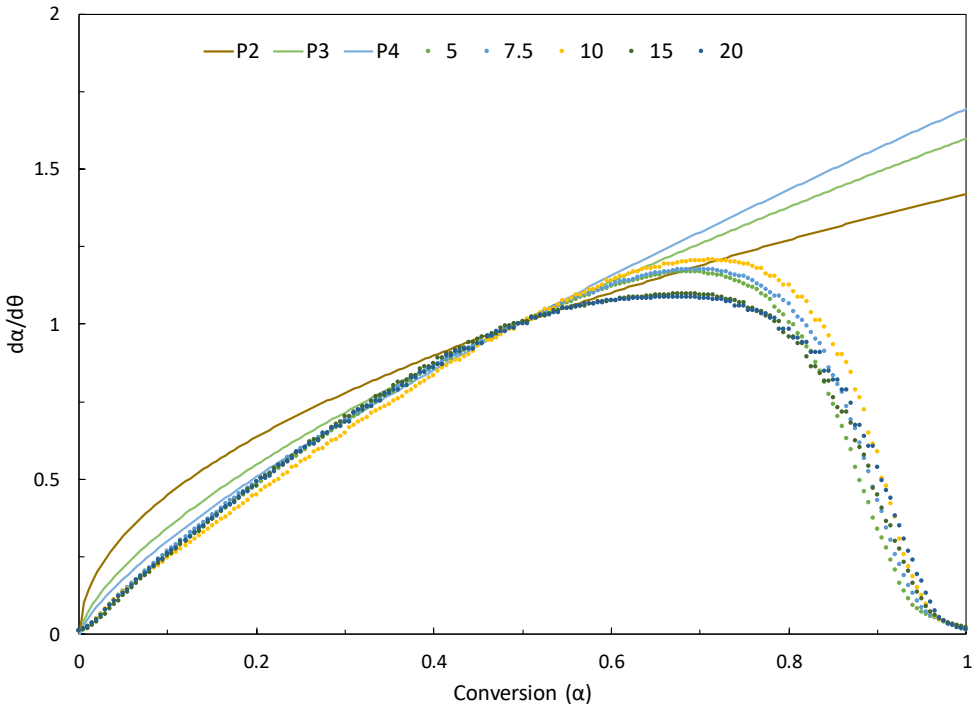

Figure 3.3-33: $\frac{d\alpha}{d\theta}$ as a function of conversion (α) for Nuvolve™ at different heating rates (ºC/min)

Table 3.3-3: Solid-State Rate Expressions for Different Reaction Models [83]

Model	Differential Form f(α)
Power law (P2)	$2\alpha^{1/2}$
Power law (P3)	$3\alpha^{2/3}$
Power law (P4)	$4\alpha^{3/4}$

The pre-exponential factor for common polysaccharides such as cellulose have been determined to be around 10^{11} min^{-1} [84]. With the knowledge of the activation energy E_a, reaction model f(α) and pre-exponential factor A; Equation 7 can be integrated and a mathematical expression of time (min) can be obtained as a function of conversion.

The integration of Equation 7 yields:

$$t = \frac{\alpha^{1/4}}{Ae^{\frac{-E_a}{RT}}} \tag{13}$$

Equation 13 can be used to determine the time-temperature behavior of Nuvolve™. Table 3.3-4 shows the time (seconds) it takes for Nuvolve™ to reach 1 and 5 % conversion at 190 and 200 ºC. The increase of temperature by 10 ºC (from 190 to 200 ºC) shows that Nuvolve™ at 1 % and 5 % conversion takes approximately half the time at 200 ºC compared to the time it would take at 190 ºC. In this study, Nuvolve™ was processed with PP using a melt temperature of 190 ºC and the results showed that Nuvolve™ is thermally stable for up to 1576 seconds before 5 % conversion occurs.

Table 3.3-4: Time-temperature behavior of Nuvolve™

Temperature (ºC)	Conversion (%)	Time (seconds)
190	1	1054
190	5	1576
200	1	567
200	5	848

Figure 3.3-34 shows the degradation of Nuvolve™ in time (seconds) as a function of increasing temperature at two conversion levels: 1 and 5 %. It is clear that with increasing temperature the time for Nuvolve™ to degrade decreases as the temperature approaches the onset thermal stability temperature of Nuvolve™. Using this data, the time-temperature behaviour of Nuvolve™ can be predicted to aid in designing new composite systems that entail manufacturing processes such as extrusion and injection molding.

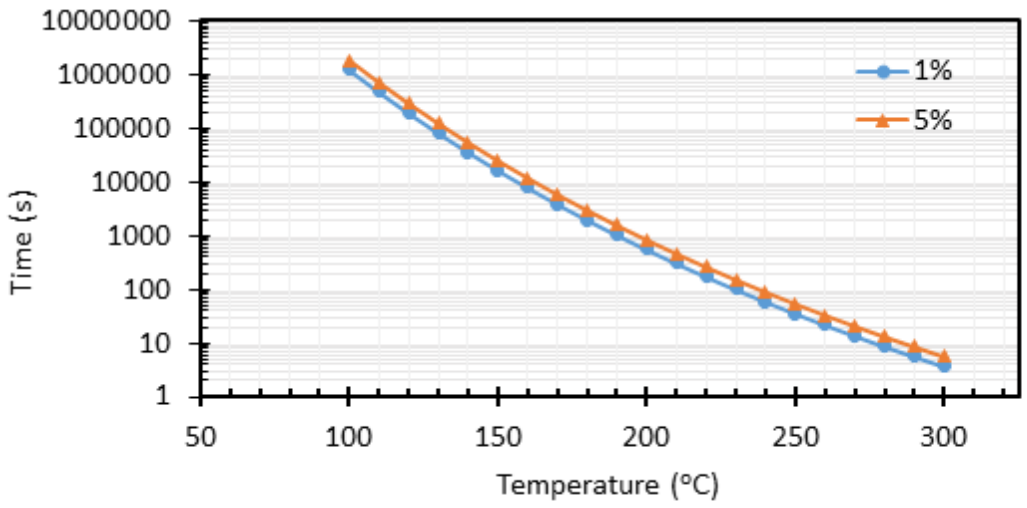

Figure 3.3-34: Time-temperature dependence of Nuvolve™ at 1 and 5 % conversion

3.3.7 Melt Rheology -Linear Viscoelastic Properties

Rheology is the science of deformation and flow of matter under controlled testing conditions. The analysis is useful to find out the effect of filler on the flowability of the melt. Industrial processes such as extrusion, injection molding, blow molding, etc. have defined shear rates that are optimal to process polymers and composites. The stress response is measured as a function of oscillatory strain (angular frequency) and complex viscosity, storage modulus, loss modulus and tan delta can be evaluated from this type of analysis. The analysis of polymer microstructures requires rheological measurements to be done in the linear viscoelastic region (LVR), where the applied shear stresses do not cause structural break down (apparent yield stress) effecting the microstructure of polymers [85]. This can be determined by performing a stress-strain sweep test. Figure 3.3-35 shows the respective shear rates related to the industrial processes (e.g. extrusion and injection molding).

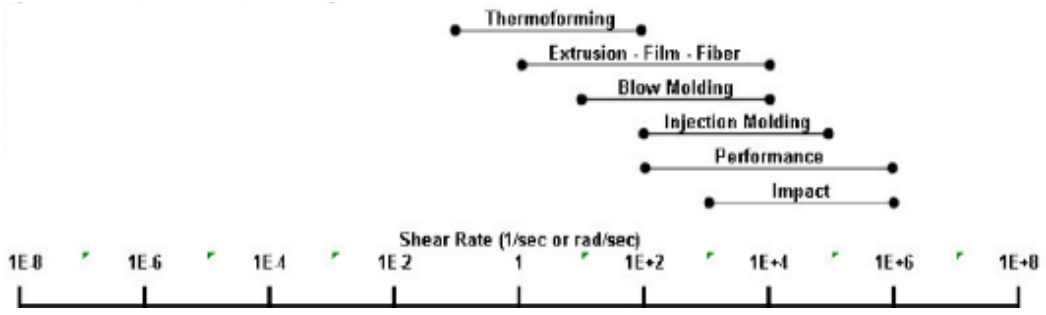

Figure 3.3-35: Shear rates for industrial processes [86]

The storage modulus measures the elastic response (ability to store energy) of a viscoelastic polymer whereas the loss modulus measures the viscous nature (ability to dissipate energy) of the viscoelastic polymer [86].

Figure 3.3-36 shows the complex viscosity of neat PP, 30B/0, 10B/15, 10B/20 and 15B/15 as a function of frequency (rad/s). It can be seen that the complex viscosity decreases as shear rate is increasing for neat PP and the hybrid composites. This is likely due the shear thinning effect of pseudoplastics [87]. For the composites the rigidity and orientation of the fillers inhibit PP from forming chain entanglements. This observation implies that the composites require higher shear stress and longer relaxation times to flow compared to neat PP [88] [89] [90] [91] [92]. It can also be noted that at higher shear rates the differences in complex viscosity is nullified due to the polymer matrix contribution dominating over the filler contribution [86]. Specifically, comparing formulation 10B/15 and 15B/15, it is observed that the 5 wt.% increase of Nuvolve™ demonstrated a threefold increase in viscosity at lower shear rates. Similar effect is observed for formulation 10B/15 and 10B/20, where an additional 5 wt.% increase in glass fiber loading effected the viscosity. Therefore, the total filler content tends to increase the viscosity albeit the result shown for 30B/0.

The storage modulus is a measure of stiffness (resistance to deformation) and the addition of filler content increases this property as compared to neat PP (Figure 3.3-37). Similarly, comparing composite 15B/15 and 10B/20 with 10B/15 there is twofold increase at low shear rates when an additional 5 wt.% filler content is added. This property is mainly controlled by the filler-matrix interface as opposed to the reinforcing fillers itself [93] as the fillers are added the stress is transferred from the matrix to the rigid fillers provided that the filler matrix interactions are strong. With good filler matrix interactions, the rigidity of the fillers (Nuvolve™ and glass fiber) restrict deformation as seen for complex viscosity [94]. This trend is seen at lower shear rates and at higher shear rates yet again the matrix contributions dominate over the filler contributions [94].

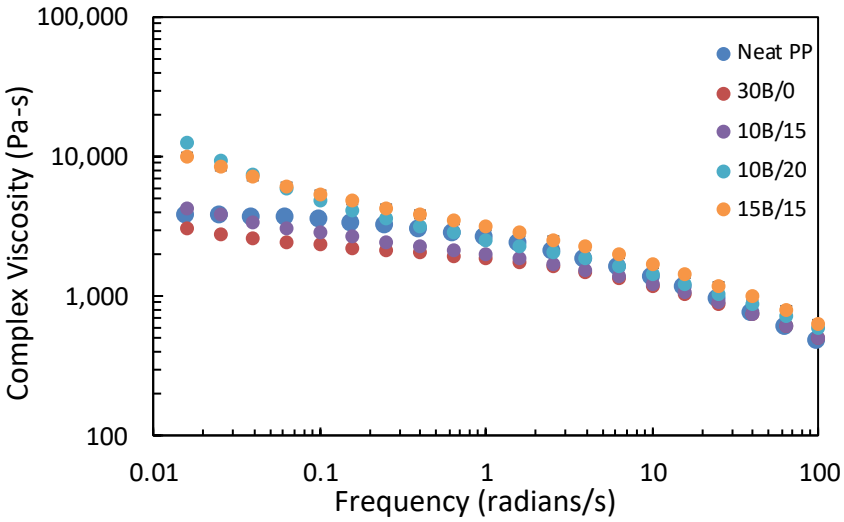

Figure 3.3-36: Complex viscosity as a function of frequency

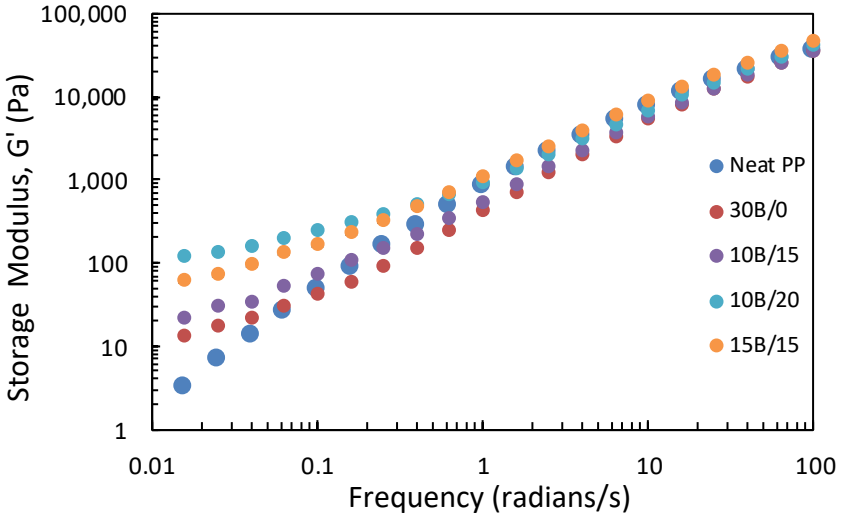

Figure 3.3-37: Storage modulus (G′) as a function of frequency

The loss modulus indicates the viscous behavior (liquid like) of the melt (energy dissipation in flow). The composites show an increase in loss modulus for the hybrid composites compared to neat PP which could indicate energy dissipation mechanisms due to filler-matrix and filler-filler interactions [93] [95].

Additionally, the tan δ is plotted as a function of frequency; where the general trend shows a decrease in tan δ as shear rate increases (Figure 3.3-39). At low shear rates, the tan δ of neat PP is higher than the hybrid composites which is contrary to what was reported in literature where the addition of filler material increased tan δ compared to PP [90] [93]. At higher shear rates, tan δ increased with the addition of filler material compared to neat PP. This is attributed to the reinforcing effect imparted by the fiber/filler adding to the viscoelastic energy dissipation in the composite [93].

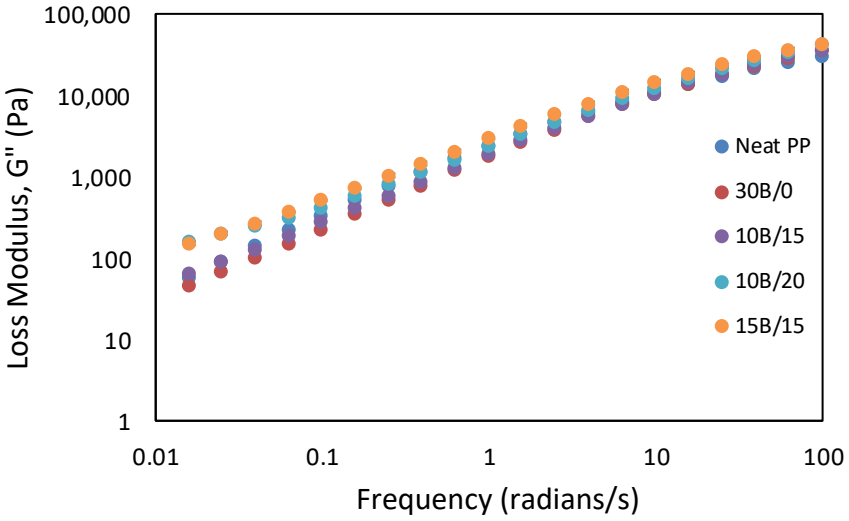

Figure 3.3-38: Loss modulus (G″) as a function of frequency

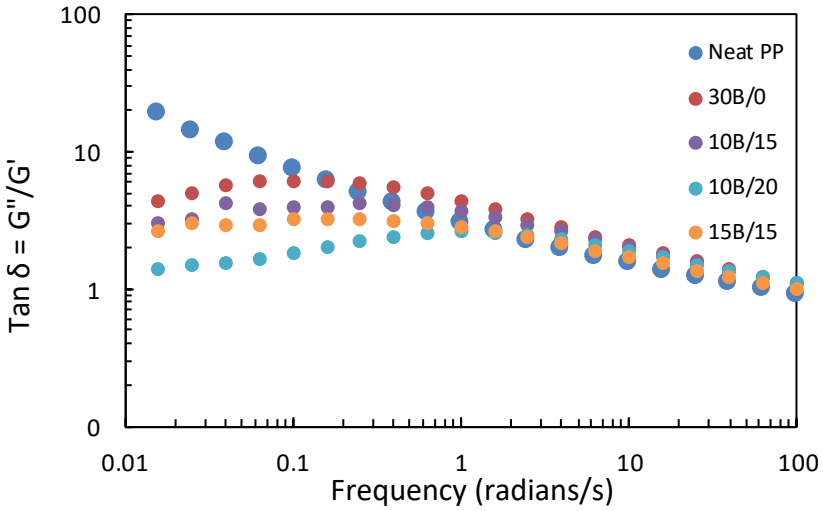

Figure 3.3-39: Tan δ as a function of frequency

Overall, the complex viscosity, storage modulus, and loss modulus increased with the addition of filler material. The study of melt rheology is in particular interest to molders and compounders for example in the injection molding process the objective is to produce a product that is free of

voids, sink marks, minimizing warpage and maximizing performance properties for end-use [96]. For this to occur the requirement is that the melt flows freely and fills the cavity where the final product is free of residual stresses. The viscosity data presented in this section suggests that the composites become more free flowing at higher shear rates. Therefore, it is important to understand the flow behavior of the polymer melt and the response of the flow to deformation under controlled conditions.

3.4 Conclusion

The development of hybrid composites with DuPont's Nuvolve™ and glass fiber as fillers in a PP matrix were investigated in this chapter. The maximum total filler content did not exceed past 30 wt. % and the mechanical, thermal and morphological properties were evaluated and compared to Ford's incumbent material for body interior and under-the-hood applications in passenger vehicles and light-duty trucks.

The mechanical properties of the composites showed general increase in performance with glass fiber content and the opposite with Nuvolve™ content. However, optimum formulations were found (10/15, 10/20) that may reduce or replace a portion of the inorganic content. The best performing composites were 10/15 and 10/20, they outperformed Ford's incumbent material that is glass filled with a loading of 35 wt. %; creating an opportunity for a reduction up to 10% in total filler content and therefore delivering weight savings per automotive part.

The thermal stability of the hybrid composites showed a decrease in thermal stability compared to neat PP. This was due to the low thermal stability of Nuvolve™. However, the addition of filler material retarded the degradation of PP. Thermal stability results showed that the hybrid composites can be utilized in challenging conditions such as under-the-hood components. The

crystallization temperature (T_c) of the composites decreased revealing that Nuvolve™ is not a nucleating agent enabling crystallization to occur at a higher temperature and thereby decrease cycling time during manufacturing processes like injection molding.

Analysis of the melt rheology showed the storage modulus, loss modulus, complex viscosity increased with the addition of filler concentration. The morphological properties of the composites showed moderate to good filler distribution. DuPont's Nuvolve™ tended to agglomerate randomly up to 100 μm in size, which can cause localized stress concentration and create active sites for crack propagation. Nuvolve™ is a hydrophilic polysaccharide, thus it has poor compatibility with hydrophobic PP. As the sole purpose of reinforcement of plastics is to effectively transfer load away from the continuous phase through shear forces, having optimal adhesion between filler and matrix is desired to attain superior performance properties. The SEM micrographs showed favorable distribution of Nuvolve™ albeit agglomeration in localized areas, as well as fiber pull-out.

The hybridization of Nuvolve™ with glass fiber yielded high performing composites that have enhanced thermal stability and can be exploited in body interior and under-the-hood applications for the automotive industry. The composites use less filler material (compared to Ford's incumbent material) providing an opportunity for lightweighting with the added benefit of integrating a sustainable material in the bill of material (BOM) of components.

Chapter: 4 Determining Mechanical, Thermal, Morphological Properties of Nanocellulose Reinforced Hybrid Composites

4.1 Introduction

The introduction of the national nanotechnology initiative (NNI) in 2001 from the U.S government helped to propel research in nanotechnology that explores control of matter in the nanoscale (1-100 nm) to isolate unique properties for novel applications such as advanced materials for automotive, military and aerospace industries [97]. Nanomaterials derived from renewable biomaterials such as cellulose (most abundant raw polymeric material) can play an undoubtedly huge role for the advancement of new materials that can exploit the intrinsic mechanical and thermal properties of cellulose while ascending away from the dependence of petroleum-based materials used in today's society.

Chapter 2 highlights the chemistry and fabrication of nanocellulose and the superior mechanical properties of nanocellulose crystals (CNC) compared to carbon nanotubes, glass fiber, steel wire, graphite and Kevlar. In the previous chapter micro-polysaccharide/glass fiber reinforced thermoplastic composites were explored and the results showed that the composites encompassed high specific mechanical properties and enhanced thermal stability compared to virgin polypropylene and Ford Motor Company's material specification used in body interior and under-the-hood applications. Beyond the performance of materials, life cycle assessment is also important as future materials should have the ability to be reused, recycled and disposed (compost) via natural pathways that do not harm the environment. At the nanoscale cellulose offers greater mechanical reinforcement with an average value of 130 GPa which is higher than cellulose microfibrils [98]. The increased surface area/volume ratio allows for better transfer of load

between the matrix and the filler material attaining high reinforcement capabilities at lower loadings of filler. As reported by Andrew Finkle, the incorporation of nanomaterials requires only a few percentages by mass to achieve desired mechanical properties that would otherwise need greater than 30 wt.% microparticle content to achieve similar performance [37].

In this chapter, cellulose nanocrystals and cellulose nanofibrils were combined with glass fiber in a polypropylene matrix to yield hybrid composites at various nanocellulose and glass fiber loadings (wt. %) for body interior and under-the-hood automotive applications. Mechanical, thermal and morphological analyses were conducted to assess the reinforcing capabilities, thermal stability and filler-matrix interactions and ultimately conclude the viability of nanocomposites for automotive applications.

4.2 Experimental

Polypropylene (PP) homopolymer pellets, chopped glass fiber filled PP pellets were provided by local suppliers and nanocrystalline-cellulose (CNC) & cellulose nanofibrils (CNF) were supplied by University of Maine's Process Development Center. CNC is 5-20 nm wide and 150-200 nm long and CNF has a nominal fiber width of 50 nm [99]. Polypropylene grafted maleic anhydride (PP-g-MA: locally sourced) was used as a coupling agent to help with the compatibility between the filler and matrix.

CNC masterbatch (5 wt.%) with PP was produced by Ford Motor Company using a wet-compounding process. The CNF masterbatch (5 wt.%) was produced using an extrusion process where dry PP, PP-g-MA and CNF were separately starve-fed into a twin-screw extruder via K-Tron gravimetric feeders using a screw speed of 120 RPM. After extrusion, the materials were immediately quenched in a water bath and kept at room temperature. The compounded materials

from the twin screw extruder were granulated using a lab scale grinder/chopper. CNC and CNF masterbatches were dried (60°C 12 h) before the injection molding step.

CNC and CNF masterbatch with PP (now grounded pellets) was hand-mixed with chopped glass fiber filled PP pellets and then transferred to the injection molder (Boy Machines Model 80M) to process ASTM test specimens for tensile (ASTM-D638), flexural (ASTM D790) and impact (ASTM D256) testing, respectively. The extrusion and injection molding temperature profiles were kept the same as described in Chapter 3.

Table 3.2-3 shows the formulations used in this study, where two variants of nanocellulose were supplied (CNC and CNF) and the control samples used were 5 & 10 wt.% glass fiber reinforced PP, neat PP and Ford Motor Company's material specification (35% total filler content).

Table 4.2-1: Composition of the composites

Formulation	Nanocellulose (wt. %)	Glass fiber (wt. %)	Total filler (wt. %)
Neat PP	---	---	---
0/5	---	5	5
0/10	---	10	10
5CNC/0	5	---	5
2.5CNC/2.5	2.5	2.5	5
2.5CNC/5	2.5	5	7.5
2.5CNC/10	2.5	10	12.5
5CNF/0	5	---	5
2.5CNF/2.5	2.5	2.5	5
2.5CNF/5	2.5	5	7.5
2.5CNF/10	2.5	10	12.5

Figure 4.2-1: Nanocellulose 5% masterbatch with PP; CNF (left) and CNC (right)

Figure 4.2-1 shows a visual representation of the 5 wt.% masterbatch of CNC (right) and CNF (left) with PP. It is clear to see that there is a pigment difference between both samples which is likely an indication of thermal degradation of cellulose related to the processing of the masterbatch.

4.2.1 Mechanical Test & Density Measurement

Tensile, flexural and impact tests were conducted using a universal testing machine (Instron 3366) and a pendulum tester (Testing Machines Inc. 43-02-03 model) in compliance with ASTM D638 (Figure 4.2-2)., ASTM D790 and ASTM D256, respectively The properties of interest were: tensile strength, strain, young's modulus, flexural modulus, flexural strength and impact strength. All mechanical tests were run in an environmentally conditioned room at 23 °C ± 2 °C and 50 ± 5 % relative humidity. Density was measured using an analytical balance (readability down to 0.1mg) and density kit ME-DNY-43 from Mettler Toledo.

Figure 4.2-2: Visual presentation of ASTM D638-10 dogbones of the composite; CNF (left) and CNC (right)

4.2.2 Thermal Characterization

Thermal transitions of the composites and the virgin polymer matrix were analyzed using a differential scanning calorimetry instrument (DSC: TA Instruments Q2000). The samples were prepared by cutting the injection molded ASTM test specimens into small chips obtained from multiple locations of multiple test specimens to minimize possible effects of poor material distribution within the composites. At first the samples were heated from room temperature to 190 °C at a rate of 50 °C/min and held isothermally for 5 min to remove any thermal history incurred from fabrication of the composites. Thereafter, the samples were cooled to 70 °C at 10 °C/min and isothermally held for 5 min before reheating to 190 °C at 10 °C/min. The melting and crystallization transitions were collected from the heat flow versus temperature curves where, melting temperature (T_m) is an endothermic transition and the crystallization temperature (T_c) is an exothermic transition denoted by the peak minimum and maximum respectively. Crystallinity, heat of fusion (ΔH_f) and heat of crystallization (ΔH_c) were also calculated.

Thermal gravimetric analysis (TGA: TA Instruments Q500) was used to study thermal stability of neat PP and the hybrid composites. The samples were heated at 20 °C/min and subjected to

nitrogen from 35 °C to 800 °C at a flowrate of 40mL/min. Samples were prepared similarly to the DSC sample preparation.

4.2.3 Morphology (SEM)

Zeiss 1550 (LEO) scanning electron microscope with accelerating voltage of 5-7 keV was used to observe the morphology of the composites and the neat PP as well as distribution of fillers within the polymer matrix. The samples were fractured from the notched Izod impact tests and sputter-coated with gold to avoid surface charging.

4.3 Results & Discussion

4.3.1 Mechanical Properties: Tensile and Flexural Properties

The effects of different fiber combinations on the tensile and flexural properties of the composites and control samples which include neat PP, PP filled with glass fiber (5 & 10 wt.%) and Ford Motor Company's material specification Figure 4.3-1, Figure 4.3-2, Figure 4.3-3 and Figure 4.3-4. Modulus is a measure of stiffness of a composite and the tensile and flexural modulus increase with the addition of glass fiber and nanocellulose (Figure 4.3-1 and Figure 4.3-2). This can be attributed to the high aspect ratio of CNC and CNF, with the addition of 5 wt.% of nanocellulose the modulus improved by 8% compared to neat PP. Comparing formulation 0/5 (5 wt.% glass fiber) and 5/0 (5 wt.% nanocellulose), the glass fiber has a greater effect on the modulus as opposed to nanocellulose. This could be a factor of the inherent agglomeration of nanocellulose to their strong intermolecular bonds (e.g. hydrogen bonding) which leads to less than desirable distribution of nanocellulose within the composite [100]. Formulation 2.5/10 was able to meet Ford Motor Company's material specification for body interior and under-the-hood applications.

Tensile strength of the composites showed a general trend of increase with increasing filler concentration (Figure 4.3-3). The addition of 5 wt.% of nanocellulose led an increase of 3% compared to neat PP whilst the addition of glass fiber (5 wt.%) led to an increase of 22.6% compared to neat PP. It is clear that the glass fiber has a greater effect on the improvement of tensile strength over nanocellulose. Similarly, this is explained due to the inherent agglomeration of nanocellulose that leads to weak dispersion [101].

Furthermore, tensile strain of the hybrid composites showed a decreasing trend with the addition of glass fiber which was expected as the rigid filler stiffens the composite and hence flexibility suffers (Figure 4.3-4). This agreed with Y. Peng *et al* [100] findings that explored the mechanical properties of CNF reinforced PP composites. Despite the reduction in tensile strain at break; the hybrid composites met the tensile strain at break requirement for body interior and under-the-hood applications detailed by Ford Motor Company with the exception of formulation 2.5/10 slightly performing below the material requirement (1.21 % reduction).

Figure 4.3-5 shows the density reduction (%) in reference to Ford Motor Company's material specification that is being used for body interior and under-the-hood applications. The hybrid composites 5/0, 2.5/2.5, 2.5/5 and 2.5/10 show a density reduction of greater than 15 %. The incorporation of just CNC and CNF showed an average density reduction of 23 % which is a significant amount and therefore the combination of inorganic and naturally sourced filler materials can offer substantial weight savings per vehicle part.

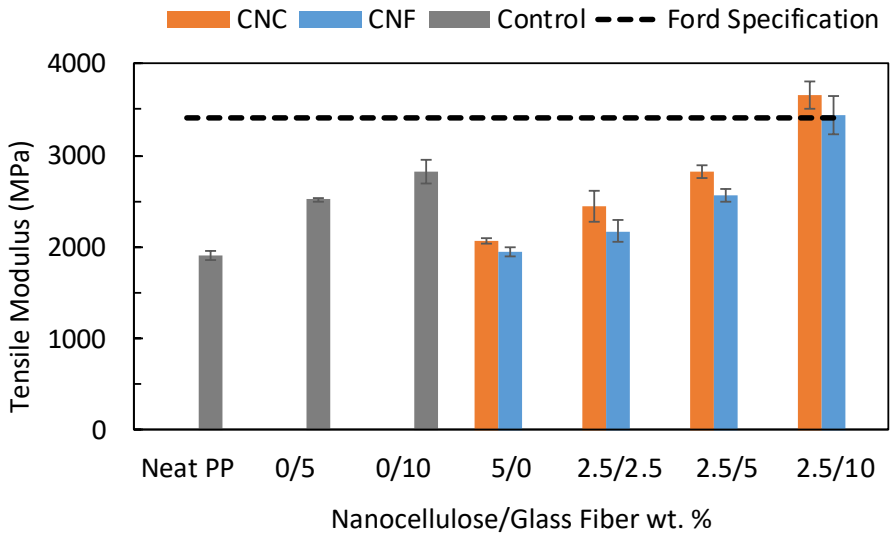

Figure 4.3-1: Tensile Modulus (MPa) of all composites and neat PP

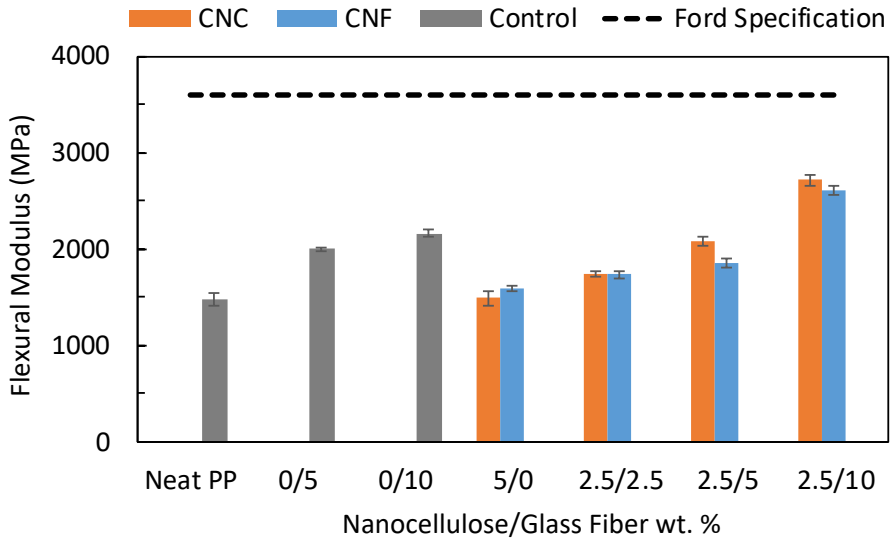

Figure 4.3-2: Flexural Modulus (MPa) of all composites and neat PP

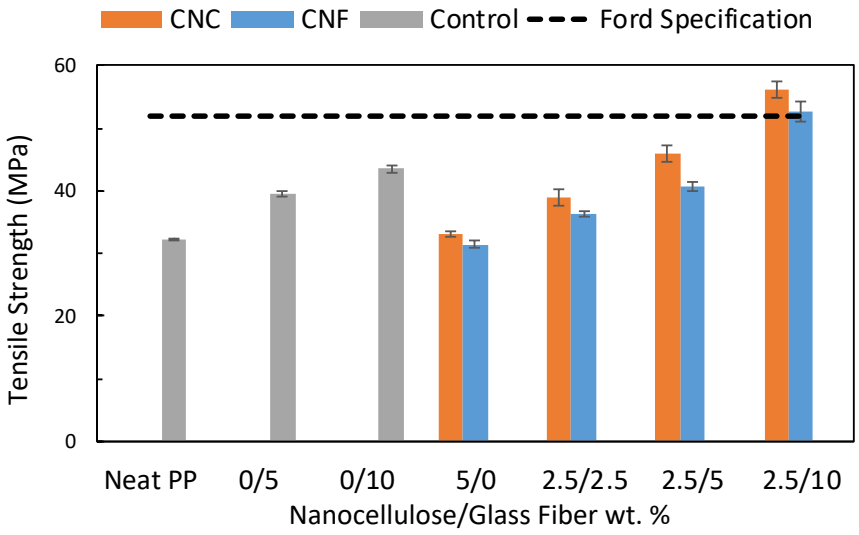

Figure 4.3-3: Tensile Strength (MPa) of all composites and neat PP

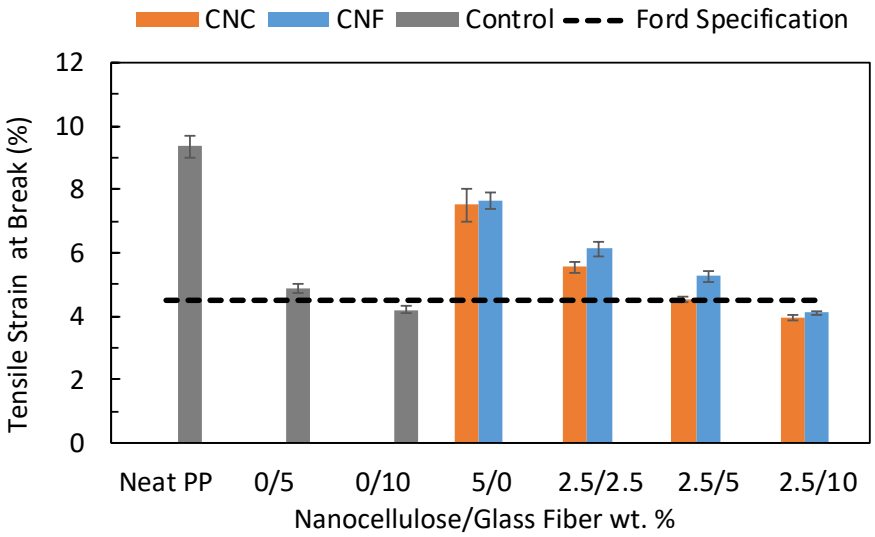

Figure 4.3-4: Tensile Strain at Break (%) of composites and neat PP

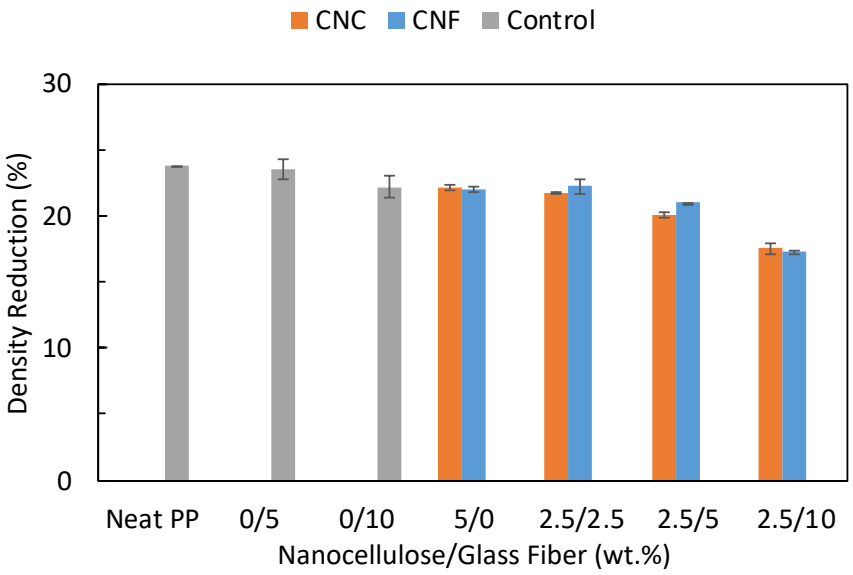

Figure 4.3-5: Density Reduction (%) of all composites and neat PP in reference to Ford's Incumbent Material

4.3.2 Mechanical Properties: Impact Properties

Figure 4.3-6 shows that impact strength decreased by 24 % for formulation 5/0 that contained no glass fiber and this can be associated with the tendency of CNC and CNF agglomerating forming stress concentration that ultimately leads to active sites for crack propagation [100] [64] [65]. This observation was further supported by A.Kiziltas *et al* [102] that showed 5 wt.% of CNF in polyethylene (PE) led to 60 % reduction in impact strength compared to virgin PE. The addition of glass fiber (5 and 10 wt.%) yielded an improvement in impact strength of up to 24 % compared to neat PP. This addition of relatively long glass fiber likely enables additional pathways for energy to dissipate such as fiber pull out as discussed in Chapter 3 [66].

When comparing; formulation 0/10 and 2.5/ an increase of 27 % with the addition of 2.5 wt.% of nanocellulose alone is observed. Moreover, all the hybrid composites showcased superior impact strength with the best performing composite being 2.5/10 showcasing an increase of 64 %

compared to neat PP meeting Ford Motor Company's material specification for body interior and under-the-hood applications.

Moreover, it should also be noted that limited differences in performance were found between CNC and CNF. X. Xu *et al* [49] studied the mechanical performance of CNC and CNF reinforced polyethylene oxide (PEO) composites and showed that CNF composites outperformed CNC composites in strength and modulus. This was attributed to the larger aspect ratio of CNF and the hydrogen bonding between CNF and PEO matrix. It is understood that the preparation of CNC using sulfuric acid hydrolysis replaces few hydroxyl groups with SO_3^{-1} and thereby reduces the potential for hydrogen bonding to occur with PEO compared to CNF. The results shown in this section do not agree with X.Xu *et al* [49] work and can be attributed to the difference in processing method and matrix selection as PEO is a hydrophilic polymer in comparison to PP being hydrophobic. It is likely that the CNC reinforced hybrid composites were dispersed more readily using the wet compounding process compared to the dry melt-blending step for CNF reinforced hybrid composites which is prone to agglomeration.

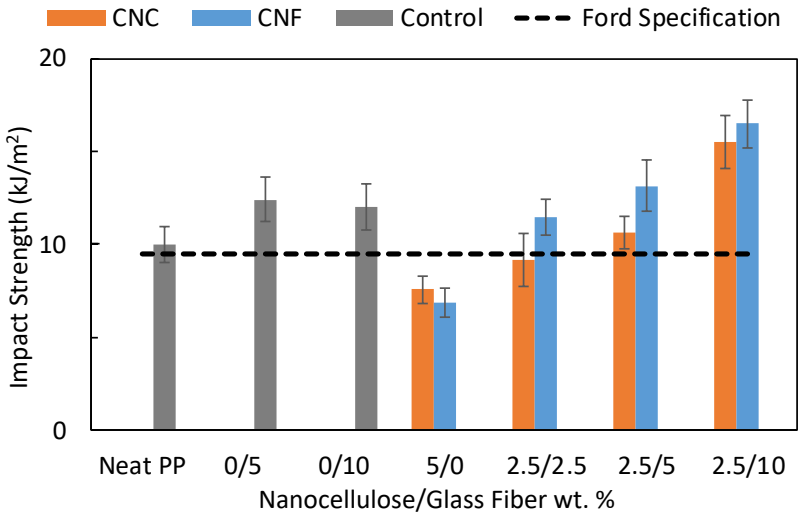

Figure 4.3-6: Impact Strength (kJ/m^2) of all composites and neat PP

4.3.3 Morphological Properties

Morphological analyses on hybrid composites were conducted to study the interfacial bonding and the degree of interaction between the continuous polymer phase and filler material which in this case is the nanocellulose (CNC and CNF) and glass fiber. As illustrated in the previous chapter, optimizing the interfacial interaction between filler and matrix is directly related to the composite's mechanical performance as the filler's sole duty is to effectively transfer load from the polymer matrix through shear stresses [45]. Figure 4.3-7 shows the SEM micrograph of neat PP.

It was apparent from previous SEM work that identifying nanocellulose on the SEM micrograph is difficult, therefore formulation 5/0 for CNC and CNF were treated with sulfuric acid (99.9% concentrated) with the same methodology described in Chapter 3 to identify and evaluate the particle distribution of nanocellulose.

Figure 4.3-8 shows moderate distribution of CNC within the composite (shown as voids). Agglomeration up to 30 μm wide and 50 μm long is observed. Similar findings were seen with formulation 5CNF/0 demonstrating agglomeration of up to 100 μm (Figure 4.3-10). Agglomeration leads creates stress concentrations and lead to the formation of crack propagation that can adversely impact mechanical properties as seen in Section 4.3.2; where the addition of solely 5 wt.% of nanocellulose reduced the impact strength by 24 % compared to neat PP. This effect is pronounced in the CNF composite (5CNF/0) more so than the CNC (5CNC/0) composite. The disparity in the degree of agglomeration formation is likely due to the difference in the fabrication process for both composites. Figure 4.3-9 shows the same sample(5CNC/0) without acid treatment clearly showing the difficulty in identifying CNC from the SEM micrograph.

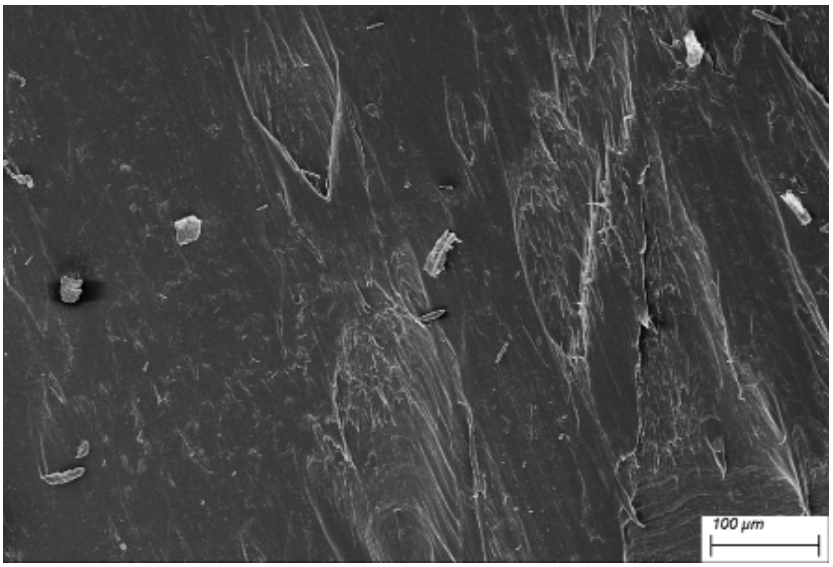

Figure 4.3-7: SEM micrograph of Neat PP at 500x magnification

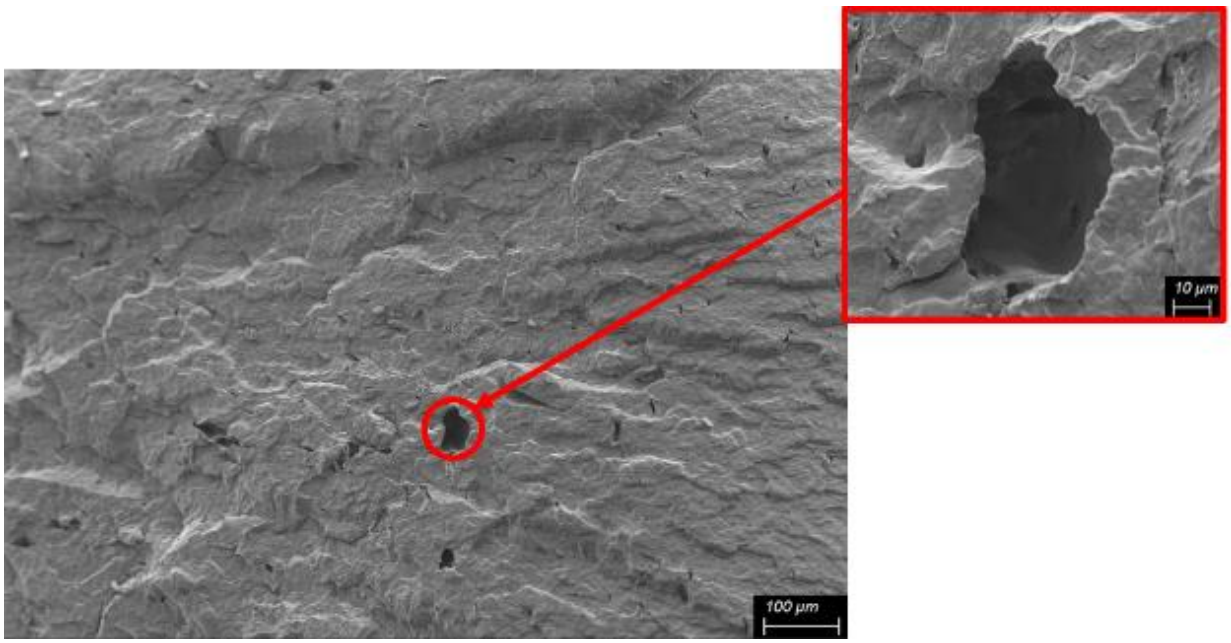

Figure 4.3-8: SEM micrograph of 5CNC/0 (treated with sulfuric acid) at 250x magnification

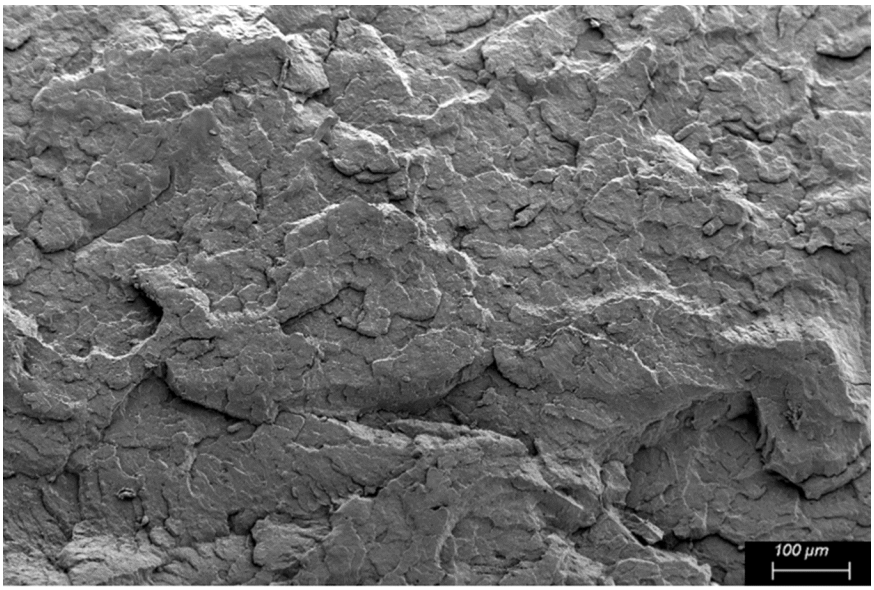

Figure 4.3-9: SEM micrograph of 5CNC/0 (no treatment) at 250x magnification

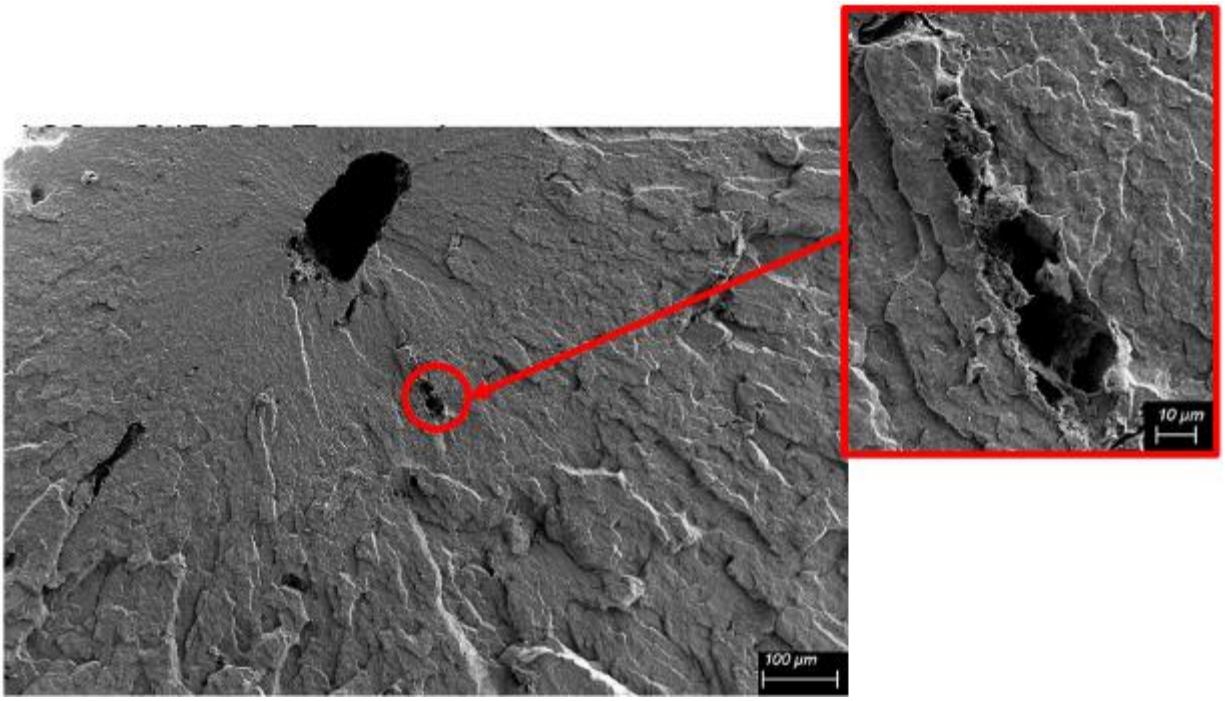

Figure 4.3-10: SEM micrograph of 5CNF/0 (treated with sulfuric acid) at 100x magnification

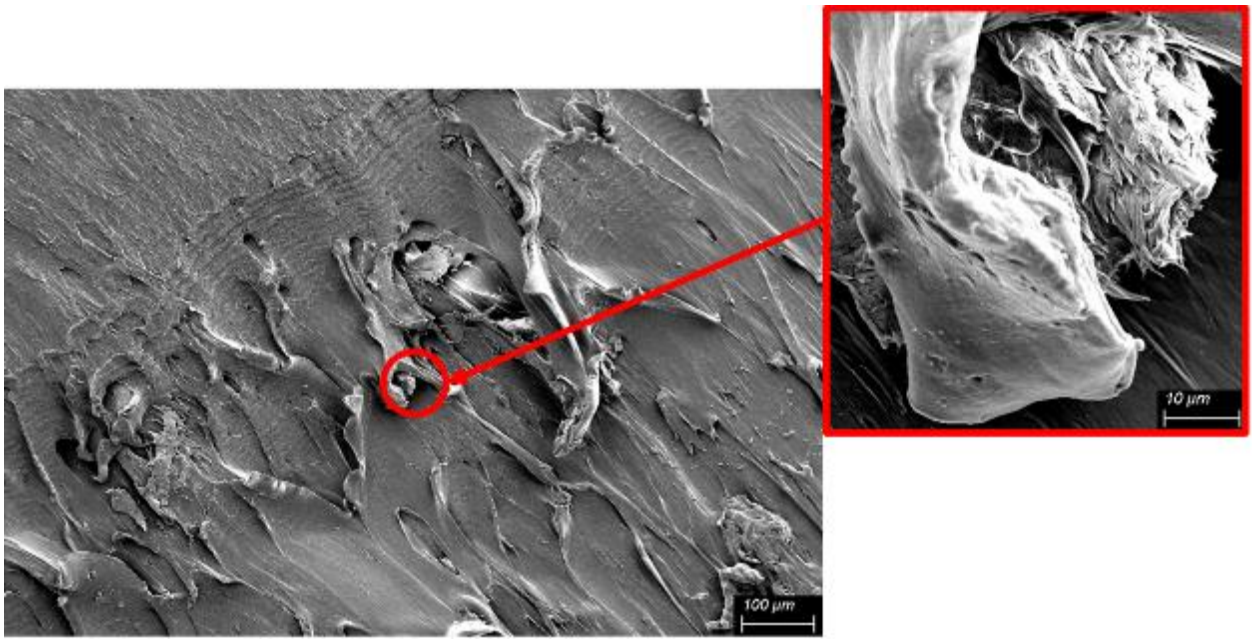

Figure 4.3-11: SEM micrograph of 5CNF/0 (untreated) at 100x magnification

Figure 4.3-12 shows another region on sample 5CNF/0 (untreated) with an agglomerated particle, this seems to be a repeated phenomenon which is likely due to the high intermolecular forces such as hydrogen bonding keeping the particles together.

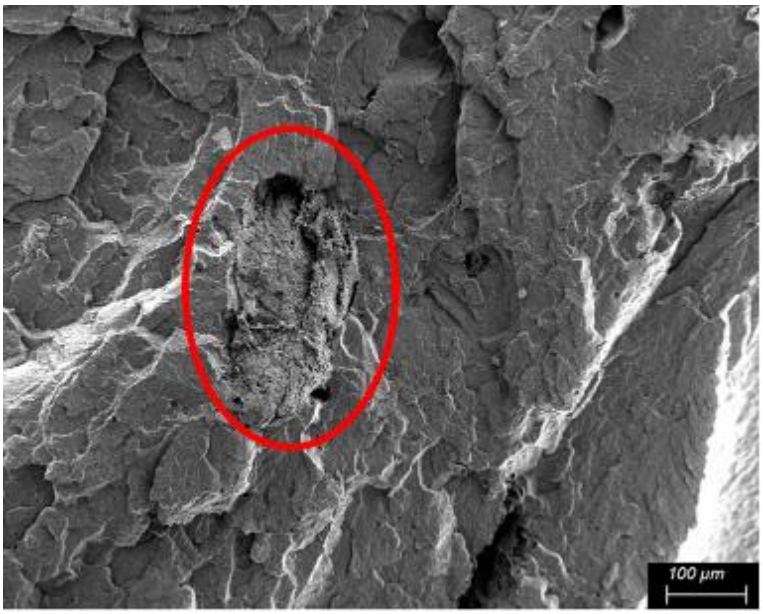

Figure 4.3-12: SEM micrograph of 5CNF/0 (untreated) at 100x magnification

The mechanical analysis suggested that the best performing composite that exceeded Ford's material specification was formulation 2.5/10 exemplifying exceptional tensile, flexural and impact properties as well as achieving a reduction in filler content by 22.5 % for body interior and under-the-hood applications. Figure 4.3-13 shows an SEM micrograph of the 2.5CNC/10 formulation and it is clear that the composite is showing good distribution of glass fiber. Further inspection shows fiber pull-out which is a fracture mechanism when the composite is exposed to a load. Fiber pull-out occurs when the stresses are transferred to the fiber from the matrix and when the stress level exceeds the fiber stress, then the fractured fibers are pulled out from the matrix [103]. This mechanism can aid in improving the impact strength of the composites as seen in Section 4.3.2 [66] [70]. This effect is further amplified by good interfacial bonding between glass fiber and PP matrix seen in Figure 4.3-14.

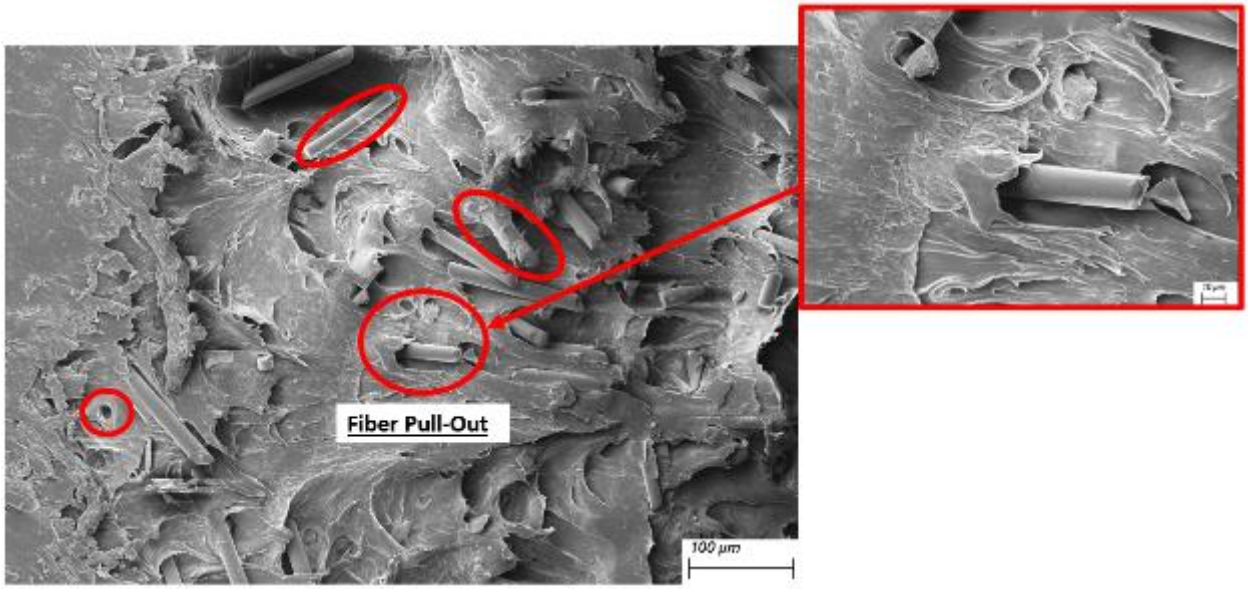

Figure 4.3-13: SEM micrograph of 2.5CNC/10 at 500x magnification, fiber pull-out (red)

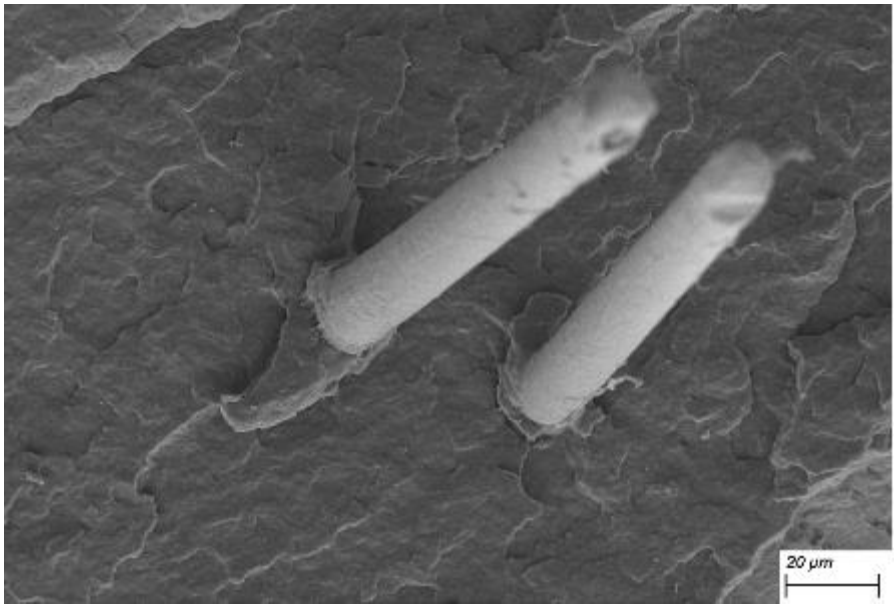

Figure 4.3-14:SEM micrograph of 2.5CNF/2.5 at 2000x magnification showing good wetting of the glass fibers by PP

Figure 4.3-15 shows a CNF fibril network of 300 µm long. This further supports the lower mechanical properties of CNF hybrid composites compared to CNC hybrid composites (although

being very small) due to the average size of the particles. Networks of that size suggests that CNF is not evenly distributed through the composite (agglomeration) yielding anisotropic properties. This is further amplified by formulation 2.5CNF/10 (Figure 4.3-16) where a 250 µm long and 120 µm wide fibril network is observed.

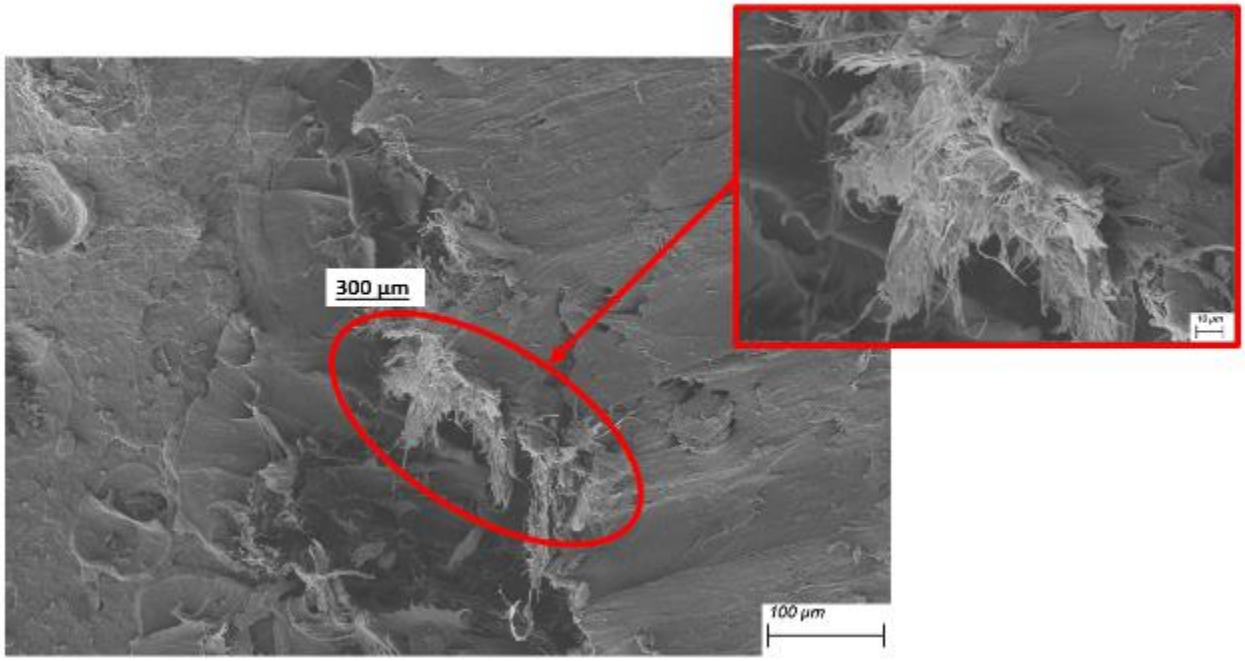

Figure 4.3-15: SEM micrograph of 5CNF/0 at 500x magnification

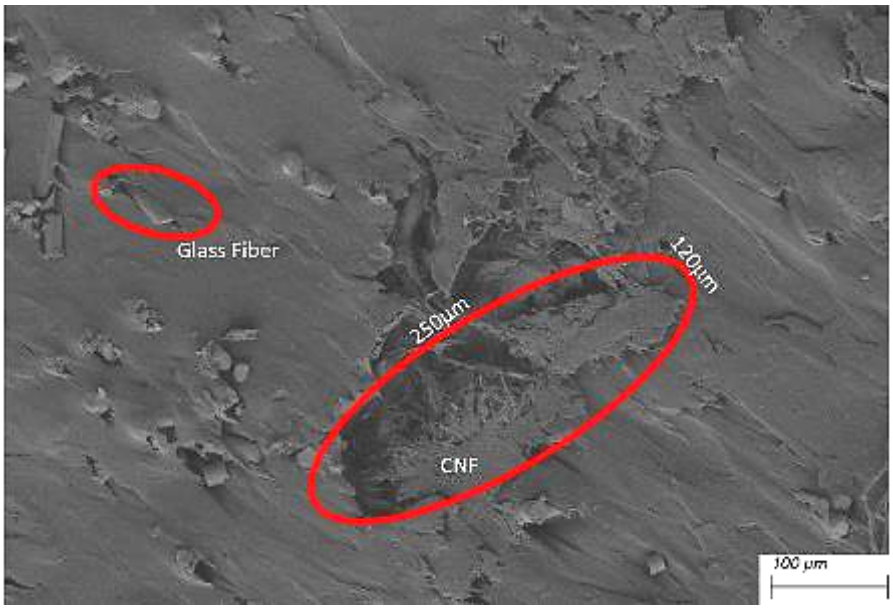

Figure 4.3-16: SEM micrograph of 2.5CNF-10 at 500x magnification

4.3.4 Performance and Cost Analysis of the Hybrid Composites

Similarly to Chapter 3, Figure 4.3-17 shows significant improvements in density by the hybridization of glass fiber and nanocellulose in PP; however the flexural modulus of the hybrid composites did not meet Ford Motor Company's material specification for body interior and under-the-hood applications. When comparing the specific flexural modulus as function of total filler loading (wt.%); it is clear that the best performing composite formulation 2.5/10 is equivalent to the Ford Motor Company's material specification while only utilizing 12.5 wt.% of total filler concentration as opposed to 35 wt.% (Figure 4.3-18).

Furthermore, the cost of the hybrid composites showed an increase in cost with the incorporation of nanocellulose (Figure 4.3-19). Formulation 5/0 for CNC reinforced hybrid composites cost 0.38 $/L more than t Ford Motor Company material specification. High cost is associated with the manufacture of CNC due to the various solvents used as well as acid hydrolysis

to alleviate amorphous domains from the cellulose structure. Formulation 2.5/10 for CNC reinforced hybrid composites showed an increase in cost of 0.19 $/L compared to the Ford Motor Company material specification. The CNF hybrid composites, specifically formulation 2.5/10 showed promising results with the specific flexural modulus being slightly below the Ford Motor Company material specification as well as being cost neutral. The incorporation of sustainable material incurs a premium price, however with the hybridization of glass fiber and nanocellulose the price can be brought down.

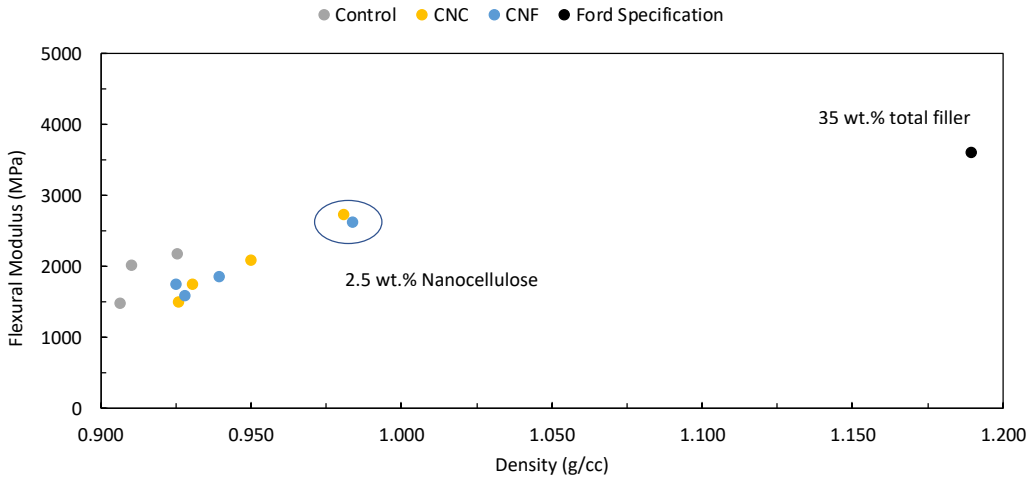

Figure 4.3-17: Flexural Modulus (MPa) vs. Density (g/cc)

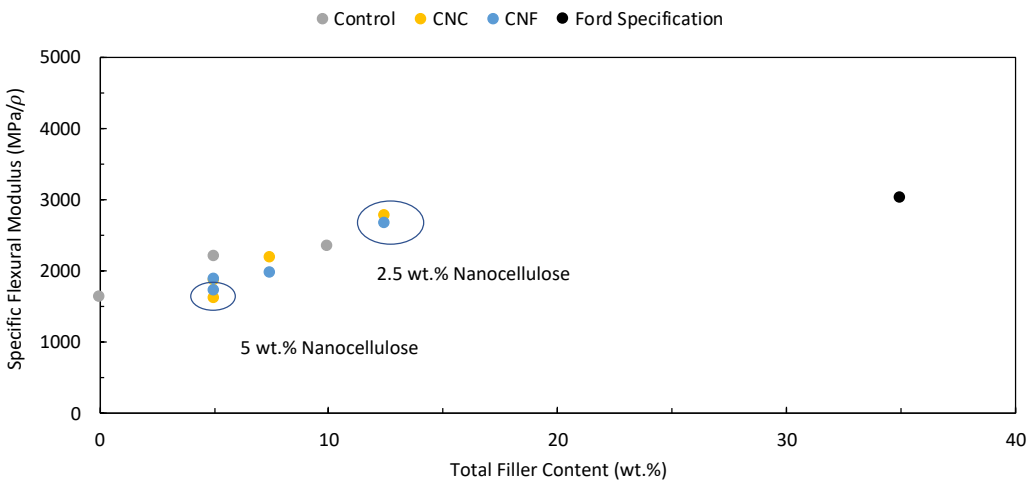

Figure 4.3-18: Specific Flexural Modulus (MPa/ρ) vs. Total Filler Concentration (wt.%)

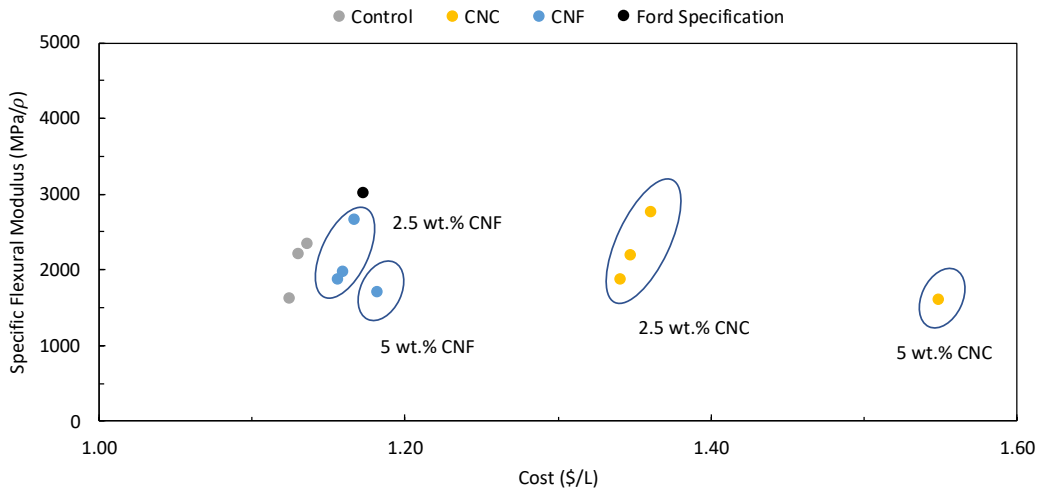

Figure 4.3-19: Specific Flexural Modulus (MPa/ρ) vs. Cost ($/L)

4.3.5 Thermal Properties

In this section the thermal stability of the hybrid composites containing nanocellulose (CNC & CNF) and glass fiber were evaluated using thermal characterization methods such as thermogravimetric analysis (TGA) and differential scanning calorimetry (DSC). Plastic usage in automobiles have steadily increased over the years to replace metals for lightweighting and cost-

reduction. Due to these changes plastic material requirements need to be compliant to be used in harsh environments. Thermogravimetric analysis (TGA) enables the study of weight change as a function of temperature, where the degradation temperature of a composite's main constituents are analyzed. Furthermore, differential scanning calorimetry (DSC) measures the difference in the amount of heat required for a sample to increase temperature as a function of temperature. This technique enables the study of endothermic and exothermic pathways the sample exhibits; characterizing the melting and crystallization temperatures.

Figure 4.3-20 shows the TGA curves for CNC and CNF reinforced hybrid composites. Two transitions (minor and major) can be observed from the TGA curves, the minor transition is more pronounced on the CNC reinforced hybrid composites. This transition happens between 250-300 ºC and is attributed to the degradation of CNC. Previous work on nanocellulose confirms this transition to happen between 200-300 ºC [104].

The onset degradation temperature of the composites were identified at 1% conversion. Table 4.3-1 outlines the results for the onset degradation temperature and temperatures at 10 and 15 % weight loss. The hybrid composites exhibited higher thermal stability compared to neat PP. The addition of 5 wt.% led to an increase 3 and 6 ºC in temperatures at 10 and 15 % weight loss compared to neat PP. The onset degradation temperature of PP was retarded by the addition of filler materials. Formulation 2.5/10 (nanocellulose/glass fiber wt.%) showed a 32 ºC increase in the onset degradation temperature of PP compared to neat PP. The increase in thermal stability is attributed to the hindered diffusion of volatile decomposition products within the polymer nanocomposites [105] [106] . Similar results were reported by M.D.R Batista *et al* [54] and A. Kiziltas *et al* [106] showing improved thermal stability with the addition of micro and nanocellulose in PP.

The thermogravimetric results showed that addition nanocellulose and glass fiber enhances the thermal stability. With respect to processing, nanocellulose (CNC and CNF) showed that it will be stable when incorporated in a melt blending step with PP with temperature profiles ranging from 190-210 ºC [72]. Equally, the hybrid composites demonstrated suitability to be employed in under-the-hood components that can withstand operating temperatures of 120 ºC [73].

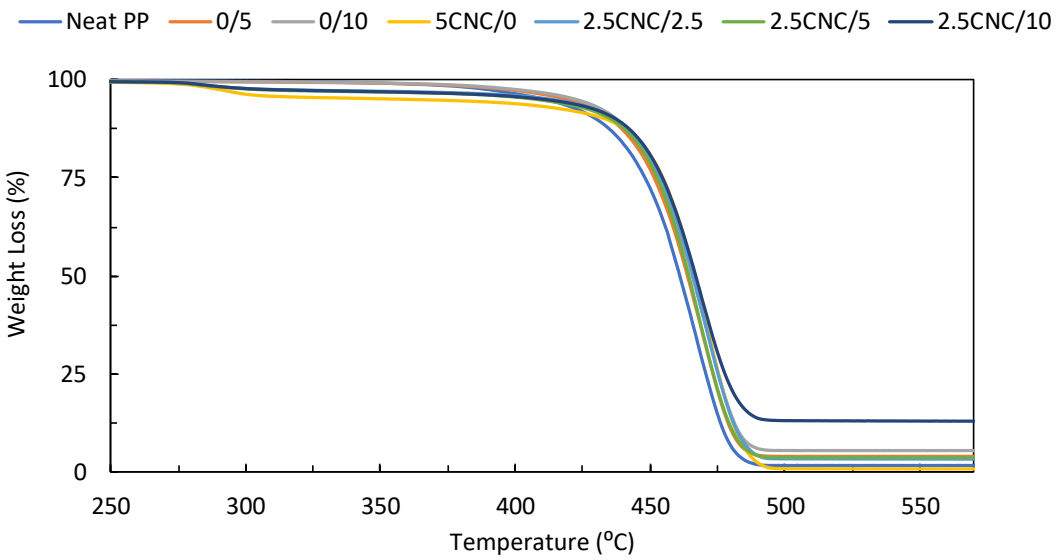

Figure 4.3-20: TGA curves for CNC hybrid composites

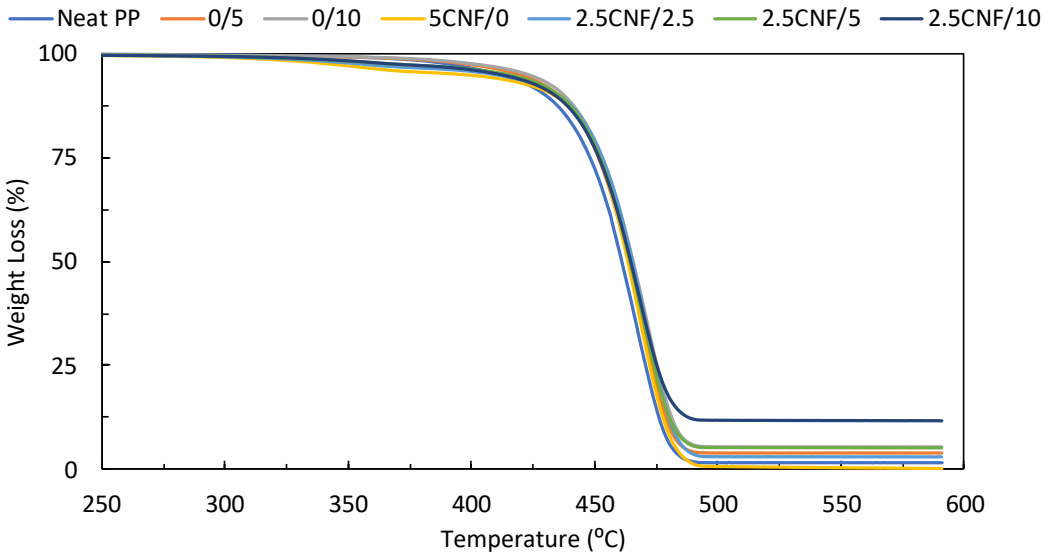

Figure 4.3-21: TGA curves for CNF hybrid composites

Table 4.3-1: Thermogravimetric data for hybrid composites reinforced by CNC and CNF

Formulation	Onset Degradation Temperature of PP (°C)	Temperature at 10% Weight Loss (°C)	Temperature at 15% Weight Loss (°C)
Neat PP	368	430	439
0/5	371	435	443
0/10	371	438	445
5CNC/0	395	434	445
2.5CNC/2.5	395	437	445
2.5CNC/5	391	436	444
2.5CNC/10	396	438	446
5CNF/0	406	433	443
2.5CNF/2.5	402	435	444
2.5CNF/5	403	436	443
2.5CNF/10	400	434	442

Figure 4.3-22 and Figure 4.3-23 show the DSC cooling curves for CNC and CNF-hybrid composites. The peak and onset crystallization temperatures of CNC and CNF-hybrid composites decreased up to 3 % compared to neat PP (Table 4.3-2). The onset crystallization temperatures were estimated at a defined temperature range of 105-160 ºC for consistency. This trend is similar to findings observed in Chapter 3, where increasing amount of total filler content had a supressing effect on the onset and peak crystallization temperature. This has been observed by A.Kiziltas *et al* [88] and A. Buchenauer [79] utilizing micro-crystalline cellulose and wood fiber in thermoplastics.

Y. Amintowlieh *et al*, [75] reported that wood fiber reinforced polyamide composites exhibited higher values for crystallization temperatures compared to neat PP inferring that the wood fiber acted like a nucleating agent. Similar results were reported by Y. Feng *et al* [74]. This type of nucleation is referred to as heterogeneous nucleation induced by the presence of foreign particles in the continuous polymer matrix [17]. Heterogeneous nucleation can result in faster part production and lower cycle times which is beneficial in a manufacturing process.

Moreover, the crystallinity of the hybrid composites (Equation (**3**) showed little to no significant changes compared to neat PP, where a slight increase of crystallinity was observed with the addition of nanocellulose (Table 4.3-2). This is supported by D.J Gardner *et al* work on CNF reinforced PP composites where negligible effects on crystallinity were observed with the addition of nanocellulose. This result was compared to micro-crystalline cellulose (MCC) reinforced PP composites showing that greater than 10 wt.% loading of MCC decreased crystallinity which was postulated to be the cause of agglomeration and phase segregation [106]. X.Xu *et al*l also reported that the crystallinity of nanocellulose reinforced PEO composites decreased at filler loading above 10 wt.%; again, credited to the formation of agglomerates [49]. In contrast, the peak and onset

melt temperatures for the hybrid composites were consistent with neat PP showing marginal effect by the addition of filler material (Figure 4.3-24 and Figure 4.3-25).

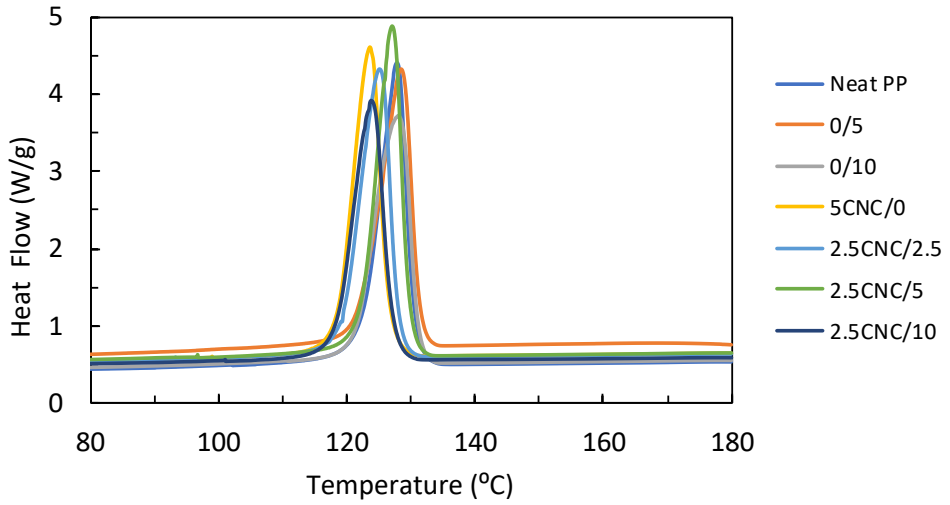

Figure 4.3-22: DSC cooling curve for CNC-hybrid composites

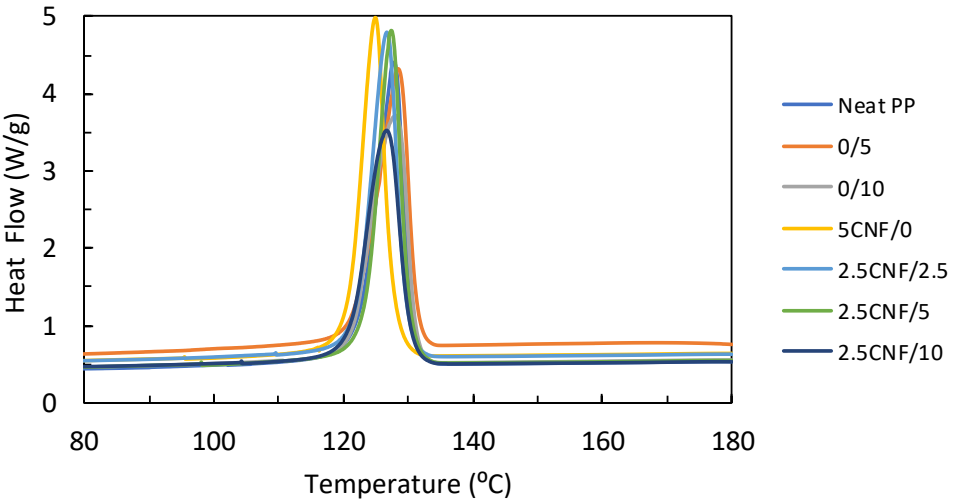

Figure 4.3-23: DSC cooling curves for CNF-hybrid composites

Table 4.3-2: Differential scanning calorimetry (DSC) data

Formulation	Peak Crystallization Temperature (ºC)	Onset Crystallization Temperature (ºC)	Crystallinity (%)
Neat PP	128	131	64
0/5	128	131	70
0/10	128	131	66
5CNC/0	124	127	69
2.5CNC/2.5	125	128	68
2.5CNC/5	127	130	72
2.5CNC/10	124	127	67
5CNF/0	125	128	68
2.5CNF/2.5	127	130	69
2.5CNF/5	127	130	67
2.5CNF/10	127	130	64

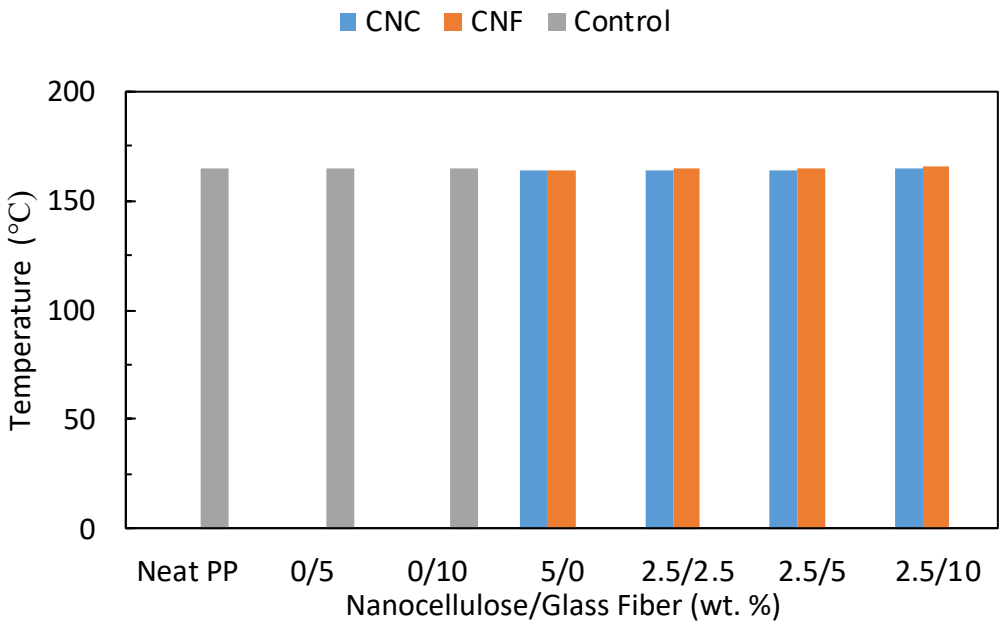

Figure 4.3-24: Peak melt temperature (T_m)

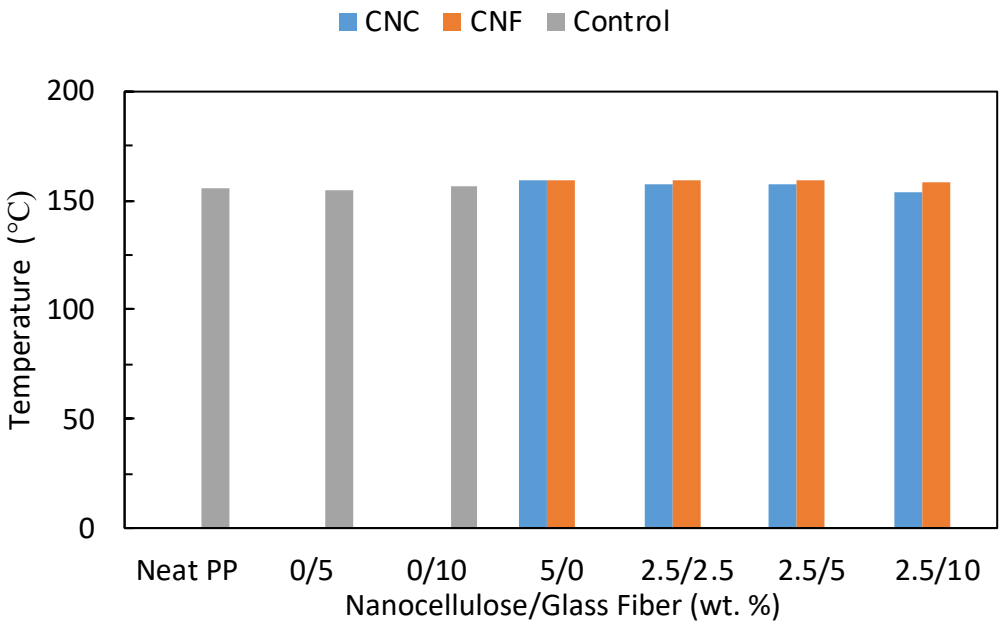

Figure 4.3-25: Onset melt temperature (T_m)

4.4 Conclusion

The development of hybrid composites with nanocellulose and glass fiber as fillers in a PP matrix were investigated. Two variants of nanocellulose were used in this study: cellulose nanocrystals (CNC) and cellulose nanofibrils (CNF. The composites were formulated by varying the nanocellulose and glass fiber loadings (wt. %) and the total filler content did not exceed 15 wt. %. Mechanical, thermal and morphological properties according to ASTM were analyzed and compared to Ford Motor Company's material specification used fleet-wide for body interior and under-the-hood applications.

The mechanical properties of the composites showed general increase in performance with glass fiber content and the opposite with nanocellulose content. The best performing formulation was 2.5/10 where only 12.5% total filler content was utilized. CNC reinforced hybrid composites performed marginally better than CNF reinforced hybrid composites. The flexural modulus of the 2.5/10 composite just fell under the Ford Motor Company's material specification and this can be improved by increasing the total filler content (not desired) or incorporating a filler with a higher aspect ratio. Formulation 2.5/10 produces a 22.5 % decrease in total filler content compared to Ford Motor Company's material specification and hence provides for significant weight savings.

The thermal stability of the composites showed improvements in comparison to neat PP, where CNC and CNF hybrid reinforced composites showed increased thermal stability. Similar to Chapter 3, the crystallization temperature (T_c) of the composites decreased revealing that nanocellulose is not a nucleating agent enabling crystallization to occur sooner and hence reducing cycle times in processing of the composites.

The SEM micrographs of the CNC hybrid composites showed moderate distribution of CNC within the composite with areas of agglomeration. CNF hybrid composites showed pronounced areas of fibril networks forming (agglomerates) thereby highlighting poor dispersion of the CNF within the PP matrix. This observation clarifies the difference in mechanical performance (although only marginally) between CNC and CNF reinforced hybrid composites. Cellulose are inherently hydrophilic whereas PP is hydrophobic; therefore, the two polymers are incompatible. For effective transfer of load through shear forces the interfacial interactions between the filler and matrix need to be optimal to attain superior performance properties. The nanocomposites shown in this study demonstrated less than desirable dispersion and adhesion properties specifically for the CNF reinforced hybrid composites. To improve the interfacial interactions, a higher concentration of maleic anhydride can be incorporated to form chemical bonds between the continuous hydrophobic polymer phase and the hydrophilic filler phase.

The Nanocomposites studied in this chapter exploited the inherent mechanical properties of nanocellulose at a fraction of the total filler content currently used by Ford Motor Company for body interior and under-the-hood applications. This improvement in physical properties and reduction in density as much as 17 % is a stepping stone for the application of nanocomposites in the automotive industry.

Chapter: 5 Conclusion and Recommendation

5.1 Conclusion

The overall objective of this study was to investigate the influence of natural, biodegradable filler material on the overall mechanical and thermal properties when combined with glass fiber in a polypropylene (PP) matrix. Two polysaccharide morphologies were explored at the micro and nanoscale that include DuPont's Nuvolve™ and nanocellulose. The results of this study demonstrated that high performing composites can be produced with varies polysaccharide morphologies (micro and nano) while providing significant lightweighting opportunities for body interior and under-the-hood applications. The following are a summary of findings presented in this thesis work:

1. Nuvolve™ reinforced hybrid composites showed enhanced mechanical properties that exceeded Ford Motor Company's material specification for body interior and under-the-hood applications. The best performing composites were formulations that contained 10 wt.% Nuvolve™ and 15 wt.% glass fiber (10/15) and 10 wt.% Nuvolve™ and 20 wt.% glass fiber (10/20). Ultimately decreasing the filler content by 10% compared to Ford Motor Company's material specification achieving a density reduction of up to 13%.

2. Incorporation of Nuvolve™ yielded composites with lower thermal stability compared to neat PP. However, the addition of the filler materials retarded the degradation of PP. The crystallization temperatures of the hybrid composites decreased unveiling that Nuvolve™ does not have a nucleating effect. Furthermore, there is little to no

difference in performance between two variants of Nuvolve™: Nuv-A (5 μm) and Nuv-B (20 μm) and thereby enabling commercial potential for Nuv-B.

3. Melt rheology of the Nuvolve™ reinforced hybrid composites showed that the addition of filler content increased the complex viscosity, storage modulus and loss modulus compared to neat PP.

4. Nanocellulose reinforced hybrid composites also showed improved mechanical properties with the best performing composite only utilizing 12.5 wt.% of total filler content (2.5 wt.% nanocellulose & 10% wt.% glass fiber). There is a 22.5% reduction in total filler content yielding a density reduction of greater than 15% compared to Ford Motor Company's material specification.

5. Thermal stability of the nanocellulose reinforced hybrid composites showed an improvement over neat PP. Similarly, to Nuvolve™, the nanocellulose did not act as a nucleating agent.

6. Overall, hybridization of natural sourced filler material with glass fiber yielded high performing composites exemplifying lightweighting and sustainability in the automotive industry.

5.2 Recommendation for Future Work

The morphological study performed on the polysaccharide reinforced hybrid composites showed that dispersion and distribution of filler materials can be further optimized. I have summarized below what can be done to improve dispersion and distribution which is related to the performance properties of the composites as well as other analysis that be performed on the composites.

1. The incorporation of an additional extrusion step could aid with the dispersion of Nuvolve™ and nanocellulose, however this would increase production cost

2. SEM micrographs also showed aggregation of Nuvolve™ and nanocellulose which has a negative impact on the physical properties of the composite. This could be improved with increasing the amount of maleic anhydride being incorporated in the formulations. Maleic anhydride helps to compatibilizer the hydrophilic polysaccharide with the hydrophobic polypropylene resulting in better dispersion. Another way to improve dispersion is using a carrier fluid such as water to create an emulsion system separating the individual particles. This of course would require extensive drying to be employed, which would add considerable cost to the fabrication process.

3. Future work should encompass accelerated aging studies for predicting long term performance such as high temperature and high humidity tests as well as water absorption test for extended application in exterior of an automobile.

Chapter: 6 Bibliography

[1] B. Fry, Working with Polyethylene (Speaking of Plastic Manufacturing), Dearborn: Society of Manufacturing Engineers, 1999.

[2] L. Miller, K. Soulliere , S. Beaulieu, S. Tseng and E. Tam, "Challenges and Alternatives to Plastics Recycling in the Automotive Sector," *Materials,* pp. 5883-5902, 2014.

[3] Department of Transportation (National Highway Traffic Safety Administration), "2017 and Later Model Year Light-Duty Vehicle Greenhouse Gas Emissions," *Federal Register,* vol. 77, no. 199, pp. 62623-63200, 2012.

[4] A. Langhorst, J. Burkholder, J. Long, A. Kiziltas and D. Mielewski, "Blue-Agave Fiber Reinforced Polypropylene Composite for Automotive Applications," *BioResources,* vol. 13, no. 1, 2018.

[5] A. Mohanty, M. Misra and L. Drzal, Natural Fibers, Biopolymers, and Biocomposites, Boca Raton: CRC Press Taylor & Francis Group, 2005.

[6] D. Sauter, M. Taoufik and C. Boisson, "Polyolefins, a Success Story," *Polymers,* vol. 9, pp. 185-198, 2017.

[7] C. Crawford and B. Quinn, "4-Physiochemical Properties and degradation," in *Microplastic Pollutants*, Elsevier, 2017, pp. 57-100.

[8] A. Shamiri, M. Chakrabatri, S. Jahan, M. Husaain, W. Kaminsky, P. Aravind and W. Yehye, "The Influence of Ziegler-Natta and Metallocene Catalysts on Polyolefin Structure, Properties and Processing Ability," *Materials,* pp. 5069-5108, 2014.

[9] A. Alshaiban, "Active Site Identification and Mathematical Modelling of Polypropylene Made with Ziegler-Natta Catalysts," Unverisity of Waterloo, Waterloo,ON, 2008.

[10] Z. Moore, "Polypropylene," ICIS Chemical Business, Houston,TX, 2018.

[11] S. Moritomi, T. Watanbe and S. Kanzaki, "Polypropylene Compounds for Automotive Applications," Sumitomo Kagaku, Japan, 2010.

[12] A. Patil, A. Patel and R. Purohit, "An overview of Polymeric Materials for Automotive Applications," in *Materials Today: Proceedings* , 2017.

[13] B. Vieille, W. Albouy, L. Taleb and L. Chevalier, "About the influence of stamping on thermoplastic-based composites for aeronautical applications," *Composites. Part B, Engineering,* vol. 45, pp. 821-834, 2013.

[14] R. Dargazany, M. Itskov and E. Poshtan, "Constitutive modeling of strain-induced crystallization in filled rubbers," *Physical Revew ,* no. 89, 2014.

[15] Princeton University, "Nucleation and Growth," Princeton University , [Online]. Available: https://scholar.princeton.edu/hajakbar/nucleation-and-growth. [Accessed 5 11 2019].

[16] University of Cambridge, "Spherulites and optical properties," [Online]. Available: https://www.doitpoms.ac.uk/tlplib/polymers/spherulites.php. [Accessed 12 11 2019].

[17] R. Huang and G. Zhong, "On transcrystallinity in semi-crystalline polymer composites," *Composites Science and Technology ,* vol. 65, pp. 999-1021, 2005.

[18] Mettler Toledo, "Different types of nucelation," 2017.

[19] M. Etcheverry and S. Barbosa, "Glass Fiber Reinforced Polypropylene Mechanical Properties Enhancment by Adhesion Improvement," *Materials,* pp. 1084-1113, 2012.

[20] Q. Li, G. Zheng, K. Dai, M. Xie, M. Liu, C. Liu, C. Liu, B. Liu, X. Zhang, B. Wang, J. Chen, C. Shen, Q. Li and X. Peng, "β-transcrystallinity developed from the novel ringed nuclei in the glass fiber/isotactic PP composite," *Materials Letters,* vol. 65, pp. 2274-2277, 2011.

[21] Y. Li, W. Shi, J. Li, C. Yang, T. Xia, X. Sheng and X. Wang, "Structure and Properties of Glass Fiber Reinforced Polypropylene/Liquid Crystal Polymer Blends," *Journal of Macromolecular Science Part B: Physics,* vol. 54, pp. 1144-1152, 2015.

[22] J. Hollbery and D. Houston, "Natural-Fiber-Reinforced Polymer Composites in Automotive Applications," *JOM,* vol. 58, no. 11, pp. 80-86, 2006.

[23] S. Joshi, L. Drzal, A. Mohanty and S. Arrora, "Are natural fiber composites environmentally superior to glass fiber reinforced composites?," *Composites Part A: applied science and engineering,* vol. 35, pp. 371-376, 2004.

[24] F. Wallenberger, J. Watson and H. Li, "Glass Fibers," *ASM Handbook,* vol. 21, 2001.

[25] P. Chu, "Glass Fiber-Reinforced Polypropylene," in *Handbook of Polypropylene and Polypropylene Composites*, New York, Marcel Dekker, Inc., 2003, pp. 1-71.

[26] G. Witucki, "A silane primer: chemistry and applications of alkoxy silanes," *Coatings Technology,* pp. 65-67, 1993.

[27] F. Ramsteiner and R. Theysohn, "The Influence of Fibre Diameter on the Tensile Behaviour of Short-glass fibre Reinforced Polymers," *Composite Science and Technology,* vol. 24, pp. 231-240, 1985.

[28] R. Clark, "Talc in Polypropylene," in *Handbook of Polypropylene and Polypropylene Composites*, New York, Marcel Dekker,Inc., 2003, pp. 1-30.

[29] P. Malacari, "Talc in Automotive Applications," in *8th Chinese Industrial Minerals Conference* , Qungdao, 2009.

[30] D. Chung, "Chapter 4: Properties of Carbon Fibers," in *Carbon Fiber Composites*, Elsevier Inc. , 1995, pp. 65-78.

[31] B. Newcomb, "Processing, structure, and properties of carbon fibers," *Composites: Part A,* vol. 91, pp. 262-282, 2016.

[32] F. Rezaei, R. Yunus, A. Ibrahim and E. Mahdi, "Development of Short-Carbon-Fiber-Reinforced Polypropylene Composite for Car Bonnet," *Polymer-Plastics Technology and Engineering,* vol. 47, pp. 351-357, 2008.

[33] J. Duflou, J. De Moor, I. Verpoest and W. Dewulf, "Environmental impact analysis of composite use in car manufacturing," *CIRP Annals-Manufacturing Technology ,* vol. 58, pp. 9-12, 2009.

[34] E. Beckman, "World Economic Forum," 12 August 2018. [Online]. Available: https://www.weforum.org/agenda/2018/08/the-world-of-plastics-in-numbers. [Accessed 16 July 2019].

[35] A. Pinket, K. Marsh, S. Pang and M. Staiger, "Ionic Liquids and Their Interaction with Cellulose," *Chemical Reviews,* vol. 109, pp. 6712-6728, 2009.

[36] I. Trachevsky and G. Marchenko, Cellulose: Biosynthesis and structure, Berlin: Springer-Verlag, 1991.

[37] A. Finkle, "Cellulose – Polycarbonate Nanocomposites: A novel automotive window alternative," University of Waterloo, Waterloo,ON, 2011.

[38] A. Chakraborty, M. Sain and M. Kortschot, "Cellulose microfibrils: A novel method of preparation using high shear refining and cryocrushing," *Holzforschung,* vol. 59, no. 1, pp. 102-107, 2005.

[39] A. Rouchi, "Discovery of guiding proteins reshapes thinking in the field of lignin and lignan biosynthesis.," *Chemical & Engineering News,* pp. 29-32, 2000.

[40] C. Miao and W. Hamad, "Cellulose reinforced polymer composites and nanocomposites: a critical review," *Cellulose,* vol. 10, pp. 2221-2262, 2013.

[41] F. Ferreira, I. Pinheiro, S. De Souza, L. Mei and L. Kona, "Polymer Composites Reinforced with Natural Fibers and Nanocellulose in the Automotive Industry," *Journal of Composites Science,* 2019.

[42] A. Karmaker and J. Youngquist, "Injection Molding of Polypropylene Reinforced with Short Jute Fibers," *Journal of Applied Polymer Science,* vol. 62, no. 8, 1996.

[43] K.-Y. Lee, Y. Aitomäki, L. A. Berglund, K. Oksman and A. Bismarck, "On the use of nanocellulose as reinforcement in polymer matrix composites," *Composite Science & Technology,* no. 105, pp. 15-27, 2014.

[44] J. Kim, B. Shim, H. Kim, Y. Lee, S. Min, D. Jang, Z. Abas and J. Kim, "Review of Nanocellulose for Sutainable Future Materials," *International Journal of Precision Engineering and Manufacturing-Green Technology,* vol. 2, no. 2, pp. 197-213, 2015.

[45] R. Moon, A. Martini, J. Nairn, J. Simonsen and J. Youngblood, "Cellulose nanomaterials review: structure, properties and nanocomposites," *Chemical Soceity Reviews,* 2011.

[46] K. Lee, A. Bismarck and J. Blaker, "Surface functionalisation of bacterial cellulose as the route to produce green polylacride nanocomposites with improved properties," *Composite Science Technology,* vol. 69, pp. 2724-2733, 2009.

[47] A. Gorgani, "Inkjet Printing," in *Printing Polymers*, Tehran, 2016, pp. 231-246.

[48] T. Saito, S. Kimura, Y. Nishiyama and A. Isogai, "Cellulose Nanofibers Prepared by TEMPO-Mediated Oxidation of Native Cellulose," *Biomacromolecules,* vol. 8, pp. 2485-2491, 2007.

[49] X. Xu, F. Liu, J. Zhu, D. Haagenson and D. Wiesenborn, "Cellulose Nanocrystals vs. Cellulose Nanofibrils: A Comparative Study on Their Microstructures and Effects as Polymer Reinforcing Agents," *Applied Materials & Interfaces,* vol. 5, pp. 2999-3009, 2013.

[50] S. Puanglek, S. Kimura, Y. Enomoto-Rogers, T. Kabe, M. Yoshida, M. Wada and T. Iwata, "In vitro synthesis of linear α-1,3-glucan and chemical modification to ester derivatives exhibiting outstanding thermal properties," *Scientific Reports,* 2016.

[51] K. Kobayashi, T. Hasegawa, R. Kusumi, S. Kimura, M. Yoshida, J. Sugiyama and M. Wada, "Characterization of crystalline linear (1 → 3)-α-D-glucan synthesized in vitro," *Carbohydrate Polymers,* vol. 177, pp. 341-346, 2017.

[52] C. Lenges, "DuPont BioMaterials: Enzymatic polymerization - A new process for engineered polysaccharides," in *Biobased Performance Materials Symposium*, Wageningen, Netherlands, 2017.

[53] N. Robertson, J. Nychka, K. Alemaskin and J. Wolodko, "Mechanical Performance and Moisture Absorption of Various Natural Fiber Reinforced Thermoplastic Composites," *Journal of Applied Polymer Science,* pp. 969-980, 2013.

[54] M. Batista, L. Drzal, A. Kiziltas and D. Mielewski, "Hybrid Cellulose-Inorganic Reinforcement Polypropylene Composites: Lightweight Materials For Automotive Applications," *SPE ACCE,* pp. 1-16, 2019.

[55] F. Fernandes, R. Gadioli, E. Yassitepe and M. De Paoli, "Polyamide-6 Composite Reinforced With Cellulose Fibers and Fabricated by Extrusion: Effect of Fiber Bleaching on Mechanical Properties and Stability," *Polymer Composites,* pp. 299-308, 2017.

[56] M. Idicula, K. Joseph and S. Thomas, "Mechanical Performance of Short Banana/Sisal Hybrid Fiber Reinforced Polyester Composites," *Journal of Reinforced Plastics and Composites,* vol. 29, no. 1, pp. 12-18, 2010.

[57] D. Ndiaye, B. Diop, C. Thianadoume, P. Fall, A. Farota and A. Tidjani, "Morphology and Thermo Mechanical Properties of Wood/Polypropylene Composites," in *Polypropylene*, 2012, pp. 416-428.

[58] R. Gauthier, H. Gauthier, C. Joly, C. Coupas and M. Escoubes, "Interfacial in Polyolefin/Cellulosic Fiber Composites: Chemical Coupling, Morphology, Correlation with Adhesion and Aging in Moisture," *Polymer Composites,* vol. 19, no. 3, pp. 287-300, 1998.

[59] A. Valadez-Gonzalez, J. Cervantes-Uc, R. Olayo and P. Herrera-Franco, "Effect of fiber surface treatment on the fiber–matrix bond strength of natural fiber reinforced composites," *Composites: Part B,* pp. 309-320, 1999.

[60] Administration of William J. Clinton, "Executive Order 13134—Developing and Promoting Biobased Products and Bioenergy," United States. Office of the Federal Register, Washington, DC, 199.

[61] .. Riley, C. Paynter, P. McGenity and J. Adams, "Factors Affecting the Impact Properties of Mineral Filled Polypropylene," *Plastics and Rubber Processing and Applications,* vol. 14, pp. 85-93, 1990.

[62] H. Ku, H. Wang, N. Pattarachaiyakoop and M. Trada, "A review on the tensile properties of natural fiber reinforced polymer composites," *Composites: Part B,* vol. 42, pp. 856-873, 2011.

[63] R. Velmurugan and V. Manikandan, "Mechanical properties of palmyra/glass fiber hybrid composites," *Composites Part A,* vol. 38, pp. 2216-2226, 2008.

[64] M. Khan, J. Ganster and H. Fink, "Hybrid composites of jute and man-made cellulose fibers with polypropylene by injection moulding," *Composites: Part A,* vol. 40, pp. 846-851, 2009.

[65] J. Thomason and J. Fernandez, "A Review of the Impact Performance of Natural Fiber Thermoplastic Composites," *Frontiers in Materials,* 2018.

[66] J. Thomason and M. Vlug, "Influence of fibre length and concentration of propertie sof glass fibre-reinforced polypropyleneL 4 Impact properties," *Composites Part A,* vol. 28, pp. 277-288, 1997.

[67] S. Panthapulakaal and M. Sain, "Injection-molded short hemp fiber/glass fiber-reinforced polypropylene hybrid composites—Mechanical, water absorption and thermal properties," *Jounral of Applied Polymer Science,* vol. 103, no. 4, pp. 2432-2441, 2007.

[68] S. Kim, J. Moon, G. Kim and C. Ha, "Mechanical properties of polypropylene/natural fiber composites: Comparison of wood fiber and cotton fiber," *Polymer Testing,* vol. 27, no. 7, pp. 801-806, 2008.

[69] H. Kim, B. Lee, S. Choi and H. Kim, "The effect of types of maleic anhydride-grafted polypropylene (MAPP) on the interfacial adhesion properties of bio-flour-filled polypropylene composites," *Composites Part A: Applied Science and Manufacturing,* vol. 38, no. 6, pp. 1473-1482, 2007.

[70] R. Tokoro, D. Vu, K. Okubo, T. Tanaka, T. Fuji and T. Fujiura, "How to improve mechanical properties of polylactic acid with bamboo fibers," *Journal of Materials Science,* vol. 43, no. 2, pp. 775-787, 2008.

[71] A. Kiziltas, D. Gardner, Y. Han and H. Yang, "Thermal properties of microcrystalline cellulose-filled PET–PTT blend polymer composites," *Journal of Thermal Analysis and Calorimetry ,* vol. 103, pp. 163-170, 2011.

[72] ASAHI KASEI PLASTICS NORTH AMERICA, "Polypropylene Processing Guidelines," 2018.

[73] N. Jia and V. Kagan, "Effects of Time and Temperature on the Tension-Tension Fatigue Behavior of Short Fiber Reinforced Polyamides," *Polymer Composites,* vol. 19, no. 4, pp. 408-414, 2004.

[74] Y. Feng, X. Jin and J. Hay, "Effect of Nucleating Agent Addition on Crystallization of Isotactic Polypropylene," *Journal of Applied Polyer Science ,* pp. 2089-2095, 1998.

[75] Y. Amintowlieh, A. Sadashti and L. Simon, "Polyamide 6–Wheat Straw Composites: Effects of Additives on Physical and Mechanical Properties of the Composite," *Polymer Composites,* vol. 33, no. 6, pp. 976-984, 2012.

[76] Y. Guan, S. Wang, A. Zheng and H. Xiao, "Crystallization Behaviors of Polypropylene and Functional Polypropylene," *Journal of Applied Polymer Science,* vol. 88, no. 4, pp. 872-877, 2002.

[77] R. Blaine, "Determination of Polymer Crystallinity by DSC," TA instruments, Deleware, USA.

[78] A. Rudin, The Elements of Polymer Science and Engineering, Sand Diego: Academic Press, 1999.

[79] A. Buchenauer, "Wood Fiber Polyamide Composites for Automotive Applications," University of Waterloo, Waterloo,ON, Canada, 2016.

[80] V. Pasangulapati, D. Ramachandriya, A. Kumar, M. Wilkins, C. Jones and R. Huhnje, "Effects of cellulose, hemicellulose and lignin on thermochemical conversion characteristics of the selected biomass," *Bioresource Technology,* vol. 114, pp. 663-669, 2012.

[81] X. Liu, Y. Wang, L. Yu, Z. Tong, L. Chen, H. Liu and X. Li, "Thermal degradation and stability of starch under different processing conditions," *Starch,* vol. 65, pp. 48-60, 2013.

[82] P. Sanchez-Jimenez, L. Perez-Maqueda, A. Perejon and J. Criado, "Generalized Master Plots as a Straightforward Approach for Determining The Kinectic Model: The Case of Cellulose Pyrolysis," University of Seville, Seville, Spain.

[83] A. Khawam and D. Flanagan, "Solid-State Kinetic Models: Basics and Mathematical Fundamentals," *The Journal of Physical Chemistry,* vol. 110, no. 35, pp. 17315-17328, 2006.

[84] J. Conesa, J. Caballero, A. Marcilla and R. Font, "Analysis of different kinetic models in the dynamic pyrolysis of cellulose," *Thermochimica Acta,* vol. 254, pp. 175-192, 1995.

[85] Malvern Instruments Worldwide, "A Basic Introduction to Rheology," Malvern Instruments Limited, 2016.

[86] TA Instruments, "Understanding Rheology of Thermoplastic Polymers".

[87] S. Nanguneri, "Rheological characteristics of glass-fibre-filled polypropylene melts," *Rheologica Acta,* vol. 26, no. 3, pp. 301-307, 1987.

[88] A. Kiziltas, D. Gardner, B. Nazari and D. Bousfield, "Polyamide 6–Cellulose Composites: Effect of Cellulose Composition on Melt Rheology and Crystallization Behaviour," *Polymer Engineering & Science,* vol. 54, no. 54, pp. 739-746, 2014.

[89] T. Li and M. Wolcott, "Rheology of HDPE–wood composites. I. Steady state shear and extensional flow," *Composites Part A: Applied Science and Manufacturing,* vol. 35, no. 3, pp. 303-311, 2004.

[90] S. Mohanty, S. Verma and S. Nayak, "Rheological characterization of PP/jute composite melts," *Journal of Applied Polymer Science,* vol. 99, no. 4, pp. 1477-1483, 2005.

[91] P. Oommen, K. Joseph and S. Thomas, "Melt Rheological Behaviour of Short Sisal Fibre Reinforced Polypropylene Composites," *Jounral of Thermoplastic Composite Materials,* vol. 15, 2002.

[92] C. Sanchez, C. Valero, A. Mendoza and R. Hurtado, "Rheological behavior of original and recycled cellulose–polyolefin composite materials," *Composites Part A: Applied Science and Manufacturing,* vol. 42, no. 9, pp. 1075-1083, 2011.

[93] S. Samal, S. Mohanty and S. Nayak, "Banana/Glass Fiber-Reinforced Polypropylene Hybrid Composites: Fabrication and Perfromance Evaluation," *Polymer-Plastics Technology and Materials,* pp. 397-414, 2009.

[94] D. Shumingin, E. Tarasova, A. Krumme and P. Meier, "Rheological and Mechanical Properties of Poly(lactic) Acid/Cellulose and LDPE/Cellulose Composites," *Materials Science,* vol. 17, no. 1, 2011.

[95] M. Kumar, S. Priya, G. Kanagaraj and G. Pugazhenthi, "Melt rheological behavior of PMMA nanocomposites reinforced with modiefied nanocaly," *Nanocomposites,* vol. 2, no. 3, pp. 109-116, 2016.

[96] J. Dealy, Melt Rheology and Its Role in Plastic Processing, Dordrecht, Netherlands: Kluwer Academic Publishers, 1999.

[97] National Science and Technology Council Committee on Technology, "National Nantoechnology Initiative Strategic Plan," National Science and Technology Council Committee on Technology, 2016.

[98] A. Dufresne, "Nanocellulose: a new agless bionanomaterial," *Materials Today,* vol. 16, no. 6, 2013.

[99] University of Maine, "CNC and CNF Product Specification," [Online]. Available: https://umaine.edu/pdc/nanocellulose/nanocellulose-spec-sheets-and-safety-data-sheets/. [Accessed 1 12 2019].

[100] Y. Peng, S. Gallegos, D. Gardner, Y. Han and C. Zhiyong , "Maleic anhydride polypropylene modified cellulose nanofibril polypropylene nanocomposites with enhanced impact strength," *Polymer Composites,* vol. 37, no. 3, pp. 783-793, 2014.

[101] Y. Peng, D. Gardner, Y. Han, Z. Cai and M. Tshabalala, "Influence of drying method on the surface energy of cellulose nanofibrils determined by inverse gas chromatography," *Journal of Colloid and Interface Science,* vol. 405, pp. 85-95, 2013.

[102] A. Kiziltas, E. Kiziltas, S. Boran and D. Gardner, "Micro-and Nanocellulose Composites for Automotive Applications," *SPE ACCE,* 2013.

[103] D. Romanzini, H. Junior, S. Amico and A. Zattera, "Preparation and characterization of ramie-glass fiber reinforced polymer matrix hybrid composites," *Materials Research,* vol. 15, pp. 415-420, 2012.

[104] S. Sam and P. Gan, "Thermal properties of nanocellulose-reinforced composites: A review," *Journal of Applied Polymer Science,* vol. 136, 2019.

[105] Q. Zhang, C. Zhao, M. Yang and S. Yang, "Thermal stability and flammability of polypropylene/montmorillonite composites," *Polymer Degradation and Stability,* vol. 85, no. 2, pp. 807-813, 2004.

[106] A. Kiziltas, H. Yang and D. Gardner, "Thermal analysis and crystallinity study of cellulose nanofibril-filled polypropylene composites," *Journal of Thermal Analysis and Calorimetry,* vol. 113, no. 2, pp. 673-682, 2013.

[107] K. Nelson, T. Retsina, M. Lakovlev and A. Van Heiningen, "American Process: Production of Low Cost Nanocellulose for Renewable, Advanced Materials Applications," in *Catalytic Materials: Nanofibers-From Research to Manufacture*, 2016, pp. 267-302.

[108] Y. Li, "ChE 640 Lecture 2 Polymerization methods-1:Conventional methods," Yuning Li, University of Waterloo, Waterloo,ON, 2018.

[109] L. Barino and R. Scordamaglia, "Modeling of isospecific Ti sites in MgCl2 supported heterogeneous Ziegler-Natta catalysts," *Macromolecular Theory and Simulations,* vol. 7, no. 4, 1998.

[110] B. Zhao, "ChE 612 Interfacial Phenomena," University of Waterloo, Department of Chemical Engineering, Waterloo, 2018.

[111] C. Curmudgeon, "August 13, 1941 Henry Ford's Soybean Car," Today in History, 13 August 2018. [Online]. Available: https://todayinhistory.blog/2018/08/13/august-13-1941-henry-fords-soybean-car/. [Accessed 28 June 2019].

[112] F. Yao, Q. Wu, Y. Lei and Y. Xu, "Thermal decomposition kinetics of natural fibers: Activation," *Polymer Degradation and Stability ,* vol. 93, pp. 90-98, 2008.

[113] C. Doyle, "Kinectic Analysis of Thermogravimetric Data," *Journal of Applied Polymer Science,* vol. 5, pp. 285-292, 1961.

[114] Y. Zare, "Study of nanoparticles aggregation/agglomeration in polymer particulate nanocomposites by mechanical properties," *Composites: Part A,* vol. 84, pp. 158-164, 2016.

[115] K. Lee, T. Tammelin, K. Schulfter, H. Kiiskinen, J. Samela and A. Bismarck, "High performance cellulose nanocomposites: Comparing the reinforcing ability of bacterial

cellulose and nanofibrillated cellulose," *ACS Applied Materials Interfaces,* vol. 4, pp. 4078-4086, 2012.

[116] M. Misra, M. Janoobi, J. Harun, A. Shakeri and K. Oksmand, " Chemical composition, crystallinity, and thermal degradation of bleached and unbleached kenaf bast (Hibiscus cannabinus) pulp and nanofibers," *BioResources,* vol. 4, pp. 626-639, 2009.

[117] M. Poletto, H. Ornaghi Junior and A. Zattera, "Native cellulose: Structure, characterization and thermal properties," *Materials,* pp. 6105-6119, 2014.

[118] S. Mostashari and H. Moafi, "Thermogravimetric analysis of a cellulosic fabric incorporated with ammonium iron (ii)-sulfate hexahydrate as a flame- retardant," *Journal of Industrial Textiles,* vol. 37, pp. 31-42, 2007.

[119] M. Poletto, A. Zattera, M. Forte and R. Santana, "Thermal decomposition of wood: Influence of wood components and cellulose crystallite size," *Bioresource Technology,* vol. 109, pp. 148-153, 2012.

[120] P. Mederic, "Talc Filled Thermoplastic Composites: Melt Rheological Properties," vol. 13, no. 6, 2019.

[121] A. Espert, S. Karlsson and F. Vilaplana, "Comparison of water absorption in natural cellulosic fibres from wood and one-year crops in polypropylene composites and its influence on their mechanical properties," *Composites Part A: Applied Science and Manufacturing ,* vol. 35, no. 11, pp. 1267-1276, 2004.

[122] E. Kiziltas, A. Kiziltas, H. Yang, S. Boran, E. Ozen and D. Gardner, "Thermal Analysis of Polyamide 6 Composites Filled by Natural Fiber Blend," *BioResources,* vol. 11, no. 2, pp. 4758-4769, 2016.

[123] S. Simon, Analysis of Fiber Attrition and Fiber-Matrix Separation during Injection Molding of Long Fiber-Reinforced Thermoplastic Parts, Tulln: Austrian Biotech University of Applied Sciences, 2016.

Chapter: 7 Appendix

7.1 Material Data Specification

Table 7.1-1: Nuvolve™ Specification [52]

Typical Properties	
Brightness [L*]	90 - 96
Degree of Polymerization	800 (400 – 2000)
PDI	1.7 - 2
Residual Sugars	<0.2 wt.%
Dry polymer solids	> 88 wt.%
Crystallinity Index	> 65%
Density (in g/cm^3)	1.5

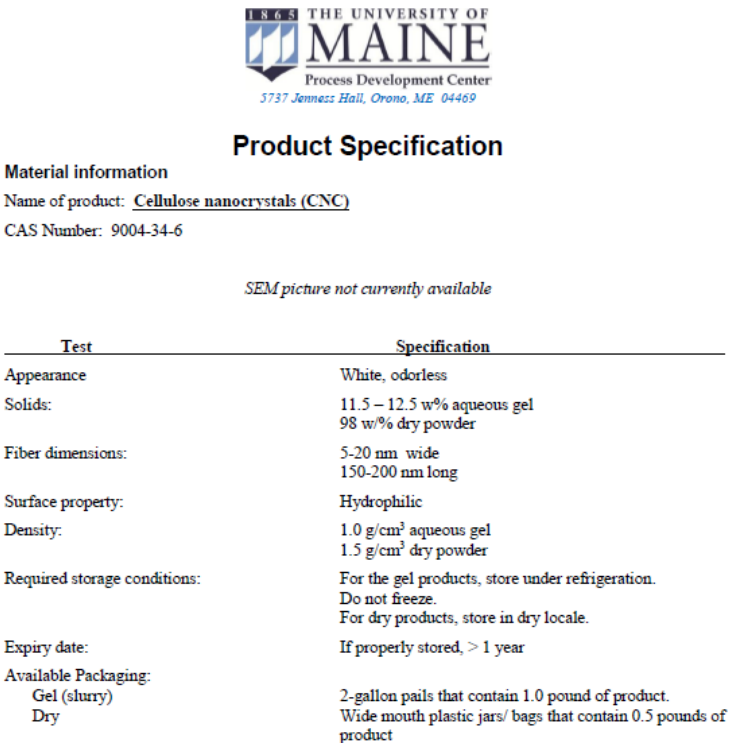

1865 THE UNIVERSITY OF MAINE
Process Development Center
5737 Jenness Hall, Orono, ME 04469

Product Specification

Material information

Name of product: **Cellulose nanocrystals (CNC)**

CAS Number: 9004-34-6

SEM picture not currently available

Test	Specification
Appearance	White, odorless
Solids:	11.5 – 12.5 w% aqueous gel 98 w/% dry powder
Fiber dimensions:	5-20 nm wide 150-200 nm long
Surface property:	Hydrophilic
Density:	1.0 g/cm^3 aqueous gel 1.5 g/cm^3 dry powder
Required storage conditions:	For the gel products, store under refrigeration. Do not freeze. For dry products, store in dry locale.
Expiry date:	If properly stored, > 1 year
Available Packaging: Gel (slurry) Dry	 2-gallon pails that contain 1.0 pound of product. Wide mouth plastic jars/ bags that contain 0.5 pounds of product

Figure 7.1-1: CNC Specification [99]

THE UNIVERSITY OF MAINE
Process Development Center
5737 Jenness Hall, Orono, ME 04469

Product Specification

Material information

Name of product: **Cellulose nanofibers (CNF)**

CAS Number: 9004-34-6

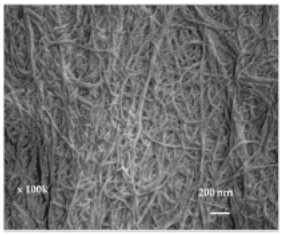

Test	Specification
Appearance	White, odorless
Solids:	3.0 w% aqueous gel 98 w/% dry powder
Fiber dimensions:	nominal fiber width of 50 nm lengths of up to several hundred microns
Surface property:	Hydrophilic 31-33 m^2/g (BET)
Density:	1.0 g/cm^3 aqueous gel 1.5 g/cm^3 dry powder
Required storage conditions:	For the gel products, store under refrigeration. Do not freeze. For dry products, store in dry locale.
Expiry date:	If properly stored, > 1 year
Available Packaging: Gel (slurry) Dry	 5-gallon pails that contain 1.0 pound of product. Wide mouth plastic jars/ bags that contain 0.25 pounds of product

Figure 7.1-2: CNF Specification [99]

PROPERTY	ASTM METHOD	VALUES Temp: 21 to 25°C Humid: 40 to 60%	UNITS
Tested			
Melt Index – Procedure A	D-1238-13	12.1 (avg.)	dg/min
Tested Minimum Quarterly			
Specific Gravity (A)	D-792-13	0.9071	
Tensile Strength – Yield	D-638-14	5,700 (39)	psi (MPa)
Flexural Modulus – 1% Sec	D-790-15e2	231,000 (1,593)	psi (MPa)
Izod Impact – Notched	D-256-10e1	0.66 (35)	ft-lbs/in (J/m)

Figure 7.1-3: Injection Mold PP Homopolymer Specification

7.2 Friedman Plots for Activation Energy of Nuvolve™

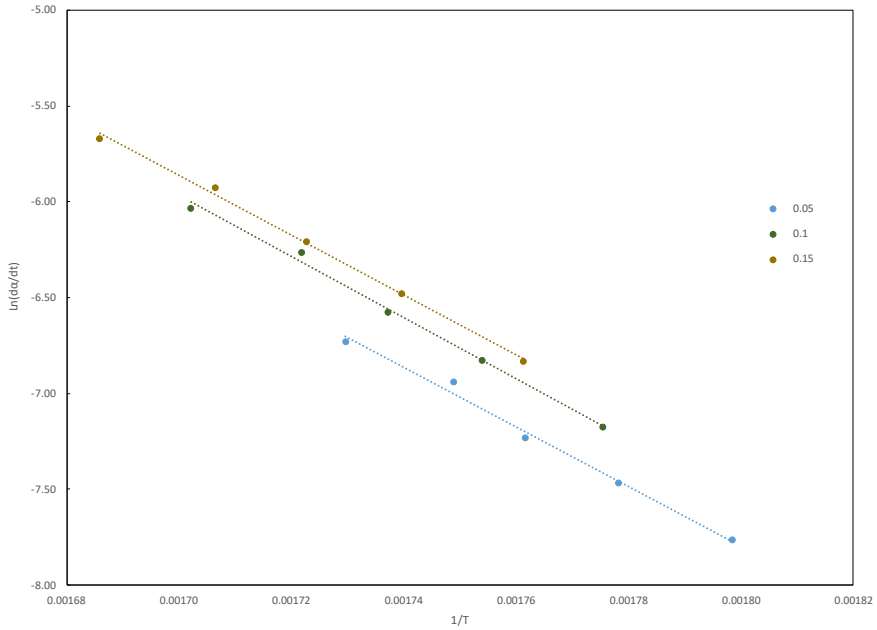

Figure 7.2-1: Friedman Plot of Nuvolve™-B in nitrogen at 5, 10 and 15 % conversion

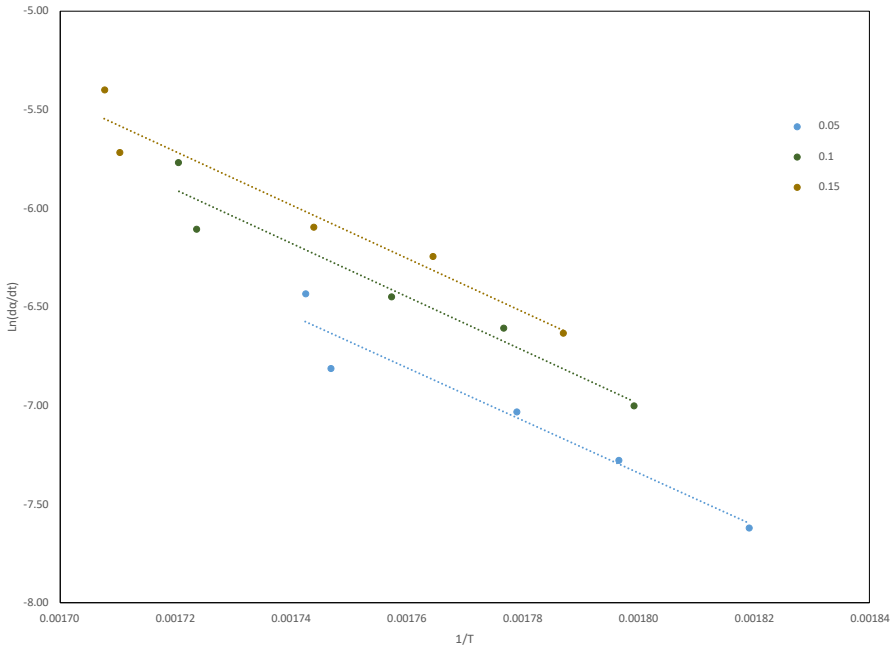

Figure 7.2-2: Friedman Plot of Nuvolve™-B in air at 5, 10 and 15 % conversion

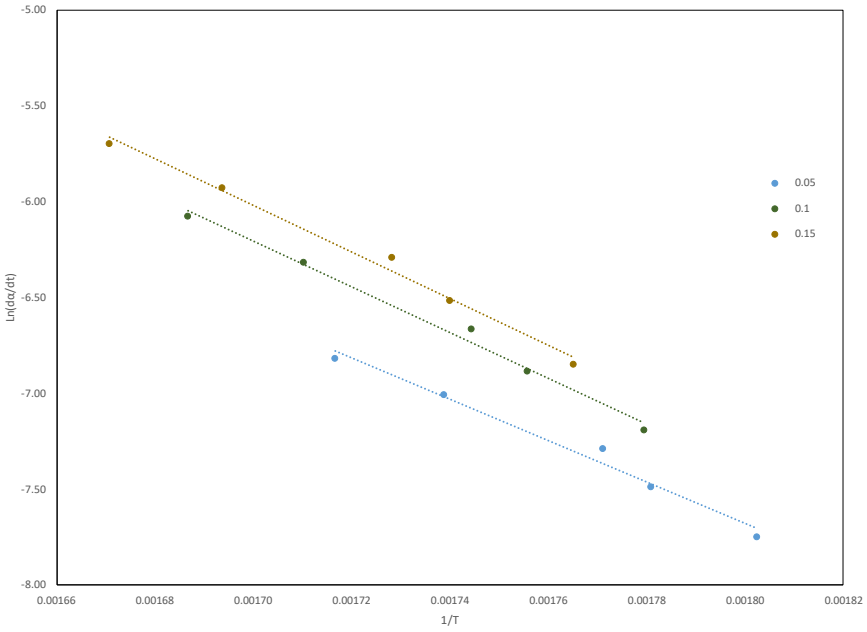

Figure 7.2-3: Friedman Plot of Nuvolve™-A in nitrogen at 5, 10 and 15 % conversion

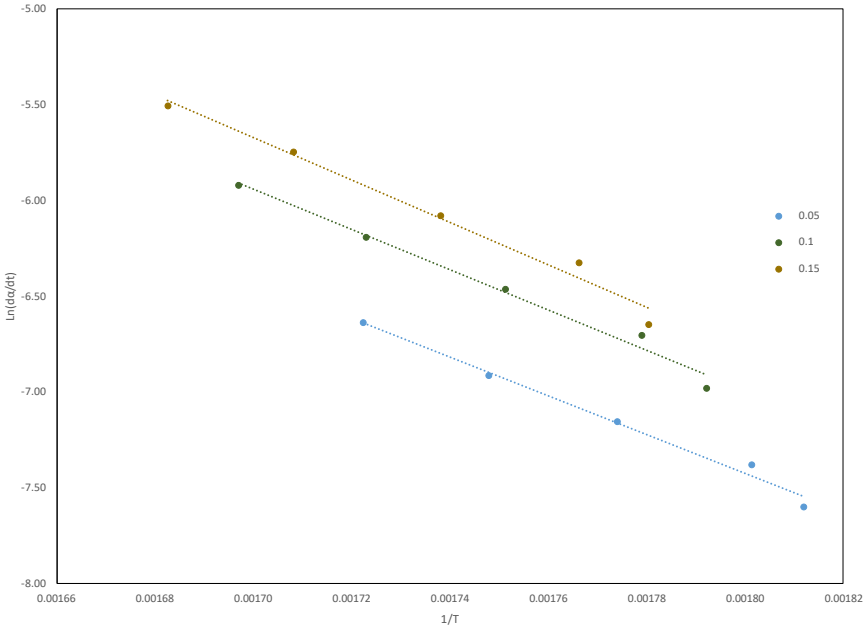

Figure 7.2-4: Friedman Plot of Nuvolve™-A in air at 5, 10 and 15 % conversion

7.3 Melt Rheology Raw Data

Table 7.3-1: Neat PP

Freq (radians/s)	Avg Vis. (Pa-s)		Avg G' (Pa)	Avg G" (Pa)	Avg, Tan Delta
100	470.9	3.2	35291.2	31183.4	0.9
63.0957	600.8	4.2	27114.7	26491.0	1.0
39.8107	754.6	5.2	20358.9	22091.2	1.1
25.1189	933.0	6.4	14927.5	18066.9	1.2
15.8489	1131.3	7.7	10643.1	14428.5	1.4
10	1351.3	9.3	7406.3	11302.2	1.5
6.30957	1588.5	11.0	5024.3	8672.4	1.7
3.98107	1835.3	13.0	3313.9	6511.5	2.0
2.51189	2084.8	15.0	2125.4	4786.2	2.3
1.58489	2332.7	17.6	1327.1	3450.6	2.6
1	2570.4	18.7	807.2	2440.4	3.0
0.630957	2793.8	20.1	477.8	1696.8	3.6
0.398107	3000.0	21.1	276.9	1161.8	4.2
0.251189	3178.8	20.9	156.0	783.1	5.0
0.158489	3332.9	23.4	86.0	521.2	6.1
0.1	3471.0	26.3	46.3	344.0	7.4
0.063096	3578.1	35.0	24.6	224.4	9.1
0.039811	3661.6	29.9	12.7	145.2	11.4
0.025119	3735.3	36.0	6.7	93.6	14.0
0.015849	3773.6	21.1	3.1	59.7	19.2

Table 7.3-2: Formulation 30B/0

Freq (radians/s)	Avg Vis. (Pa-s)		Avg G' (Pa)	Avg G" (Pa)	Avg, Tan Delta
100	501.0	210.8	33811.7	36973.3	1.1
63.0957	615.5	258.9	24549.0	30094.9	1.2
39.8107	742.8	310.3	17331.8	23960.6	1.4
25.1189	884.2	368.3	11931.6	18734.4	1.6
15.8489	1034.8	429.9	7983.3	14326.9	1.8
10	1188.0	492.1	5180.3	10691.2	2.1
6.30957	1341.3	553.6	3267.4	7806.6	2.4
3.98107	1488.7	612.5	2003.9	5577.4	2.8
2.51189	1625.7	666.9	1198.4	3903.6	3.2
1.58489	1752.5	714.9	704.1	2686.6	3.7
1	1865.1	755.4	409.8	1819.1	4.3
0.630957	1966.5	786.7	239.5	1217.0	4.9

0.398107	2061.6	806.4	143.7	807.4	5.5
0.251189	2148.5	819.9	90.0	531.3	5.9
0.158489	2242.0	809.2	58.5	349.7	6.2
0.1	2349.3	784.7	41.0	230.5	6.2
0.0630957	2473.4	754.9	29.4	152.4	6.1
0.0398107	2626.2	696.2	21.6	101.7	5.6
0.0251189	2835.7	611.3	16.8	68.7	4.9
0.0158489	3073.1	523.9	13.0	46.5	4.4

Table 7.3-3: Formulation 10B/15

Freq (radians/s)	Avg Vis. (Pa-s)		Avg G' (Pa)	Avg G" (Pa)	Avg, Tan Delta
100	505.5	34167.4	37260.5	1.1	100
63.0957	622.0	24927.2	30312.7	1.2	63.0957
39.8107	755.4	17767.3	24263.3	1.4	39.8107
25.1189	901.6	12321.0	19001.3	1.5	25.1189
15.8489	1058.7	8322.6	14569.7	1.7	15.8489
10	1220.1	5466.3	10907.9	2.0	10
6.30957	1385.2	3519.7	7999.6	2.3	6.30957
3.98107	1549.2	2219.3	5754.2	2.6	3.98107
2.51189	1702.7	1376.9	4049.1	2.9	2.51189
1.58489	1868.3	863.1	2832.2	3.3	1.58489
1	2000.5	530.2	1928.6	3.6	1
0.630957	2152.3	336.0	1315.4	3.9	0.630957
0.398107	2302.3	221.2	889.0	4.1	0.398107
0.251189	2461.6	145.8	600.6	4.2	0.251189
0.158489	2700.9	107.5	414.1	3.9	0.158489
0.1	2867.1	73.0	277.1	3.9	0.1
0.0630957	3112.8	50.7	189.7	3.8	0.0630957
0.0398107	3364.0	34.0	129.2	4.2	0.0398107
0.0251189	3897.0	29.1	93.4	3.2	0.0251189
0.0158489	4325.8	21.7	65.0	3.0	0.0158489

Table 7.3-4: Formulation 10B/20

Freq (radians/s)	Avg Vis. (Pa-s)		Avg G' (Pa)	Avg G" (Pa)	Avg, Tan Delta
100	586.9	39810.5	43125.9	1.1	100
63.0957	722.2	29139.4	35029.2	1.2	63.0957
39.8107	878.3	20906.6	28028.9	1.3	39.8107
25.1189	1051.1	14666.8	21954.5	1.5	25.1189
15.8489	1238.8	10065.8	16856.1	1.7	15.8489
10	1436.2	6777.5	12662.4	1.9	10
6.30957	1642.9	4504.9	9336.1	2.1	6.30957

3.98107	1855.6	2979.0	6759.6	2.3	3.98107
2.51189	2074.1	1973.3	4821.5	2.4	2.51189
1.58489	2305.8	1323.8	3406.1	2.6	1.58489
1	2559.5	921.7	2387.6	2.6	1
0.630957	2843.5	658.9	1668.6	2.5	0.630957
0.398107	3190.0	488.2	1172.2	2.4	0.398107
0.251189	3632.9	374.3	832.2	2.2	0.251189
0.158489	4193.8	299.0	593.6	2.0	0.158489
0.1	4957.0	237.9	434.9	1.8	0.1
0.0630957	5959.6	193.9	322.2	1.7	0.0630957
0.0398107	7419.2	159.5	248.6	1.6	0.0398107
0.0251189	9494.4	133.3	197.7	1.5	0.0251189
0.0158489	12722.2	117.6	163.7	1.4	0.0158489

Table 7.3-5: Formulation 15B/15

Freq (radians/s)	Avg Vis. (Pa-s)		Avg G' (Pa)	Avg G" (Pa)	Avg, Tan Delta
100	641.1	45679.2	44982.8	1.0	100
63.0957	801.5	34201.2	37247.9	1.1	63.0957
39.8107	990.7	25117.1	30407.9	1.2	39.8107
25.1189	1205.4	18020.3	24330.4	1.3	25.1189
15.8489	1445.0	12637.8	19097.5	1.5	15.8489
10	1702.3	8654.4	14658.5	1.7	10
6.30957	1977.9	5816.8	11040.2	1.9	6.30957
3.98107	2259.9	3831.8	8139.2	2.1	3.98107
2.51189	2555.5	2508.4	5908.0	2.4	2.51189
1.58489	2856.5	1627.6	4223.8	2.6	1.58489
1	3171.5	1065.6	2986.3	2.8	1
0.630957	3504.6	702.0	2096.2	3.0	0.630957
0.398107	3883.7	474.5	1471.0	3.1	0.398107
0.251189	4312.6	325.7	1032.8	3.2	0.251189
0.158489	4820.7	228.8	728.7	3.2	0.158489
0.1	5445.8	165.4	518.6	3.2	0.1
0.0630957	6213.7	130.9	369.0	2.9	0.0630957
0.0398107	7178.8	95.6	268.8	2.9	0.0398107
0.0251189	8516.3	70.6	201.4	3.0	0.0251189
0.0158489	10227.0	59.5	150.5	2.6	0.0158489

7.4 Tensile, Flexural and Impact Raw Data

Table 7.4-1: Tensile properties of Nuvolve™ and Nanocellulose Reinforced Hybrid Composites

Material Code	Tensile Strength MPa	Elongation @ Break, %	Tensile Modulus, MPa
Neat PP	32.21	9.39	1885.10
	32.26	9.63	1841.62
	32.14	9.85	1872.45
	32.51	9.08	1901.51
	32.34	9.11	1991.71
	32.22	9.02	1904.88
0/5	40.04	4.86	2515.79
	40.11	4.72	2517.61
	39.49	4.97	2526.09
	38.9	5.15	2485.52
	39.46	4.89	2530.36
	39.47	4.82	2525.47
0/10	43.82	4.11	3072.10
	43.17	4.22	2752.79
	44.3	4.07	2893.92
	42.78	4.3	2740.33
	43.42	4.38	2754.17
	44.1	4.18	2724.63
30A/0	25.04	1.64	2384.32
	26.53	2.65	2455.34
	27.53	2.22	2523.44
	28.06	2.6	2492.21
	27.26	2.39	2396.52
	27.79	2.69	2427.87
10A/10	52.13	3.21	3906.32
	56.96	3.03	3607.55
	53.75	3.47	3561.25
	52.04	2.63	3585.95
	51.56	3.29	3413.61
	53.49	3.26	3562.03
10A/15	61.19	2.98	4339.72
	57.59	2.58	4139.66
	59.87	2.94	4308.70
	57.6	2.94	4092.69
	61.12	2.92	4338.52
	60.42	2.87	4198.63
10A/20	65.14	2.1	5128.94
	70.3	2.75	5448.45
	71.95	2.44	5582.96
	67.19	2.71	5115.46

	68.67	2.76	5402.69
	64.86	2.14	5281.46
15A/15	56.84	2.76	4253.49
	56.5	3.11	4330.23
	54.41	2.68	4226.57
	56.15	3.04	4191.59
	55.2	2.92	4374.98
	52.94	2.66	4420.90
20A/10	45.42	3.2	3449.66
	44.47	3.06	3505.95
	46.11	3.46	3328.25
	42.2	3.05	3221.34
	45.28	3.35	3251.62
	45.88	3.33	3809.03
30B/0	25.58	1.96	2329.92
	27.99	2.82	2302.43
	27.75	3	2362.37
	26.95	2.03	2522.40
	24.18	1.45	2384.47
	27.7	2.33	2351.96
10B/10	54.22	3.34	3441.62
	53.11	3.38	3233.69
	52.23	3.49	3327.79
	52.05	3.38	3278.14
	53.16	3.01	3676.09
	52.46	3.25	3409.09
10B/15	58.57	2.51	4304.71
	60.61	3	3984.82
	60.2	3.15	3981.20
	55.48	2.94	3836.65
	56.56	2.93	3857.09
10B/20	69.77	2.42	5465.97
	69.89	2.75	5825.19
	74.15	2.84	5412.01
	71.25	2.68	5368.83
	72.97	2.82	5495.47
15B/15	51.4	2.52	4287.50
	53.25	2.78	4459.16
	51.09	2.56	4457.84
	51.41	2.67	4291.66
	51.23	2.92	4214.95
	50.59	2.23	4428.77
20B/10	45.42	3.2	3449.66
	44.47	3.06	3505.95
	46.11	3.46	3328.25
	42.2	3.05	3221.34
	45.28	3.35	3251.62
	45.88	3.33	3809.03
5CNC/0	32.91	7.93	2029.91

	33.15	8.01	2023.71
	33.43	7.62	2085.24
	33.35	7.37	2034.62
	33.72	7.5	2089.65
	32.54	6.62	2076.38
2.5CNC/2.5	41.6	5.46	2501.98
	38.07	5.58	2325.72
	38.69	5.43	2374.02
	39.11	5.36	2327.44
	38.41	5.73	2384.68
	38.01	5.74	2749.38
2.5CNC/5	48.27	4.44	2859.46
	45.14	4.6	2831.31
	45.68	4.46	2777.32
	45.43	4.61	2844.18
	46.76	4.48	2889.75
	44.74	4.51	2714.27
2.5CNC/10	56.2	3.93	3596.69
	55.3	3.8	3545.65
	56.71	3.85	3722.30
	54.22	4.07	3916.60
	55.99	4.02	3520.37
	58.22	4.04	3639.65
5CNF/0	32.34	7.45	1953.15
	31.29	7.33	1919.41
	31.75	7.65	2023.40
	30.82	8.01	1903.14
	31.26	7.73	1926.03
2.5CNF/2.5	36.44	5.97	2193.11
	36.62	6.14	2110.55
	36.57	5.93	2165.22
	36.2	6.37	2116.40
	35.71	6.44	2060.87
	37.03	5.86	2399.06
2.5CNF/5	40.15	5.28	2497.72
	39.58	5.62	2487.70
	40.88	5.13	2590.84
	41.28	5.17	2669.39
	41.61	5.11	2511.80
	40.41	5.2	2594.13
2.5CNF/10	51.38	4.13	3372.00
	50.8	4	3192.67
	54.09	4.16	3819.38
	53.21	4.1	3514.92
	54.67	4.15	3430.69
	51.72	4.12	3319.21

Table 7.4-2: Flexural properties of Nuvolve™ and Nanocellulose Reinforced Hybrid Composites

Material Code	Flexural Modulus MPa
Neat PP	1558.05
	1523.03
	1443.69
	1389.48
	1442.94
0/5	1970.88
	2004.73
	2014.95
	2016.02
	1997.71
0/10	2189.72
	2193.51
	2134.94
	2165.51
	2112.44
30A/0	1927.99
	1833.94
	1856.11
	1836.49
	1804.65
10A/10	2989.21
	2699.55
	2819.72
	2788.75
	2892.19
10A/15	3308.53
	3426.07
	3344.94
	3469.06
	3381.74
10A/20	4404.59
	4181.71
	4236.20
	4306.73
	4470.12
15A/15	3541.12
	3580.74
	3474.63
	3495.61
	3351.65
20A/10	2866.83
	2658.84
	2703.13

	2803.30
	2632.30
30B/0	1839.26
	1801.36
	1814.92
	1766.78
	1802.31
10B/10	2758.31
	2742.36
	2736.21
	2806.98
	2787.93
10B/15	3478.59
	3563.35
	3497.51
	3766.23
	3653.04
10B/20	4496.59
	4211.36
	4498.46
	4375.98
	4354.23
15B/15	3448.88
	3324.35
	3281.94
	3569.43
	3603.61
20B/10	3197.11
	2726.55
	2764.33
	2910.20
	2939.31
5CNC/0	1557.56
	1488.03
	1445.37
	1559.46
	1375.06
2.5CNC/2.5	1750.00
	1706.62
	1770.35
	1750.81
	1706.44
2.5CNC/5	2012.16
	2083.82
	2130.33
	2078.49
	2088.65

2.5CNC/10	2725.78
	2678.70
	2718.13
	2790.72
	2649.78
	58.22
5CNF/0	1644.39
	1576.02
	1566.33
	1564.49
	1568.82
2.5CNF/2.5	1781.57
	1737.94
	1720.21
	1716.59
	1696.87
2.5CNF/5	1897.26
	1839.57
	1836.91
	1786.75
	1876.38
2.5CNF/10	2545.20
	2610.30
	2680.11
	2601.76
	2621.62

Table 7.4-3: Impact properties of Nuvolve™ and Nanocellulose Reinforced Hybrid Composites

Material Code	Impact Strength (kJ/m^2)
Neat PP	9.45
	11.73
	9.70
	10.54
	8.76
	10.46
	9.45
0/5	13.00
	12.74
	13.77
	13.00
	11.47
	10.46
0/10	12.22
	10.96

	11.72
	10.71
	11.47
	13.50
	11.21
	14.27
30A/0	4.76
	6.52
	3.68
	3.68
	5.68
	6.67
	2.94
	3.45
	4.44
	3.68
10A/10	14.54
	16.08
	16.34
	14.02
	15.57
	14.79
	13.77
	12.09
	16.09
10A/15	18.14
	17.37
	17.89
	19.18
	18.66
	18.39
	18.66
	15.82
	18.17
	16.34
10A/20	22.56
	22.04
	21.79
	23.87
	22.83
	22.86
	23.54
	21.52
	23.20
	21.17
15A/15	22.76
	22.21

	21.95
	23.03
	20.33
	22.48
	21.70
	23.29
	22.21
	23.83
20A/10	11.84
	14.47
	15.26
	13.94
	16.59
	16.06
	16.18
	14.73
	15.00
30B/0	3.95
	4.12
	4.20
	5.19
	4.20
10B/10	13.77
	13.77
	13.25
	14.79
	14.02
	15.82
	14.27
	13.77
	11.21
	13.77
10B/15	15.80
	19.42
	18.64
	22.29
	17.57
	18.90
	19.16
	19.42
	18.39
	18.64
10B/20	22.56
	23.60
	23.08
	21.79
	21.79

	21.85
	24.14
	20.73
	20.73
	23.35
15B/15	20.84
	17.39
	20.33
	20.06
	20.60
	20.33
	21.13
	21.41
	22.48
	21.68
20B/10	10.96
	11.73
	12.49
	13.77
	9.95
	13.52
	13.00
	10.71
5CNC/0	7.18
	5.98
	6.99
	7.68
	7.93
	8.00
	7.93
	8.19
	8.25
2.5CNC/2.5	8.00
	9.70
	7.43
	9.52
	10.20
	8.44
	12.32
	8.76
	8.00
	9.26
2.5CNC/5	11.97
	12.22
	10.96
	10.46
	10.20
	10.79
	9.20

	10.10
	10.46
	10.02
2.5CNC/10	15.05
	13.73
	15.82
	16.07
	14.39
	17.62
	15.05
	15.30
	14.02
	17.89
5CNF/0	6.13
	6.65
	6.90
	6.65
	7.41
	5.86
	6.13
	7.16
	7.67
	8.39
2.5CNF/2.5	12.11
	11.33
	11.58
	11.84
	11.84
	12.11
	8.97
	12.37
	11.33
	10.80
2.5CNF/5	13.77
	14.27
	14.27
	14.41
	13.25
	11.99
	10.46
	12.73
2.5CNF/10	16.12
	18.71
	15.10
	15.87
	16.39
	16.39
	15.10
	18.19

7.5 Differential Scanning Calorimetry Data

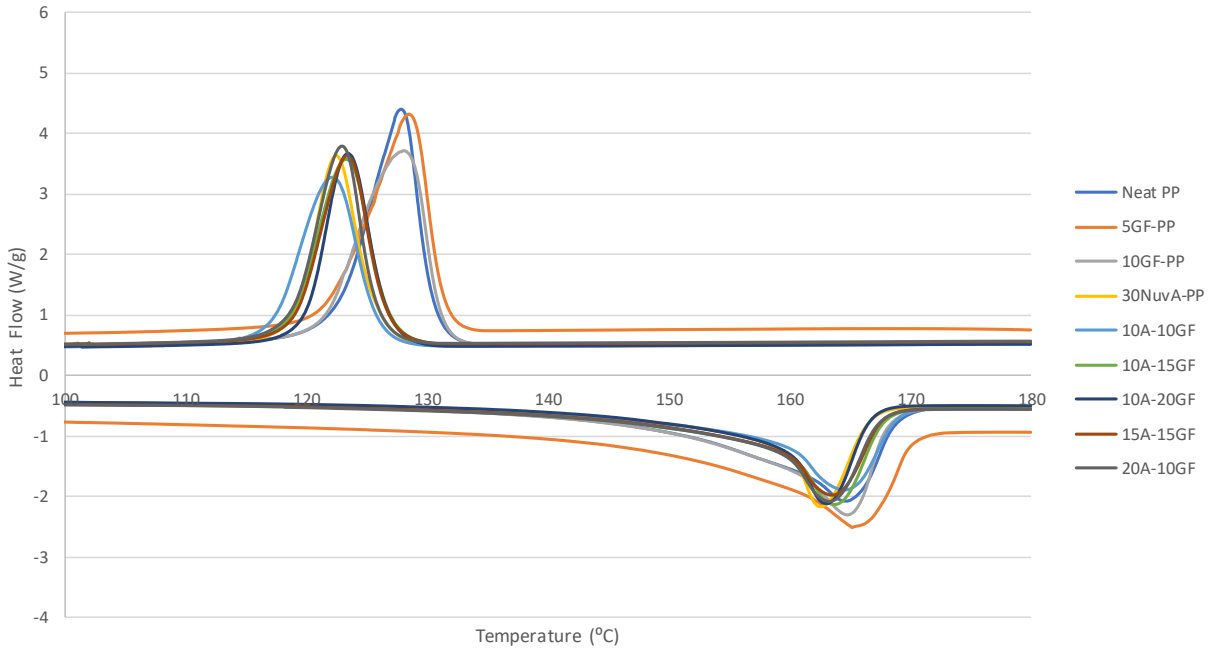

Figure 7.5-1: Nuv-A Reinforced Hybrid Composites

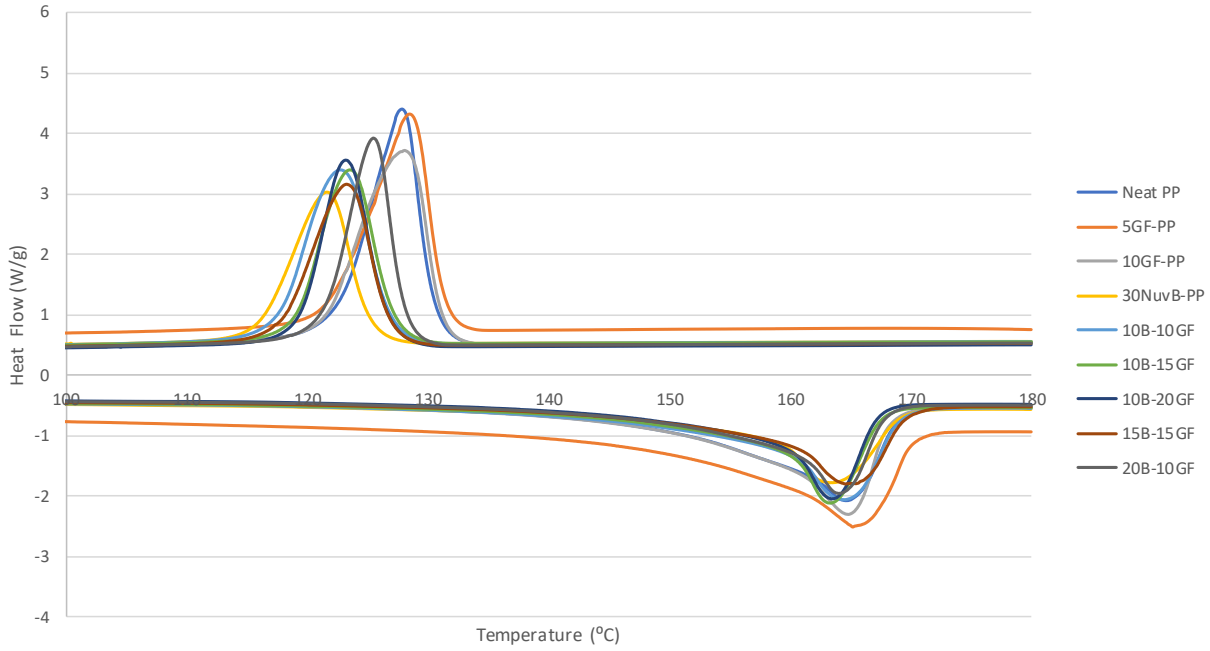

Figure 7.5-2: Nuv-B Reinforced Hybrid Composites

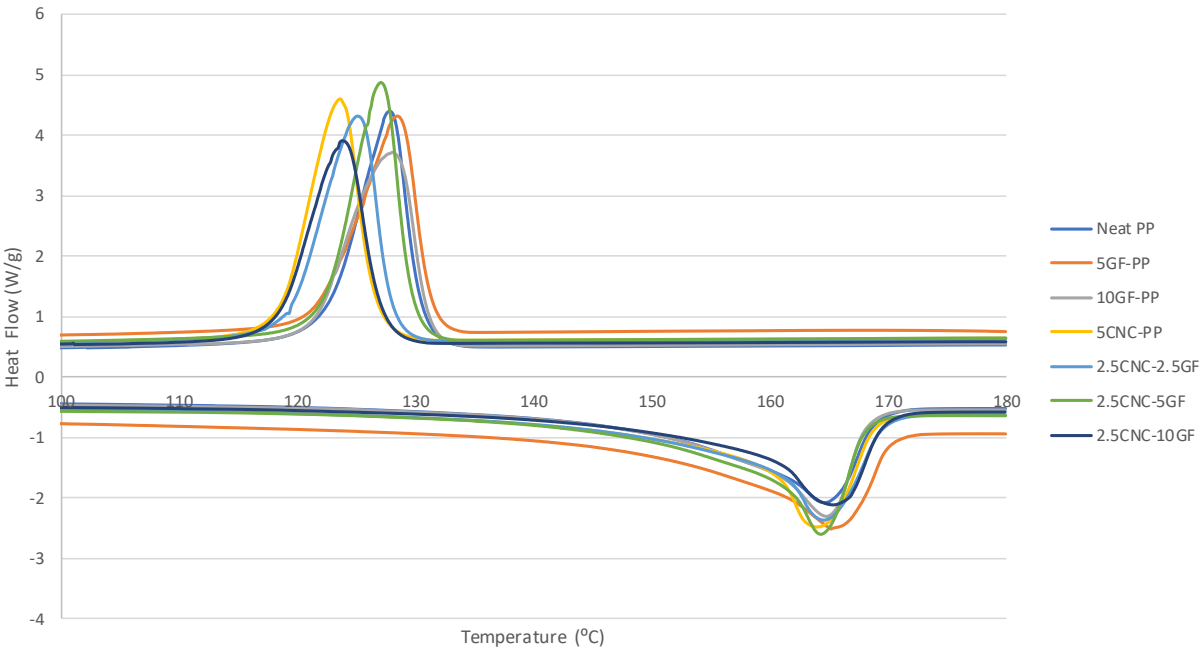

Figure 7.5-3: CNC Reinforced Hybrid Composites

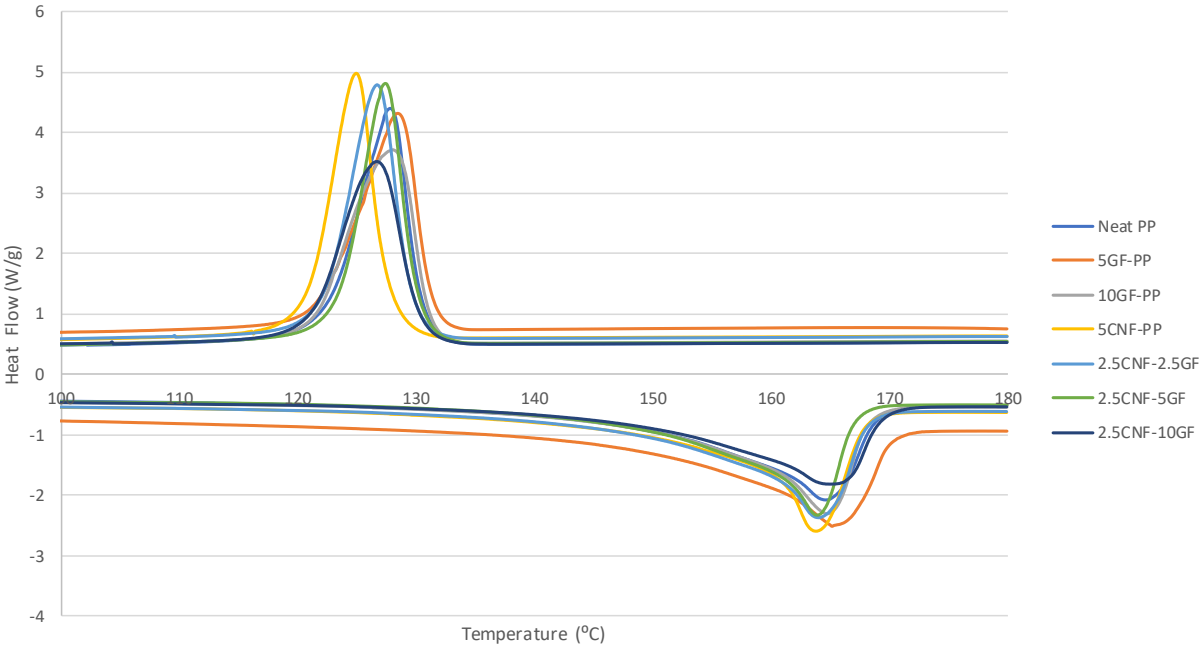

Figure 7.5-4: CNF Reinforced Hybrid Composites

7.6 Performance and Cost Analysis

Table 7.6-1: Estimated cost of materials [107]

Materials	USD ($)/tonne
Nuvolve™	2000
CNC	10000
CNF	2000
PP	1250
Glass Fiber	500

Table 7.6-2: Raw data for cost analysis of hybrid reinforced composites

Materials	Density (g/cc)	Specific Modulus (MPa/ρ)	Total filler (wt.%)	Natural Filler Conc. (wt.%)	GF (wt.%)	Cost ($/L)
Ford Spec	1.190	3025.21	35	0	35	1.17
Neat PP	0.907	1622.31	0	0	0	1.13
0/5	0.911	2197.49	5	0	5	1.13
0/10	0.926	2331.75	10	0	10	1.14
30A/0	1.015	1823.83	30	30	0	1.51
10A/10	1.003	2828.17	20	10	10	1.26
10A/15	1.037	3264.19	25	10	15	1.27
10A/20	1.075	4017.15	30	10	20	1.29
15A/15	1.063	3281.32	30	15	15	1.34
20A/10	1.029	2655.45	30	20	10	1.40
30B/0	1.021	1767.31	30	30	0	1.51
10B/10	0.995	2781.21	20	10	10	1.26
10B/15	1.044	3441.32	25	10	15	1.27
10B/20	1.075	3915.91	30	10	20	1.29
15B/15	1.071	3216.61	30	15	15	1.34
20B/10	1.038	2801.84	30	20	10	1.40
5CNC/0	0.926	1603.53	5	5	0	1.55
2.5CNC/2.5	0.931	1865.48	5	2.5	2.5	1.34
2.5CNC/5	0.950	2187.10	7.5	2.5	5	1.35
2.5CNC/10	0.981	2764.22	12.5	2.5	10	1.36
5CNF/0	0.928	1706.06	5	5	0	1.18
2.5CNF/2.5	0.925	1870.50	5	2.5	2.5	1.16
2.5CNF/5	0.940	1965.53	7.5	2.5	5	1.16
2.5CNF/10	0.984	2653.32	12.5	2.5	10	1.17

7.7 Time-Temperature Behavior of Nuvolve™

Table 7.7-1: Raw Data used to determine reaction model of Nuvolve™

Conversion	$\frac{d\alpha}{d\theta}$				
	Heating Rate (ºC/min)				
	5	**7.5**	**10**	**15**	**20**
0	0.003606	0.005162987	0.006606	0.009065	0.012352
0	0.010489	0.010515639	0.012826	0.010068	0.012244
0.005	0.014475	0.015893429	0.017951	0.013898	0.017934
0.01	0.023246	0.022664305	0.025612	0.020025	0.026112
0.015	0.034635	0.03300039	0.035347	0.028112	0.03546
0.02	0.048899	0.047948653	0.050638	0.040173	0.047455
0.025	0.065367	0.06357619	0.064028	0.053667	0.061807
0.03	0.080438	0.079001054	0.080931	0.066443	0.079144
0.035	0.09638	0.093458379	0.094921	0.082407	0.093103
0.04	0.111914	0.10944527	0.111473	0.096566	0.107198
0.045	0.125759	0.123860277	0.122486	0.107932	0.120512
0.05	0.139314	0.136785044	0.137011	0.124734	0.132774
0.055	0.150248	0.150756072	0.147579	0.137483	0.142982
0.06	0.16258	0.164565881	0.158748	0.151319	0.156955
0.065	0.173456	0.176643048	0.168715	0.166142	0.174218
0.07	0.18695	0.19041197	0.181212	0.177976	0.187445
0.075	0.198233	0.202126397	0.19143	0.188178	0.195752
0.08	0.209399	0.21452468	0.201427	0.201099	0.211013
0.085	0.220217	0.227728951	0.212689	0.216217	0.220167
0.09	0.233535	0.244032142	0.222275	0.227483	0.237462
0.095	0.244352	0.254617762	0.233694	0.24008	0.242378
0.1	0.257902	0.266935777	0.244861	0.252283	0.259163
0.105	0.269358	0.278205104	0.256122	0.26167	0.272725
0.11	0.282035	0.288871517	0.265295	0.274762	0.278657
0.115	0.293606	0.301911457	0.276144	0.288842	0.300528
0.12	0.303899	0.313986288	0.285824	0.299463	0.304256
0.125	0.31675	0.327349345	0.295818	0.314531	0.31324
0.13	0.326635	0.338578165	0.308059	0.324163	0.327821
0.135	0.338672	0.350611502	0.319288	0.330832	0.34138
0.14	0.350417	0.361316096	0.326879	0.347134	0.351042
0.145	0.360418	0.369646562	0.33858	0.359977	0.366639
0.15	0.37321	0.384618178	0.348385	0.372081	0.373757
0.155	0.384023	0.394035402	0.361037	0.383935	0.381214
0.16	0.39792	0.406630909	0.369576	0.39678	0.397828

0.165	0.406117	0.419107616	0.379696	0.41061	0.408675
0.17	0.421525	0.430776471	0.388234	0.416537	0.416471
0.175	0.430246	0.439629325	0.401834	0.429628	0.424774
0.18	0.439839	0.45170271	0.411321	0.438025	0.442913
0.185	0.449082	0.460555015	0.422073	0.451113	0.454946
0.19	0.459605	0.470615073	0.431876	0.465933	0.460197
0.195	0.471698	0.479869599	0.445159	0.4726	0.472569
0.2	0.482279	0.493149852	0.450851	0.479514	0.492402
0.205	0.492626	0.501196478	0.462551	0.504213	0.501722
0.21	0.504951	0.511658132	0.472669	0.511373	0.501722
0.215	0.516055	0.520106785	0.483107	0.51804	0.511211
0.22	0.528787	0.532983383	0.493541	0.5336	0.524599
0.225	0.535064	0.544249741	0.499865	0.543478	0.545786
0.23	0.546574	0.556723089	0.513779	0.550639	0.545786
0.235	0.55541	0.570001497	0.518837	0.558046	0.555783
0.24	0.566048	0.575634365	0.536863	0.574347	0.565779
0.245	0.57372	0.586094636	0.542238	0.584965	0.588152
0.25	0.589126	0.597762304	0.55615	0.589902	0.588152
0.255	0.596682	0.602187313	0.563423	0.601261	0.602726
0.26	0.610052	0.617477408	0.570695	0.620031	0.61323
0.265	0.61819	0.621499736	0.587138	0.628426	0.61323
0.27	0.625164	0.63356925	0.594093	0.628426	0.624073
0.275	0.633883	0.645236014	0.599467	0.636821	0.648139
0.28	0.64667	0.649660635	0.614644	0.648674	0.648139
0.285	0.657134	0.666156958	0.622548	0.667196	0.663559
0.29	0.666434	0.670581153	0.628554	0.67559	0.670163
0.295	0.675152	0.683857242	0.636775	0.684479	0.670163
0.3	0.685034	0.690696307	0.64974	0.703741	0.68609
0.305	0.692589	0.695523069	0.664916	0.703741	0.68609
0.31	0.701307	0.712823362	0.673768	0.715593	0.711341
0.315	0.708862	0.717247174	0.682937	0.724234	0.722861
0.32	0.720487	0.73011987	0.691474	0.733122	0.722861
0.325	0.729786	0.73655627	0.697796	0.733122	0.734549
0.33	0.739667	0.743394807	0.711393	0.752137	0.734549
0.335	0.748384	0.75948658	0.719613	0.764729	0.751153
0.34	0.760591	0.766324901	0.725618	0.770158	0.751153
0.345	0.768145	0.771150756	0.734154	0.770158	0.77725
0.35	0.776862	0.777988952	0.743006	0.782504	0.77725
0.355	0.779767	0.792067923	0.751542	0.802506	0.789277
0.36	0.792555	0.79729603	0.757863	0.811393	0.789277
0.365	0.801271	0.804133964	0.766714	0.811393	0.801302
0.37	0.811151	0.814996822	0.781892	0.820774	0.801302
0.375	0.8158	0.826257857	0.788529	0.833612	0.827737

0.38	0.827424	0.832693056	0.798646	0.833612	0.827737
0.385	0.836141	0.83993311	0.808129	0.854107	0.844848
0.39	0.844857	0.846770966	0.817613	0.863488	0.844848
0.395	0.850088	0.851596148	0.827412	0.863488	0.857212
0.4	0.857641	0.862458088	0.834366	0.872374	0.857212
0.405	0.868682	0.874120746	0.849542	0.892128	0.869575
0.41	0.873331	0.88136073	0.859025	0.892128	0.869575
0.415	0.882628	0.888600304	0.865978	0.905213	0.896516
0.42	0.887858	0.895839807	0.875461	0.905213	0.896516
0.425	0.900062	0.900664588	0.88526	0.914098	0.913794
0.43	0.905874	0.907501873	0.88526	0.922737	0.913794
0.435	0.914589	0.918363476	0.895059	0.922737	0.921072
0.44	0.924467	0.923590874	0.902328	0.941749	0.921072
0.445	0.927953	0.930427602	0.912443	0.941749	0.921072
0.45	0.940157	0.937264263	0.928883	0.953104	0.937842
0.455	0.943061	0.944101223	0.936151	0.958285	0.937842
0.46	0.951775	0.950937753	0.946266	0.958285	0.963425
0.465	0.956424	0.956164882	0.946266	0.968899	0.963425
0.47	0.965138	0.966623108	0.95638	0.968899	0.974769
0.475	0.973856	0.973861853	0.966495	0.985688	0.974769
0.48	0.979086	0.986327421	0.976925	0.993091	0.974769
0.485	0.987219	0.993163934	0.984194	0.993091	0.985605
0.49	0.991867	1	0.984194	1	0.985605
0.495	1	1	1	1	1
0.5	1.004648	1.004824325	1.009798	1.009132	1
0.505	1.015106	1.012062681	1.016749	1.009132	1
0.51	1.020336	1.022923039	1.016749	1.021968	1.020835
0.515	1.024983	1.027746799	1.026547	1.021968	1.020835
0.52	1.03486	1.034582935	1.036344	1.027396	1.029637
0.525	1.038345	1.041418609	1.046141	1.027396	1.029637
0.53	1.0459	1.047852219	1.046141	1.032575	1.029637
0.535	1.05345	1.054285772	1.052776	1.043436	1.037251
0.54	1.057517	1.058707281	1.062256	1.043436	1.037251
0.545	1.061583	1.069164272	1.077113	1.049603	1.052323
0.55	1.067971	1.075195248	1.077113	1.049603	1.052323
0.555	1.072619	1.07961619	1.083747	1.053795	1.052323
0.56	1.079591	1.085647064	1.092912	1.053795	1.059937
0.565	1.08656	1.091275496	1.092912	1.05774	1.059937
0.57	1.090626	1.097305845	1.102076	1.05774	1.065178
0.575	1.095274	1.097305845	1.110606	1.065883	1.065178
0.58	1.102243	1.101324639	1.110606	1.065883	1.065178
0.585	1.108634	1.107354884	1.119454	1.070816	1.069403
0.59	1.113281	1.116604538	1.125772	1.070816	1.069403

0.595	1.116184	1.120220386	1.139046	1.072291	1.077016
0.6	1.123153	1.125848512	1.139046	1.076483	1.077016
0.605	1.126637	1.131476155	1.147577	1.076483	1.077016
0.61	1.12954	1.136299435	1.153262	1.082897	1.080732
0.615	1.132443	1.141525043	1.153262	1.082897	1.080732
0.62	1.13825	1.141525043	1.16116	1.085607	1.080732
0.625	1.140571	1.144738325	1.168426	1.085607	1.082244
0.63	1.142893	1.151573315	1.168426	1.087823	1.082244
0.635	1.145795	1.155994056	1.17506	1.087823	1.084774
0.64	1.150438	1.158402944	1.178847	1.090286	1.084774
0.645	1.153922	1.162018453	1.178847	1.090286	1.084774
0.65	1.156243	1.16523157	1.184532	1.093736	1.087473
0.655	1.158565	1.16523157	1.184532	1.093736	1.087473
0.66	1.16437	1.1680423	1.192114	1.095211	1.087473
0.665	1.166692	1.169646385	1.195268	1.095211	1.087969
0.67	1.168432	1.171652811	1.195268	1.096192	1.087969
0.675	1.16901	1.174463477	1.19874	1.096192	1.087617
0.68	1.169587	1.175262818	1.200945	1.096926	1.087617
0.685	1.16958	1.175262818	1.200945	1.096926	1.087617
0.69	1.169576	1.176061708	1.203151	1.095685	1.086587
0.695	1.16841	1.176458693	1.204409	1.095685	1.086587
0.7	1.167825	1.176453332	1.204409	1.094937	1.082169
0.705	1.166659	1.176045186	1.20535	1.094937	1.082169
0.71	1.163163	1.175235152	1.206291	1.092708	1.082169
0.715	1.161416	1.175235152	1.206291	1.092708	1.078937
0.72	1.159668	1.172010655	1.205967	1.085787	1.078937
0.725	1.156758	1.169188971	1.205967	1.085787	1.078937
0.73	1.150357	1.167171541	1.205011	1.079607	1.073502
0.735	1.146284	1.163142913	1.202474	1.079607	1.073502
0.74	1.14163	1.158711993	1.202474	1.076637	1.058408
0.745	1.136976	1.153073693	1.198356	1.068235	1.058408
0.75	1.12825	1.153073693	1.192974	1.068235	1.058408
0.755	1.123014	1.148642431	1.192974	1.049955	1.044839
0.76	1.119523	1.141797699	1.187592	1.049955	1.044839
0.765	1.112544	1.128515437	1.179997	1.040071	1.044839
0.77	1.097424	1.122073186	1.179997	1.040071	1.033983
0.775	1.089283	1.112412023	1.163232	1.027472	1.033983
0.78	1.081142	1.101544421	1.154372	1.027472	1.019398
0.785	1.053816	1.089469973	1.154372	1.008452	1.019398
0.79	1.042188	1.089469973	1.140137	1.008452	0.983125
0.795	1.030559	1.075786383	1.124321	0.97437	0.983125
0.8	1.00614	1.065321011	1.124321	0.957079	0.983125
0.805	0.996837	1.0407753	1.106293	0.957079	0.954986

0.81	0.968931	1.024275971	1.087	0.937813	0.954986
0.815	0.958465	1.011799854	1.087	0.937813	0.941759
0.82	0.927654	0.99288661	1.071817	0.893362	0.941759
0.825	0.911376	0.973169315	1.036716	0.863479	0.908199
0.83	0.877078	0.952244939	1.0111	0.863479	0.908199
0.835	0.848014	0.936148703	1.0111	0.84051	0.908199
0.84	0.81139	0.913213569	0.992124	0.816801	0.848886
0.845	0.773606	0.858895449	0.963663	0.816801	0.848886
0.85	0.740472	0.833144949	0.933623	0.764449	0.820241
0.855	0.702107	0.80699209	0.902001	0.730371	0.820241
0.86	0.668392	0.780035206	0.902001	0.715305	0.789056
0.865	0.631772	0.734167845	0.877968	0.715305	0.789056
0.87	0.596314	0.691522401	0.843501	0.680486	0.744656
0.875	0.538944	0.664164008	0.787537	0.625421	0.67264
0.88	0.494478	0.617896049	0.761292	0.600726	0.67264
0.885	0.458207	0.566801904	0.723982	0.576526	0.639594
0.89	0.424261	0.525362936	0.649679	0.54245	0.607056
0.895	0.375903	0.474270209	0.613319	0.469854	0.607056
0.9	0.338122	0.433235323	0.588024	0.449605	0.536569
0.905	0.309002	0.396505182	0.501395	0.407383	0.494038
0.91	0.278661	0.342034686	0.478314	0.364912	0.464553
0.915	0.239196	0.305023329	0.420456	0.349355	0.43761
0.92	0.207056	0.258438227	0.376826	0.298985	0.381189
0.925	0.165152	0.226053927	0.306228	0.275033	0.348826
0.93	0.138882	0.190411809	0.257509	0.231528	0.307651
0.935	0.114763	0.157023054	0.217801	0.202097	0.268514
0.94	0.094828	0.13135776	0.185142	0.163925	0.237676
0.945	0.08175	0.106256807	0.151093	0.135284	0.19261
0.95	0.072275	0.086987878	0.124506	0.113384	0.1716
0.955	0.06466	0.072747338	0.095548	0.088374	0.1336
0.96	0.059195	0.062448281	0.072218	0.07314	0.103324
0.965	0.052917	0.053316201	0.059319	0.059363	0.076473
0.97	0.045536	0.046597265	0.048412	0.050942	0.055381
0.975	0.04067	0.041527248	0.041677	0.043535	0.041693
0.98	0.034574	0.035465145	0.035511	0.037954	0.033865
0.985	0.028183	0.029021685	0.02989	0.033065	0.028002
0.99	0.023569	0.022824609	0.023909	0.028546	0.023274
0.995	0.017685	0.017239421	0.018274	0.024719	0.018971
1	0.014715	0.01390119	0.013417	0.021689	0.01517

7.7.1 Derivation and Worked Example for Determination of Time-Temperature Behavior of Nuvolve™

$$\frac{d\alpha}{dt} = Aexp\left(-\frac{E_a}{RT}\right) f(\alpha) \tag{14}$$

$$\int_0^{\alpha_t} \frac{d\alpha}{f(\alpha)} = \int_0^t Aexp\left(-\frac{E_a}{RT}\right) dt \tag{15}$$

Substituting $f(\alpha) = 4\alpha^{3/4}$ in Equation 15 yields:

$$\alpha^{1/4} = Aexp\left(-\frac{E_a}{RT}\right) t \tag{16}$$

$$t = \frac{\alpha^{1/4}}{Ae^{\frac{-E_a}{RT}}} \tag{17}$$

Provided that A= 10^{11} min^{-1}, E_a= 113,000 J/mol (Nuv-B in Air), R=8.314 J/mol.K and temperature = 190 ºC= 463 K then the calculation produces the following for 1% conversion

$$t = \frac{(0.01)^{1/4}}{10^{11} * e^{\frac{-113{,}000}{8.314*463}}} * 60 = 1054\ seconds$$

Table 7.7-2: Time-temperature dependence of Nuvolve™ at 1 and 5 % conversion

Temperature (ºC)	Time (sec) at 1 % Conversion	Time (sec) at 5 % Conversion
100	1249674	1868698
110	482991	722240
120	195922	292972
130	83113	124283
140	36752	54957
150	16891	25257
160	8046	12032
170	3964	5927
180	2014	3012
190	1054	1576
200	567	848
210	313	468
220	177	264
230	102	153
240	60	90
250	36	54
260	22	33
270	14	21
280	9	13
290	6	9
300	4	6